IDENTIFICATION OF CLEAR AND CLOUDY AREAS FROM AVHRR RADIANCES

by

Nikolaos Sakellariou

Department of Meteorology
McGill University
Montreal

A thesis submitted to the Faculty of Graduate Studies and Research
in partial fulfillment of the requirements for the degree of
Doctor of Philosophy

September 1988

IDENTIFICATION OF CLEAR AND CLOUDY AREAS FROM AVHRR RADIANCES

ABSTRACT

Automatic analysis methods based on multichannel radiance data measured by the Advanced Very High Resolution Radiometer (AVHRR) on the NOAA7 and NOAA9 satellites are used to:

a) detect clear and cloudy areas above coastal regions; and

b) detect clouds and to estimate cloud amount above the Arctic

Channels 1 2 and 4 of the AVHRR were employed to separate clear from cloudy radiances above coastal regions.

All AVHRR channels were used above the Arctic. A large number of orbits were analysed automatically and the analysis results were compared to manual analyses performed by an independent observer and to published analyses The comparisons yield that the present algorithm provides a reliable method for the automatic detection of clouds in the Arctic.

RESUME

Des méthodes automatisées d'analyse basées sur les données de rayonnement provenant de canaux multiples mesurées par l'AVHRR (Advanced Very High Resolution Radiometer) des satellites NOAA7 et NOAA9 sont utilisées pour:

a) distinguer les zones claires et ennuagées au-dessus des régions cotières; et

b) discerner les nuages et estimer l'ennuagement au-dessus de l'Arctique.

Les canaux 1, 2 et 4 de l'AVHRR sont utilisés pour distinguer le rayonnement par temps clair et par temps nuageux au-dessus des régions cotières

Tous les canaux de l'AVHRR sont utilisés pour l'Arctique. Les données provenant d'un grand nombre d'orbites différentes sont analysées automatiquement et le résultat de ces analyses est comparé aux analyses manuelles produites par un observateur indépendant, de même qu'aux analyses publiées. Ces comparaisons permettent de croire que le présent algorithme constitue une méthode sûre d'auto-détection des nuages au-dessus de l'Arctique.

ACKNOWLEDGEMENTS

The author wishes to express his gratitude to Dr. H.G. Leighton for his help at all phases of this study, consultation encouragement and guidance.

He is also grateful for the assistance of Graeme Morissey and John Lewis of the Satellite Data Laboratory ir providing the AVHRR data used in the first part of the thesis and to Philip Gabriel for his helpful comments.

The financial assistance from the Natural Sciences and Engineering Research Council of Canada and rrom the Atmospheric Environment Service of Canada is greatly appreciated.

The author wishes to thank Ms Vicki Trimarchi for the editing of the manuscript, Ms Ursula Seidenfus and Mr Saolin Si for making the drawings.

The author wishes also to thank his wife for her support during these years, and his parents for their faithful encouragement until their deaths.

STATEMENT OF ORIGINALITY

The present thesis introduces: i) a new method for the identification of cloud-free pixels that can be succesfully applied to inhomogenous surfaces consisting of land and water, where previous methods become less reliable; ii) a new method to identify cloud and measure cloud amount above snow and ice covered surfaces.

Both methods are completely automated and rely on multispectral AVHRR data. The method that estimates cloud amounts above snow and ice covered surfaces was used to analyse large areas of the Arctic. Comparisons to manual analyses of the same data performed by an independent observer, and to automatic and manual analyses published elsewhere, confirm the applicability of the method. This work is viewed as a contribution to the polar cloud project of the International Satellite Cloud Climatology Project.

Chapter 2 is essentially a copy of the manuscript titled "Identification of cloud-free pixels in inhomogenous surfaces from AVHRR radiances", published in the Journal of Geophysical Research (May 1988) with the joint authorship of Dr. H. G. Leighton.

The author of the thesis contributed the idea, the method and the analysis of the data, while Dr. H. G. Leighton provided consultation and also rewrote the original draft in a style more suitable for publication.

TABLE OF CONTENTS

LIST OF FIGURES

CHAPTER 1

INTRODUCTION

1.1 Cloud Detection from Satellites

The importance of clouds in both weather and climate was emphasized long before the satellite era, and cloud observations are routinely taken by surface meteorological stations. Cloud fields are generated by the general circulation of the earth's atmosphere and oceans. But they also have a great impact on atmospheric general circulation as they control the radiation budget at the earth's surface and in the atmosphere. Therefore cloud fields form a major feedback mechanism with a profound importance for the understanding of the earth's climate.

Conventional ground-based observations of clouds are of limited value due to the limited spatial and temporal coverage. They also suffer from the observer's subjectivity. In addition, over the oceans, biases arise as ships avoid areas where severe storms are in action. Cloud climatologies based on surface observations have been constructed (e.g. Telegadas and London 1954), but sampling was sparse especially over the oceans and polar regions.

In contrast to the surface network of meteorological stations that provides point measurements of the atmosphere from selected sample sites, the network of meteorological satellites already available provides spatially continuous global observations with high spatial and temporal resolution. Satellite cloud climatologies have also been compiled (e.g Sadlers et al. 1976) but according to Schiffer and Rossow

(1983), these data sets as well as those based on conventional observations do not contain adequate information for climate modelers to calculate the effect of clouds on the earth's radiation budget. The need to create a reliable climatology of cloud radiative properties and promote relevant research using these data led to the establishement of the International Satellite Cloud Climatology Project (ISCCP). During the five-year period starting in mid-1983, data were collected from geostationary and polar orbiting satellites to form the data base that will eventually create the new climatology.

As the volume of the data prohibits the use of manual analysis, these data should be automatically analysed. The choice of a particular algorithm for the extraction of cloud parameters is crucial, and therefore the ISCCP inspired a wide-spread effort for the evaluation of the already existing algorithms and for the creation of new improved ones. Detailed intercomparison of six promising cloud detection methods took place (Rossow et al. 1985). This intercomparison yielded that regions with complex spatial distribution of surface albedo and temperature, such as for example the St. Lawrence river valley during the winter, are responsible for the largest disagreements among the results of the algorithms. Also, it was concluded that all algorithms benefit from accurate specification of clear-sky radiance values. Elements of several methods were incorporated into a new algorithm that will be used for the analysis of the ISCCP data. This algorithm repeatedly failed to detect low lying clouds, while other clouds were satisfactorily detected (Goodman and Henderson-Sellers 1988).

Reviewing the recent progress in cloud detection and analysis, Goodman and Henderson-Sellers (1988) concluded that: "while many new

echniques, are quite successful in certain well defined situations, they are usually not, and probably they will never be applicable to other areas, climates and configurations."

In most methods clouds are most readily detected above uniform backgrounds, particularly the oceans (e.g. Coakley and Bretherton 1982). Common inhomogenous backgrounds, such as coastal regions where water surfaces appear dark and often relatively cold while nearby land is warmer and brighter in the reflected sunlight, or snow-covered land with varying snow fraction, make cloud detection difficult. Sea-ice attached to the land or regions where sea-ice and open water coexist are also examples of spatially variable backgrounds that complicate recognition of clouds. Temporal variability such as might be generated by a moving snowstorm may also lead to misidentification of clear and cloudy regions by some algorithms. When the underlying surface is bright and cold, the contrast between clear and cloudy radiances is generally low, and cloud detection becomes even more difficult. Therefore snow- and ice-covered areas are probably the most unfavorable backgrounds for cloud detection. As a result there have been far fewer attempts at cloud identification above these areas than above snow-free and ice-free regions (Rossow 1987).

Polar orbiting satellites cover high latitudes not viewed by the geostationary satellites. They are equipped with the Advanced Very High Resolution Radiometer (AVHRR) that offers adequate spatial resolution (1.1 km at the subsatellite point) and five channels. The potential of the AVHRR data to detect and quantify clouds and surface properties over polar regions was investigated by various groups working on the same problem (Polar Cloud Project) within the ISCCP at a

workshop in Tokyo in 1986. All participants reported their main findings resulting from the analysis of radiation fields in polar regions, included in a data set that had been distributed among them (Raschke, 1987)

They stated (Raschke, 1987) that the study of polar cloudiness and surfaces using current satellite observations encounters four significant obstacles:

i) low radiances in general;

ii) low radiance contrasts between cloudy and clear scenes;

iii) complex surface property variations caused by changes in snow and sea-ice; and

iv) non-monotonic relations between radiances and cloud properties.

In addition to the aforementioned obstacles, it should be noticed that prevailing cold temperatures limit the amount of water vapor that can be sustained in the atmosphere and that the clouds, on average, contain less condensed material than in lower latitudes and so they tend to be optically less thick. Thin clouds tend to be less readily detectable from satellites than thick ones.

We may conclude that inhomogenous backgrounds as well as snow and ice covered surfaces pose serious problems to many cloud detection algorithms. Cloud detection schemes are generally helped by high spatial resolution data and more channels. Therefore, polar orbiting satellites, in addition to being the only source of information in high latitudes, also provide some advantages in detecting clouds at lower latitudes due to their multichannel AVHRR sensor. Arking and Childs (1985) and Coakley and Bretherton (1982) have already used AVHRR data

to detect clouds in the low and middle latitudes.

The present study will use AVHRR data to identify clear-sky radiances and to detect clouds over areas that were previously found to discourage cloud detection due to their spatially and/or temporally varying clear-sky radiances. It is partly related to the problem of exploiting the AVHRR capabilities. The goal is to provide new methods that are potentially useful for the analysis of the ISCCP data, in areas where previously existing algorithms are less reliable. First, coastal areas will be examined as they are considered to be the simplest of the aforementioned difficult situations. A new method of identifying clear-sky radiances above these areas will be formulated. Next, more complex backgrounds composed of a mixture of land, ice or snow, and water will be examined, to yield a new method for cloud identification in high latitudes. Finally radiation fields above the Arctic will be analysed and the cloud fields obtained will be compared to manual analyses by an independent observer, and to a previously published manual and automatic analysis (Ebert 1988).

1.2 Cloud Detection Algorithms

Cloud detection algorithms include a variety of assumptions and a complexity of mathematical calculations. Recent progress in cloud detection and analysis was reviewed by Goodman and Henderson-Sellers (1988). They summarize the basic principles and characteristics of various cloud detection algorithms amd also emphasize the need for validation. Each algorithm is based on a set of assumptions that is

used to associate the Earth's surface, the atmosphere and the clouds with the satellite measurements (Goodman and Henderson-Sellers, 1988). Three major groups of cloud detection algorithms can be distinguished on the basis of the aforementioned assumptions and their gross characteristics:

1) threshold type algorithms;

2) statistical type algorithms;

3) radiative transfer type algorithms;

We outline some of the basic principles, advantages and disadvantages of each group.

1) The threshold methods treat every pixel separately, and if the radiance from a particular pixel exceeds a certain threshold then the pixel is either cloud-free or overcast. Time series of extreme values of each pixel are used to derive the clear-sky radiance. The pixel's minimum reflectance for that period is assumed to represent the clear sky reflectance, on the basis that at some time during the examined time period cloud-free conditions prevail over each pixel. Initially, thresholds in a single channel were used, but soon afterwards methods that imposed thresholds in two channels were developed (Goodman and Henderson-Sellers 1988).

Simplicity, computational efficiency, and easy implementation are their main advantages.

Disadvantages are that there is no allowance made for partially cloud-covered pixels, and it is necessary to know the clear-sky radiances. Furthermore, due to spatial inhomogeneities and temporal surface variations such as fresh snowfalls or changes in atmospheric turbidity, thresholds should be tuned with the help of auxiliary data

such as surface observations of clouds and atmospheric temperature structure.

2) Statistical methods treat large groups of pixels at a time and use multidimensional frequency histograms in order to recognize clear and cloudy areas. Multidimensional histograms produce areas of relatively high pixel density associated with relatively homogenously emitting and reflecting clear water, land or cloudy regions. In principle, they can provide for partly cloudy pixels, but occasionaly the data cannot produce distinct clusters. They are generally more complex than threshold techniques, and consume more computer time.

Gaussian histogram analysis (Simmer et al. 1982), the dynamic cluster algorithm (Desbois et al. 1982), and spatial coherence algorithms (Coakley and Bretherton 1982) are examples of statistical methods developed along three different directions. The first fits Gaussian distribution functions to the histogram, to separate distinct clusters. The second automatically separates the multidimensional histograms into groups of pixels (kernels), each group representing a surface or cloud type. The third type of algorithm relies on local spatial variances of radiances. Homogenous surfaces, such as ocean and cloud layers, produce small variances while inhomogenous regions, such as partly cloudy areas between clear and overcast regions, produce considerably higher variances, allowing the separation of clear and overcast radiances. Pattern recognition algorithms like those of Garand (1986) and Ebert (1987b) are also included in the class of the statistical algorithms.

3) Radiative transfer type algorithms fit a radiative transfer model to the observed radiances in order to determine cloud parameters.

Hybrids of radiative transfer models with statistical and threshold elements have been tried (Rossow et al. 1985). The radiative transfer model uses climatologically derived values for the vertical temperature profile. The atmosphere is assumed to be composed of a Rayleigh scattering gas above and a plane parallel cloud model. Cloud parameters can be deduced directly from the model. We believe that this type of plane parallel cloud model poorly represents many cloud types that are encountered in nature, and this therefore constitutes a weak point in this procedure.

Algorithms dedicated to cloud detection above polar regions must be able to overcome the obstacles mentioned in the previous section. As data will be mostly extracted from the AVHRR, five channels can be used for cloud detection during the summer.

The main directions taken by the various research groups in the Tokyo workshop (Raschke 1987) are to extensively use the difference between the visible (0.7) and the near-infrared (0.9) channel, as independently suggested by Arking (1987) and Raschke (1987), and also to use the brightness temperature difference between the split window channels 4 and 5 (T_4-T_5), independently suggested by Inoue (1987a) and Yamanouchi (1987a).

Ebert (1987a) proposed a cloud detection method based on pattern recognition techniques; Raschke et al. (1987), a threshold method that uses thresholds at all five channels, Yamanouchi et al. (1987a), a threshold method based on T_4-T_5 values, and Rossow (1987), a bispectral threshold method with some statistical elements.

1.3 Method and Validation

The first step in every cloud analysis algorithm has the task of separating the observed radiances into either a cloudy or clear category. This step becomes increasingly difficult with increasing surface complexity.

We have developed methods to:

a) improve the aforementioned separation of radiances, above a surface that exhibits the limited complexity of being composed of vegetated land and water. We may encounter this surface type at all latitudes, and solving this problem is an introductory step towards the separation of cloudy and clear radiances in the more complex Arctic environment.

b) identify signatures of snow, ice covered water or land surfaces, and surfaces composed of combinations of the above. Channels 1 and 2 are particularly useful for the recognition of these signatures, but finally all AVHRR channels are employed in order to separate cloudy from clear pixels.

When trying to validate the whole performance of the algorithm, we keep in mind that in general, validation of cloud detection algorithms is limited in two ways:

1) Properties of the available data, such as spatial and temporal resolution, are limited by the need to have a manageable data volume.

2) There is no "truth" data set against which to compare the results (Rossow et al. 1985).

The most readily available method of validation is comparison with surface synoptic reports (Goodman and Henderson-Sellers 1988). This

kind of validation is more difficult in the Arctic than in middle latitudes due to the sparse network of observing sites. In order to validate the performance of the algorithm in the present study, we used:

1) synoptic observations that are included in the European Meteorological Bulletin;

2) sea-ice analysis charts;

3) cloud cover reports from meteorological stations;

4) manual cloud analysis performed by a meteorologist not involved in any other aspect of this work, using visible and infrared satellite images, ice charts and synoptic maps;

5) comparison between results of the algorithm obtained by low resolution and high resolution satellite data above the same area; and

6) comparison between results derived by the present algorithm and published results obtained by another investigator (Ebert 1988).

1.4 Satellite Data and Products of the Algorithm

In the first part of this study which deals with coastal areas, we identified clear and cloudy regions along the east coast of North America, the Great Lakes and the St. Lawrence river valley. The data used were radiances from the NOAA9 AVHRR obtained from the Canadian Atmospheric Environment Service and which had the full spatial resolution of 1.1 km at the sub-satellite point (Local Area Coverage, LAC), but reduced radiance resolution (see section 2.1).

The second part of the thesis deals with the identification of clouds over the polar regions. The data set analysed is that which was distributed to all participants of the Polar Cloud Project and consists of 10 bit AVHRR radiances from 97 orbits of NOAA7 from July 1, 1984 to July 7, 1984. The data are of the lower spatial resolution Global Area Coverage (GAC) form (see section 2.1 for details).

The N. Hemisphere data from all orbits were analysed to generate maps of average cloud cover in a 2.5 x 2.5 latitude-longitude cell and will be used in an intercomparison study with other participants in the Polar Cloud Project. However, in the thesis we only discuss results from July 1, July 2, and July 5, 1984.

A few problems were encountered when trying to group the pixels into the aforementioned cells. At very high latitudes, the longitude lines converge and assigning a pixel to a cell becomes ambiguous. At the poleward extremities of the satellite orbit, very few pixels may exist in a particular cell because that cell is only partly covered by the satellite orbit. Therefore, the assigned cloud amount at that cell may poorly represent the actual cloud amount.

To avoid problems associated with the aforementioned situations, we did not assign pixels into cells that lie at latitudes higher than 85^{o}. In addition, the 34 most northward lying pixels of every scan line were not assigned to any cell. We did not report any values for a cell when the total number of pixels, assigned to that cell was less than 50.

1.5 Research Areas Related to the Present Thesis

We have already mentioned the ISCCP project and its intention to provide the climatological community with a reliable satellite-derived cloud climatology. The development of algorithms that can detect cloud-free or cloudy pixels above complicated backgrounds and the development of algorithms that are effective for the polar environment are steps forward toward the completion of that goal. They are also useful for satellite based studies of surface properties, such as emissivity, temperature and reflectivity and vegetation studies, where cloud-contaminated pixels must be rejected.

The importance of satellite-derived, cloud-free and cloudy radiances for climatic studies is well known. Surface energy budgets, cloud amounts and cloud distribution, can be derived from these radiances. Furthermore, cloud amounts can be used as an input quantity for the initialization of General Circulation Climatic Models, and cloud amounts generated by GCCMs can be validated by comparison with the actual climatological cloud field.

Taking into account the time-consuming nature of manual cloud analysis based on the interpretation of satellite images, it is also conceivable that a simple, fast and efficient automatic analysis of the cloud field may facilitate operational forecasting. It is likely that the Arctic region will be served more than the rest by automatic cloud analysis based on AVHRR satellite data. Over Arctic areas, where surface observations are more sparce than at mid-latitudes, polar-orbiting satellites offer high spatial resolution and relatively high temporal resolution and so, changes in cloud fields with implications concerning the corresponding weather systems can be frequently

observed.

1.6 Structure of the Thesis

During the first part of the thesis, chapter 2, the difficulties associated with the inhomogenous backgrounds and particularly with the coastal regions are examined. The basic principles yielding identification of cloud-free and cloudy pixels, details of the method, as well as possible applications are presented.

During the second part, chapter 3, the problems that are encountered in the Arctic environment, concerning identification of cloud-free and cloudy pixels are examined. Description of the capabilities of the various AVHRR channels for cloud detection in the Arctic-Antarctic environment, based on:

a) the characteristics of the channels, and

b) methods of using these channels for the same purpose already suggested by other researchers, is presented in Sections 3.21, to 3.24. The present algorithm is described in Sections 3.3 to 3.34. The validation procedure of the present algorithm is presented in chapter 4. Our conclusions and suggestions for future work are given in chapter 5.

CHAPTER 2

2.1 AVHRR and Available Satellite Data

The Advanced Very High Resolution Radiometer on board in recent NOAA satellites, is sensitive in five spectral regions. They are centered at around 0.6, 0.9, 3.7, 10.8, and 12 μm. It scans cross the satellite orbit, at a rate of 360 lines per minute. The maximum scaning angle, is ± 55.4° from nadir. It has an optical field of view 1.3 milliradians, which results in 1.1 km maximum resolution at nadir.

There is no on-flight calibration for the solar reflected radiation channels. But the infrared channels are continuously calibrated, using a black body inside the spacecraft whose temperature can be calculated, and the outer space as points of reference.

The AVHRR data are transmitted at full resolution 1.1 km Local Area Coverage (LAC) data, or reduced resolution ~4 km Global Area Coverage (GAC) data. The data reduction process that creates the GAC data from LAC, takes four out of every five LAC pixels, along every third scan line, to compute one average value per channel. The spatial resolution of the degraded data GAC, is actually 4 x 3.3 km at the subsatellite point, but it is generally referred to as 4 km resolution. The data are transmitted to Command and Data Aquisition stations (CDA). Further processing provides for Earth location, Solar zenith angle, and calibration information (B1-data).

When we analysed radiation fields above coastal regions we used

LAC data. The data were obtained from the Satellite Data Laboratory of the Canadian Atmospheric Environment Service in the form of 8-bit counts. The scheme to compress the original 10-bit data to 8 bits in channels 1 and 2 is described by Wannamaker (1985) and is designed to retain the full resolution at the lowest reflectivity values at the expense of the highest values. Therefore estimates of clear-sky reflectivities should not be affected by the data compression. In channel 4 the 10-bit values were all divided by 4, resulting in uniform degradation of the resolution. The calibration scheme presented by Lauritson et al. (1979) was used to calibrate the data. Non-linearities in the IR channels were not taken into account.

In the analysis of cloud fields above the Arctic, GAC data obtained by NOAA7 were employed. For some satellite orbits, higher resolution LAC data were also available.

2.2 Cloud Detection Algorithms and Inhomogenous Background

As it was mentioned in Section 1.3, identification of cloud-free pixels is a first step in every cloud analysis algorithm, used to determine fractional cloud cover; it is also essential in satellite-based studies of surface properties and processes such as temperature, emissivity, reflectivity, and energy budgets.

Several methods of identifying cloud-contaminated pixels have been formulated (e.g., Coakley and Bretherton 1982; Rossow et al. 1985; Saunders 1986), the more successful methods tending to work well when the background is uniform, especially over oceans, but having dif-

ficulty in distinguishing clear from cloud-contaminated pixels when the surface temperature and reflectivity are variable. Coakley and Baldwin (1984) point out that their spatial coherence method does not work well over the continents, and Saunders (1986) finds that the preferred method deduced from a comparison of four different schemes, the spatial coherence visible technique (Llewellyn-Jones et al. 1984), required simpler criteria when applied over coastal regions, with the result that clouds would be less readily detected. England and Hunt (1985) have also drawn attention to the geographic limitations of most methods and have described a bispectral (visible and 11-μm infrared) technique that overcomes many of these limitations. However, there are a number of advantages to the method described here.

The reason that many methods have difficulty identifying cloud-contaminated pixels over scenes with complex backgrounds is that they either rely on some kind of a threshold in a solar or infrared window channel or both, or on some type of clustering of radiances in these channels. However, surface reflectivity may vary considerably from one surface type to another, and surface temperatures will also vary as the nature of the surface changes, particularly if the surface contains both land and water. These variations will normally hinder the ability of algorithms to distinguish between clear and cloud-contaminated pixels.

The method described here complements other techniques in that it works best when the background is a mixture of water and land, i.e., over coastal regions or continental regions in which the surface is covered to a significant extent by lakes. The method uses the radiances measured in channels 1, 2, and 4, centered at 0.63, 0.91, and

10.8 μm of the AVHRR, respectively, on the NOAA 9 satellite.

In section 2.3 the general principles underlying the method will be described, and in section 2.4 the details of the algorithm are given. Section 2.5 discusses an application of the method to the extraction of cloud amount and section 2.6 contains a brief summary.

2.3 Principles of the Method

Comparison of the radiances measured in channels 1 and 2 provides a useful tool for the identification of cloud-free pixels. The spectral albedo of soils, bare surfaces, and vegetated surfaces all increase with increasing wavelength, up to wavelengths beyond 1 μm (Kondratyev, 1969), suggesting that the reflectance difference in channels 2 and 1, R_2-R_1, will be positive. For water surfaces, on the other hand, the albedo is small, and except for solar zenith angles greater than about 70°, it decreases with increasing wavelength, implying that R_2-R_1 will be small and negative. Theoretical calculations (Welch et al. 1980; Wiscombe et al. 1984) and observations (Twomey and Cocks, 1982) for clouds find that reflectances in the wavelength region of interest decrease slowly with increasing wavelength, except for sharp minima at around 0.95 and 1.1 μm. Thus thick clouds would also be expected to be characterized by small negative values of R_2-R_1 but with much larger values of R_2 than for water.

These characteristics are demonstrated in a plot of R_2-R_1 against R_2 (Figure 2.1). Figure 2.1 is a composite of three scenes, each consisting of 32 x 32 pixels of full resolution (≈1.1 km at the

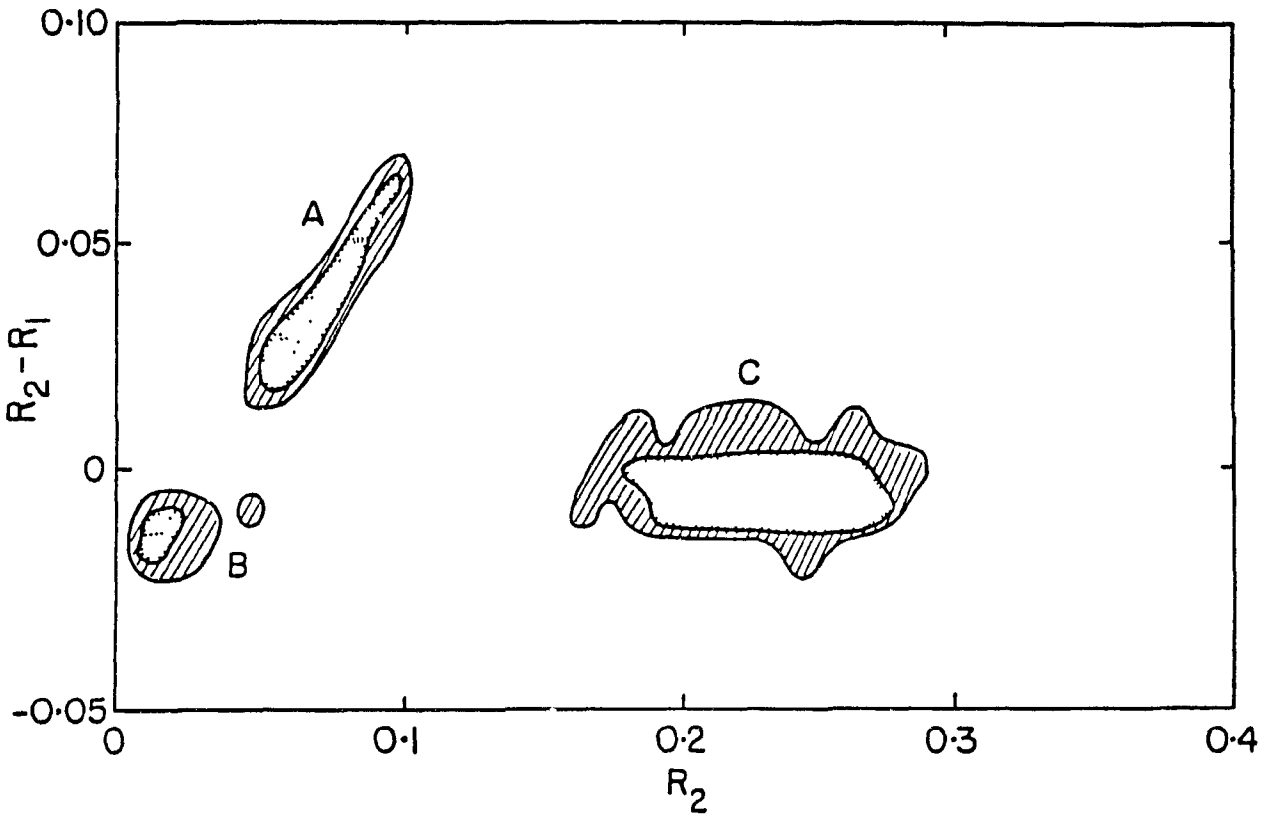

Figure 2.1. Composite of the reflectivity differences in channels 1 and 2 of the AVHRR as a function of the channel 2 reflectivity for three scenes of 32X32 pixels of local area coverage. A indicates a clear scene over southern Quebec; B, a clear scene over the Atlantic; and C, overcast cloud. The hatched and dotted regions contain pixel densities of 1-9 and greater than 9, respectively, in arbitrary units.

subsatellite point) data from channels 1 and 2 of the AVHRR on NOAA 9. The group of pixels identified as A is from a completely clear scene over southern Quebec in October. The cluster labeled B is from a cloud-free scene over the Atlantic Ocean off the coast of Florida, and the pixels clustered at large values of R_2 and with $R_2 \leq R_1$, labeled C, are from a scene with overcast cloud.

Scenes consisting of two surfaces types with quite different radiative properties at 0.65 and 0.9 μm might be expected to contain some pixels of one type, some of the second, and others that have radiances corresponding to a linear combination of the radiances of the constituent types. This situation is likely to obtain in scenes that contain both land and water surfaces, but other possibilities are scenes that consist of vegetated surface and bare soil and scenes consisting of two predominant vegetation types with different reflection properties. In such cases the channel 1 and channel 2 radiances from individual pixels, when plotted on coordinates of R_2-R_1 versus R_2 (for convenience referred to from now on simply as an R_2-R_1 plot), should lie along a line with end-points corresponding to the coordinates of pixels that are uniformly filled by each of the two surface types. This linear pattern is evident in Figure 2.1. Two other examples of the linear arrangement of points on an R_2-R_1 plot under cloud-free conditions are shown in Figures 2.2a and 2.3a. Figure 2.2a is for a cloud-free scene containing part of the northeast coast of North America, and Figure 2.3a is a cloud-free scene over southern Ontario, both in April.

To demonstrate how a band is broadened and distorted by the presence of clouds, Figures 2.4a-2.4c show a sequence of three plots for the same region of southern Quebec: (1) with almost clear skies

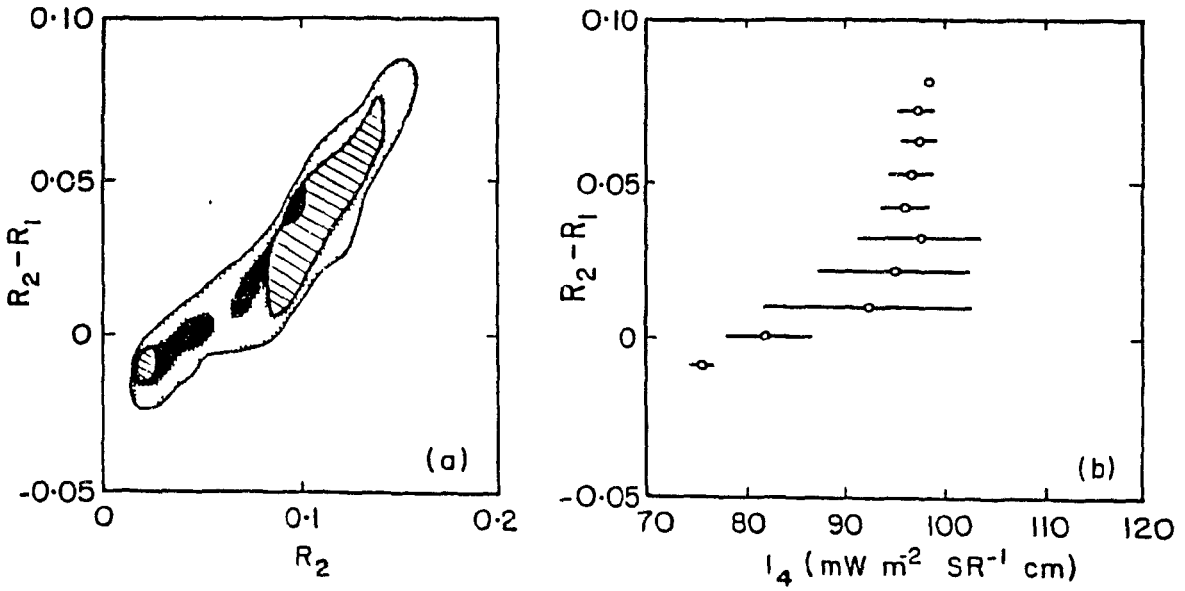

Figure 2.2. Reflectivity differences in channels 1 and 2 plotted against (a) the channel 2 reflectivity and (b) the radiance in channel 4, averaged over all pixels with the same value of R_2-R_1 The scene is a cloud free region of the northeast coast of North America. In Figure 2.2a, the dotted, shaded and hatched regions denote pixel concentrations of 1-5, 5-9 and greater than 9 respectively, in arbitrary units. In Figure 2.2b, the lengths of the lines are plus or minus one standard deviation.

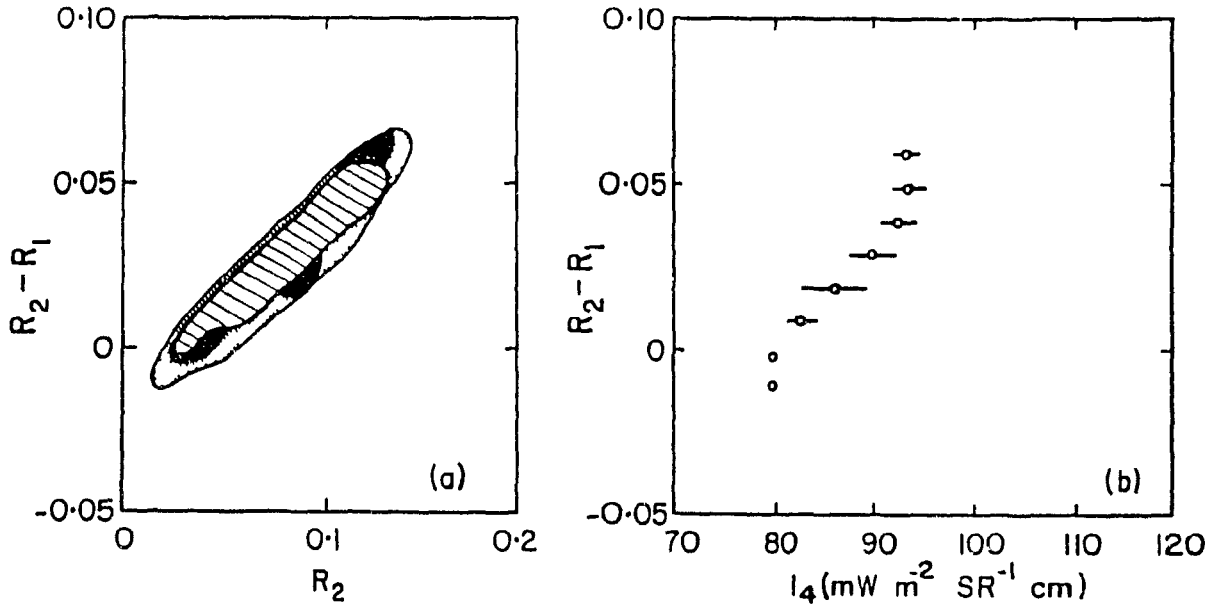

Figure 2.3. As in Figure 2.2, but for a cloud-free region over northern Ontario.

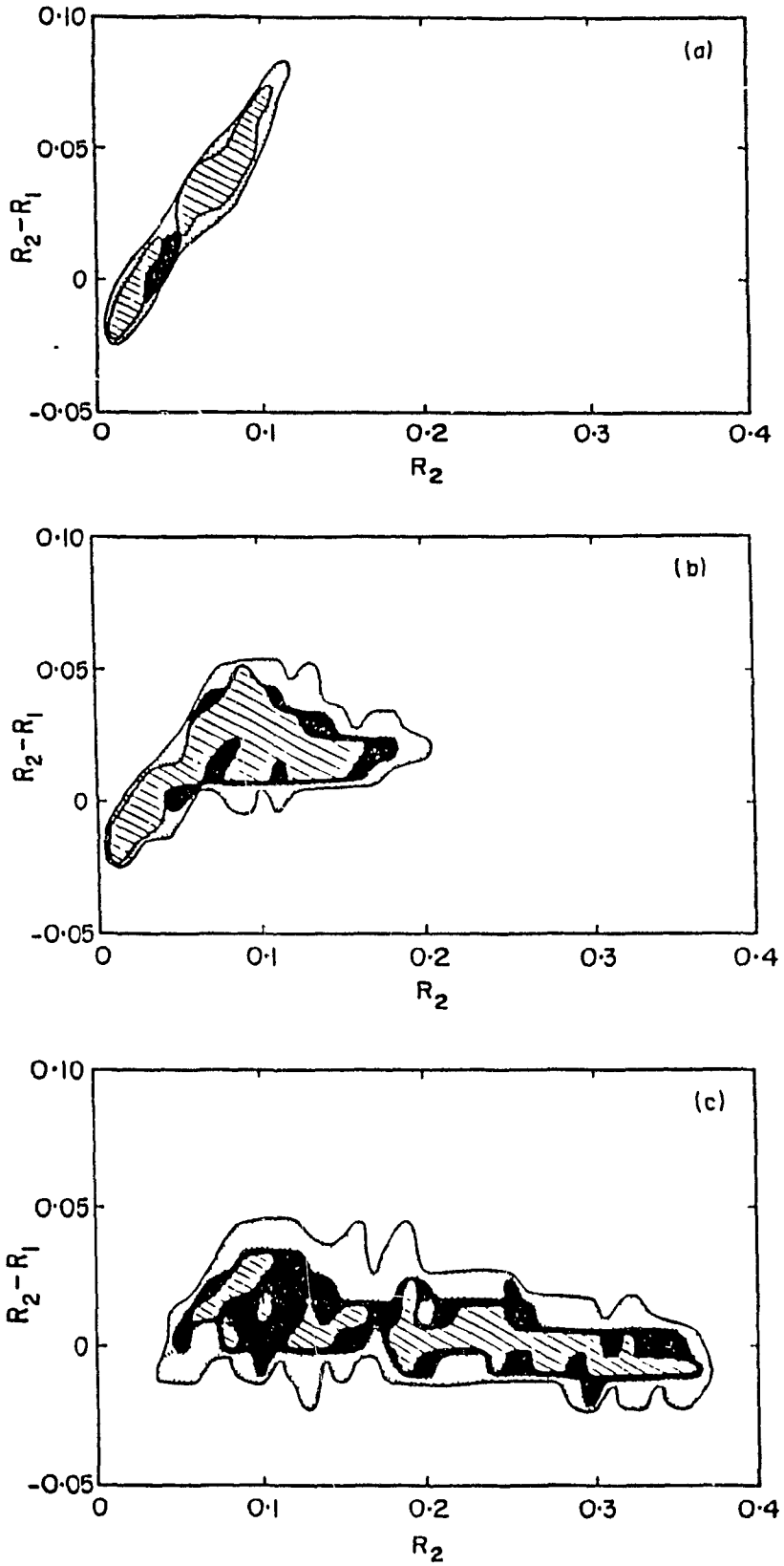

Figure 2.4. R_2-R_1 plots for the same region of southern Quebec, showing (a) almost clear skies (≈0.1 Ci). (b) a small amount of thicker cloud (≈0.1 Ac and Cu), and (c) extensive cloud (≈0.7 Sc and Cu).

(0.1 Ci according to surface observations), (2) with a small amount of cloud (0.1 Ac and Cu), and (3) with extensive cloud (0.7 Sc and Cu). As the cloud cover increases, pixels move to smaller values of R_2-R_1 and larger values of R_2, and the band of cloud-free pixels becomes less well defined.

These examples, together with the numerous others that have been examined, show that under cloud-free conditions and for vegetated surfaces and surfaces containing a combination of land and water, the channel 1 and channel 2 radiances, when plotted on the coordinates of Figure 2.2, tend to fall along a linear band. Section 3 gives the details of how this band of clear pixels is identified.

2.3 Details of the Algorithm

The method of identifying cloud-free pixels will be described with reference to a 32 x 32 pixel scene of local area coverage over southern Ontario containing clear regions and broken cloud. The R_2-R_1 plot for this scene is shown in Figure 2.5a.

First, in order to group pixels with similar properties, the reflectivities were rounded to the nearest 0.01. The effect of doing this is illustrated in Figures 2.5b and 2.5c, where in order to keep the diagrams to manageable size, they have been truncated at $R_2 = 0.2$. The identification of cloud-free pixels is based on the following assumptions:

1. For a given value of R_2-R_1, provided there is at least one pixel that is cloud free, the pixels with the minimum value of R_2 are

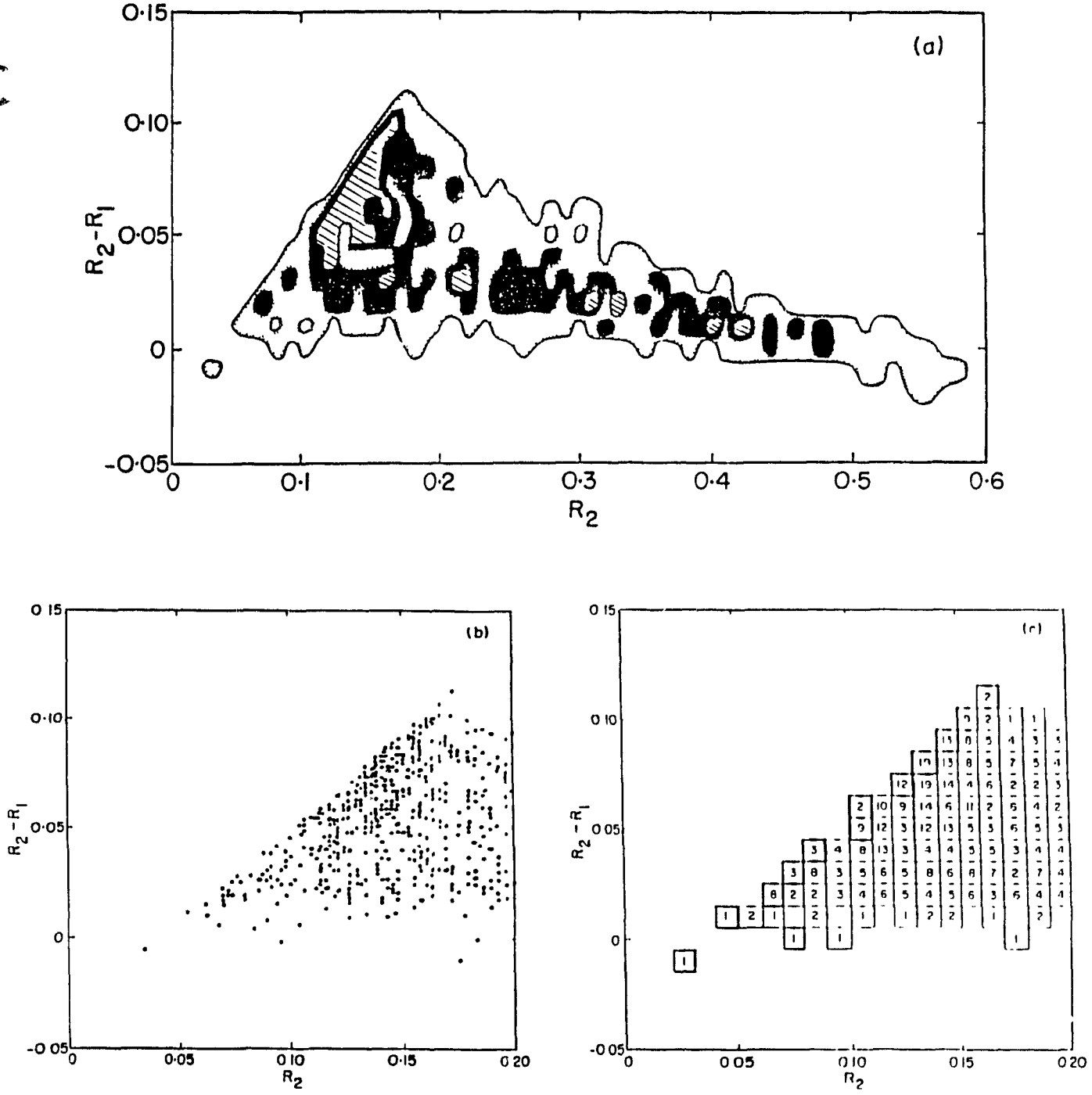

Figure 2.5. Identification of cloud-free pixels for a partially cloud scene. (a) The full R_2-R_1 plot. (b) The reflectances of individual pixels in the form of an R_2-R_1 plot truncated at R_2 = 0.2. (c) The number of pixels grouped within the specified reflectivity intervals, with the boxes with the heavy perimeters indicating pixels with minimum R_2 for fixed R_2-R_1.

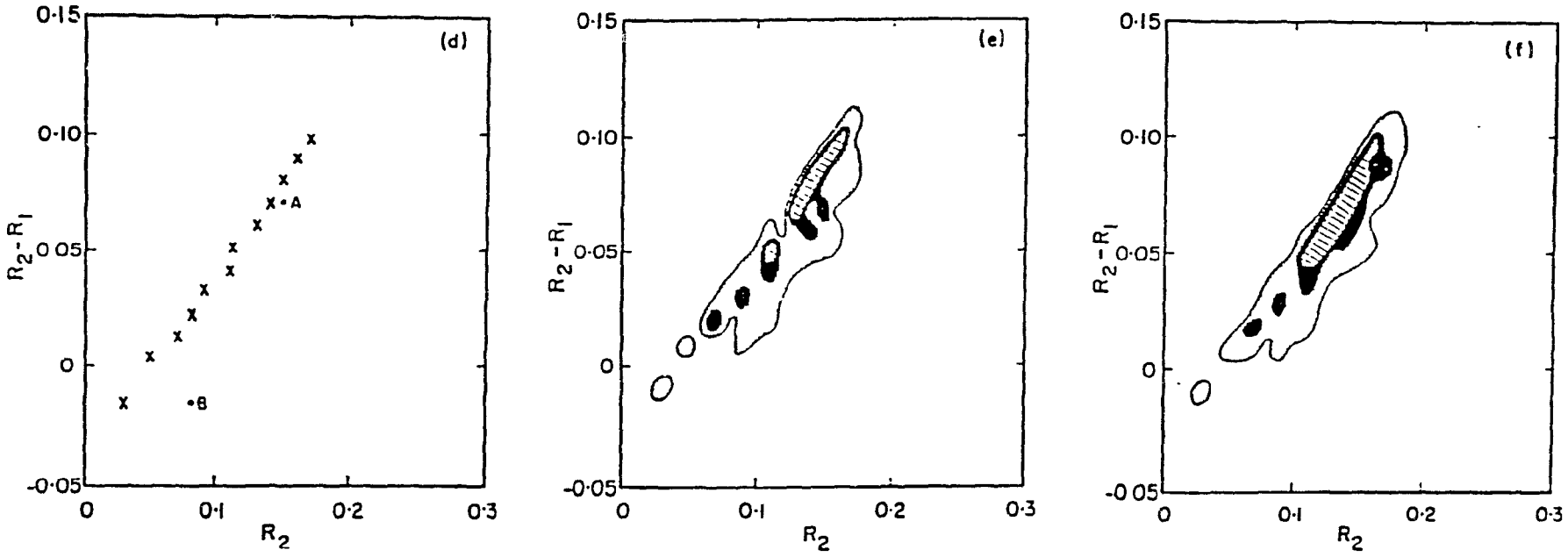

Figure 2.5 (d) Cloud free pixels that satisfy assumptions 1 and 2. (e) Pixels in Figure 2.5d as well as pixels whose I4 radiance exceeds the variable threshold described in the text. (f) All of the pixels in Figure 5e as well as pixels that lie within a specified distance from a line fitted to the pixels in Figure 2.5e.

cloud-free.

2. Pixels that are cloud-free and that have the minimum R_2 for a particular value of R_2-R_1 tend to lie on a straight line on an R_2-R_1 plot.

3. Over land, pixels with partial cloud cover will have greater values of R_2 and smaller values of R_2-R_1 than pixels with similar surface properties and no cloud.

4. Pixels with partial cloud cover will have smaller values of I_4, the radiance in channel 4, than pixels with similar surface-properties and no cloud.

The first three assumptions are based on the discussion in section 2.2, and the last is equivalent to assuming that the clouds are colder than the underlying surface.

Those pixels that have the minimum value of R_2 for each value of R_2-R_1 in Figure 2.5c are identified by the boxes with heavy perimeters. Not all of these pixels are necessarily cloud-free, since for some values of R_2-R_1 there may not be any cloud-free pixels. The second assumption is implemented by fitting a line to the points in the R_2-R_1 plot defined by these boxes and rejecting pixels in boxes that have R_2 more than 0.01 greater than the value of R_2 given by the line for the same value of R_2-R_1. This procedure is repeated as many times as necessary, typically once or twice, until there is no further rejection of pixels. The pixels that are retained satisfy assumptions 1 and 2 in as much as they lie along a line in the R_2-R_1 plot and have minimum values of R_2-R_1. The results of this step are shown in Figure 5d.

The selection of cloud-free pixels up to this point is almost certainly too restrictive. Consideration of the channel 4 radiances

and the fourth assumption suggest other pixels that should also be identified as being cloud-free. The value of I_4 for cloud-free pixels will normally vary systematically with their position along the line of cloud-free pixels on the R_2-R_1 plot. That this is so follows from the interpretation of the line as resulting from a linear combination of the reflectivities of two different surface types. To the extent that the different surface types have different temperatures, position on the line will correlate with I_4. The most favorable examples are again scenes that contain a combination of land and water. Pixels that have a relatively large proportion of land to water and hence relatively large values of R_2-R_1 will normally be warmer than those that contain predominantly water. Although the same argument holds for combinations of other surface types, the temperature contrasts are not likely to be as great. The systematic variation of I_4 is illustrated in Figures 2.2b and 2.3b. In these figures the mean values of the channel 4 radiance, I_4, averaged over all pixels with the same value of R_2-R_1 are plotted against R_2-R_1. In Figure 2.2b the mean value of I_4 is uniform for R_2-$R_1 \geq 0.03$ but then decreases sharply, suggesting that water does not cover a significant fraction of the area of pixels with R_2-R_1 > 0.03. The linear arrangement of the pixels for the larger values of R_2-R_1 must be due to variations in the nature of the land, and, in fact, there is some indication of a slight change in slope of the band at about R_2-$R_1 = 0.03$. In Figure 2.3b the mean value of I_4 decreases monotonically with decreasing R_2-R_1, which is consistent with the interpretation that lakes occupy varying fractions of the surface of individual pixels, ranging from all land to all water.

This consideration suggests the use of a variable threshold on I_4

which, if exceeded, identifies a pixel as being cloud-free. The threshold is defined as being the maximum value of I_4 of all pixels so far identified as being cloud-free which lie above and to the left of the pixel being tested on the R_2-R_1 plot. To illustrate this, suppose that the pixel plotted at point A in Figure 2.5d is cloud-contaminated. Since by assumption 3 cloud cover increases R_2 and decreases R_2-R_1, if the cloud were to disappear, the position of the pixel at A would move to a point in the diagram in one of the two cloud-free boxes above and to the left of A. Pixels with surface characteristics defined by these two boxes but which are contaminated with cloud will be colder than the pixels in these two boxes. Hence an appropriate threshold on I_4 to identify a pixel at A as being cloud-free is the maximum value of I_4 of all pixels in these two boxes. Similarly, the threshold to identify cloud-free pixels at B would be the maximum value of I_4 of all pixels in the bottom four boxes. Application of this procedure to the example, results in the pixels shown in Figure 2.5e are identified as being cloud-free.

In the next step of the procedure, a new line is fitted to all the points thus far identified as being cloud-free (Figure 2.5e). A correlation coefficient of greater than 0.7 is taken as the indication that the pixels that have been identified as being cloud-free form a linear band on the R_2-R_1 plot, consistent with our initial assumption. If the correlation coefficient is less than 0.7, the technique is rejected and one of the conventional methods of identifying cloud-free pixels may be applied. The technique is most likely to fail where the underlying surface is particularly homogenous, with cloud-free pixels being clustered within a restricted region of the diagram and not defining a band. In this circumstance, conventional methods are most

successful, and an alternative technique may be called automatically. The procedure may also fail when there are relatively few completely cloud-free pixels. Since it will normally be quite evident which of these two situations is occurring, this presents no difficulty. One exception is for the case when clouds are present over a snow or ice background, for then no cloud-free band will be present, and it may not be obvious whether the scene contains a uniform snow or ice background or uniform cloud cover.

Finally, pixels that lie close to those pixels that have been identified as being cloud-free on the R_2-R_1 plot may also be cloud-free. To allow for this, all pixels that lie within 0.67 standard errors of the line in Figure 2.5e (corresponding to 50% probability for a Gaussian distribution) are also assumed to be cloud-free, provided that their value of R_2 is not more than 0.01 greater than the value on the line with the same value of R_2-R_1 (Figure 2.5f). This step, though somewhat arbitrary, contains something of the approach of the clustering methods (e.g., Simmer et al. 1982; Desbois et al. 1982) which group together pixels with a certain probability of having common characteristics.

It is appropriate at this point to compare this method with the method of England and Hunt (1985) that is also designed to solve the problem of inhomogenous backgrounds. The basis of the England and Hunt method is the setting of thresholds in the visible channel which are adjusted by reference to the mean infrared radiance of the various surface and cloud types. However, consideration of the R_2-R_1 plots (Figures 2.2-2.4) for complex backgrounds demonstrates that there can be substantial overlap in the values of R_2 for clear and cloud-contami-

nated pixels and that this overlap will also be present in R_1. The use of the two solar radiation channels available on the AVHRR alleviates this problem.

2.4 Application to Cloud Cover Estimation

Although, as was pointed out earlier, identification of cloud-free pixels has many applications, for the purposes of illustrating the potential of the present method, an example of its application to the spatial coherence method (SCM) of determining cloud amount (Coakley and Bretherton 1982) is presented.

The essence of the SCM is illustrated in plots of the local standard deviation of I_4 of small (2 x 2) arrays of pixels plotted against the mean value of I_4 of the array. Characteristically, the plot has the form of an arch with clusters of pixels at each foot of the arch (i.e., with small local standard deviation) identifying completely clear and completely cloudy pixels. The partial cloud cover of a pixel in the body of the arch is found by linear interpolation of I_4 between the clear and overcast values.

The SCM will run into trouble for complicated surfaces with varying 11 μm radiance, especially if both water and land are present. Figure 2.6a shows the arch plot for a scene over northern Ontario. Rather than a single arch, there is a double arch which is normally characteristic of a double cloud layer (see Figure 2 of Coakley and Baldwin [1984]). In fact, when R_1 and R_2 are used to identify the cloud-free pixels (Figure 2.6b), it is seen that the two warmer feet

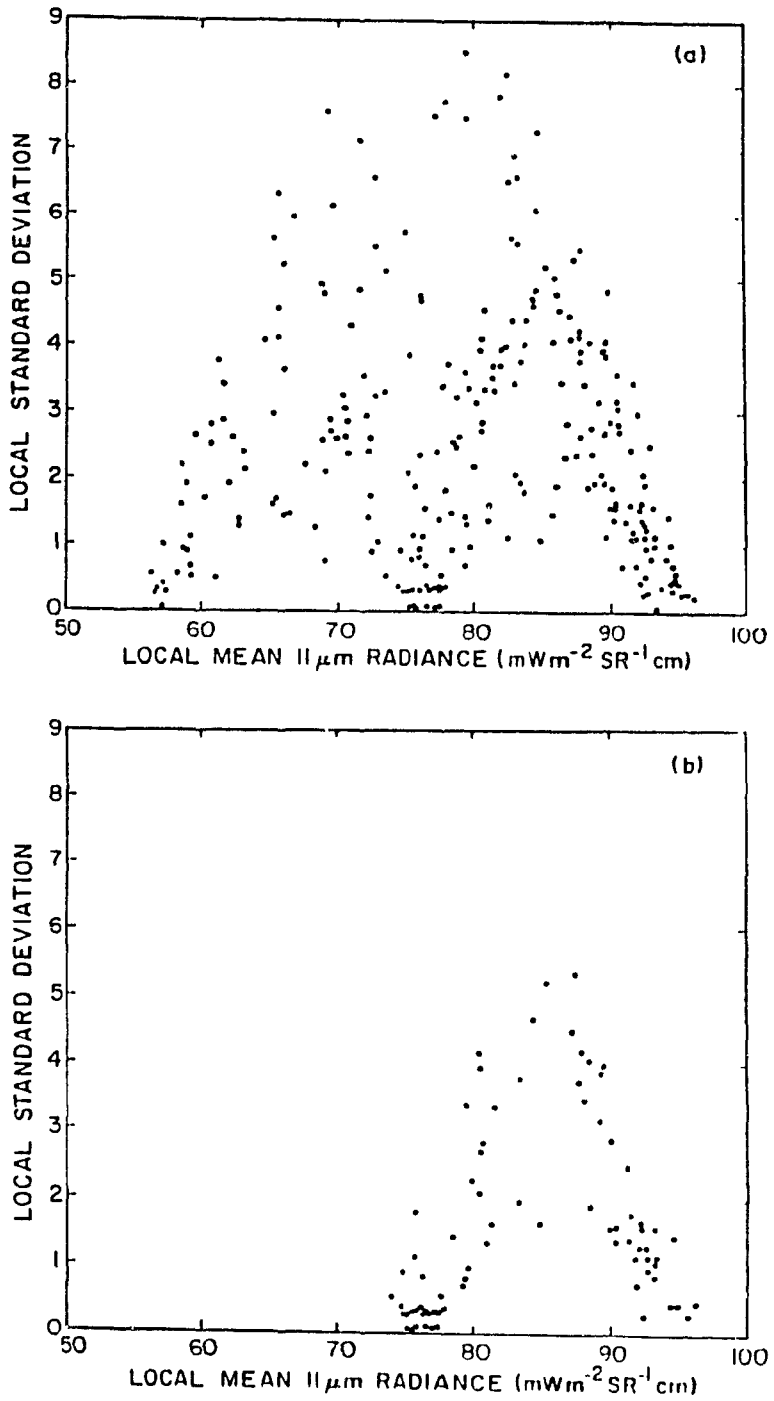

Figure 2.6. (a) Local standard deviation of the channel 4 radiance against the local mean radiance of 2 X 2 arrays for a scene over northern Ontario. (b) Same as figure 2.6a, but only for those pixels that are identified as being cloud-free on the basis of the procedure illustrated in Figure 2.5.

both correspond to cloud-free scenes, the warmer of the two corresponding to ground and the cooler to lakes. The coldest foot arises from a single, low-cloud layer.

Furthermore, in such cases, even when the two clear feet are correctly identified, application of the SCM may lead to large errors in cloud amount estimates because of the large variation in the clear-sky values of I_4. However, by using an equivalent argument to that invoked to define the variable threshold value of I_4 for each pixel that was discussed in section 3, the range of possible values of I_4 of the clear pixels that could be associated with a particular partially cloudy pixel is reduced. In this case, the value of I_4 to be used for the clear radiance when computing the cloud cover of a particular pixel is the mean value of I_4 of all clear pixels that lie above and to the left of the pixel in question on the R_2-R_1 plot. This procedure will usually restrict the uncertainty in the appropriate value of I_4 to be used in the interpolation formula to determine the partial cloud cover of each pixel.

In section 3.32, a much simpler version of this method is used for cloud detection and cloud amount estimation in high latitudes, when the backgound consists of land, or land and ice.

2.5. Discussion

The automatic identification of cloud-free regions from satellite data has many applications, and to this end, a variety of techniques have previously been used. Essentially all of these techniques work

best when the surface is uniform, and they become less reliable when the surface becomes more complex, such as is the case for coastal regions and regions that contain both land and lakes. The method described here takes advantage of a simple pattern in the two-dimensional histogram of the reflectivities in channels 1 and 2 of the AVHRR (displayed in the form of an R_2-R_1 plot) that is present for cloud-free scenes that contain vegetated surfaces or land and water surfaces. For these types of surfaces a linear arrangement of points was always observed. That the points should lie along a band is understandable in terms of the surface being composed of a linear combination of varying proportions of two surface types with different reflection properties. To the extent that the different surface types also have different temperatures, such as is often the case for water and adjacent land, the thermal radiance, I_4, will correlate with R_2-R_1.

Exploiting these ideas, we have developed a technique that identifies cloud-free pixels in circumstances where previously proposed techniques have been least reliable. The method is readily automated and may be combined with other techniques that may be more appropriate over ocean backgrounds. For applications in which cloud amount is determined by interpolating the measured radiance between clear- and cloudy-sky radiances, the method described here may be simply extended, as described in section 4, to provide narrower bounds on the clear-sky radiance associated with each pixel.

When there is considerable specular reflection from the sun (sunglint), the arrangement of cloud-free pixels is destroyed. But as we can predict when and where this error will occur we can avoid analysing data associated with sunglint.

CHAPTER 3

3.1 Arctic Environment

The Arctic region is covered by polar orbiting satellites, and GAC data taken by NOAA7 during the first week of July 1984 were distributed among the various research groups investigating the problem of cloud identification above these areas. Higher resolution LAC data were also available for a satellite orbit.

Before attempting to identify cloud-free and cloudy radiances above Arctic regions and to estimate cloud amounts, it is worth noting some of the characteristics of the region.

In Figure 3.1 where the geography of the Arctic region is given, we observe extended coast lines. They contain an area where the principles of the previously presented method of distinguishing clear from cloudy areas may be applied. During the summer most of the coast lines are generally ice-free, as the sea-ice retreats northward. But during the winter the sea-ice greatly increases and the sea freezes, except for part of the Norwegian and the Barents Sea where the Gulf Stream keeps large areas open in all seasons.

The altitude of the land is generally low, and during the short Arctic summer it is mainly covered by tundra vegetation. There is a remarkable exception to this rule. The interior of Greenland contains mountains with a maximum altitude of 3700 m and is covered by snow hardened with age. Greenland is a cold source in a cold region and it is relatively sunny by the standards of its latitude (Scorer 1988).

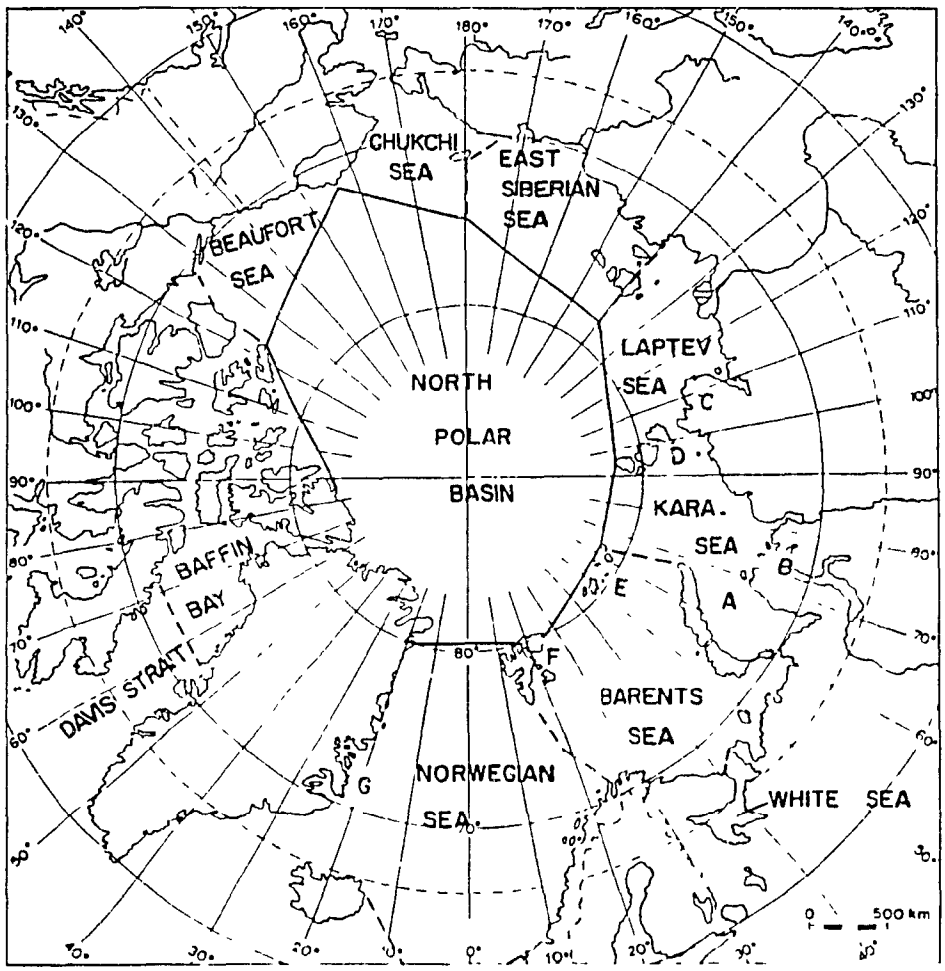

Figure 3.1. Map of the Arctic regions and the Arctic seas. Letter a, denotes Novaya Zemlya, b Obskaya Guba, c Taymyr Peninsula, d Severnaya Zemlya, e Franz Zoseph Land, f Spitsbergen island, g Scoresbysund Fjord (Vowinckel and Orvig).

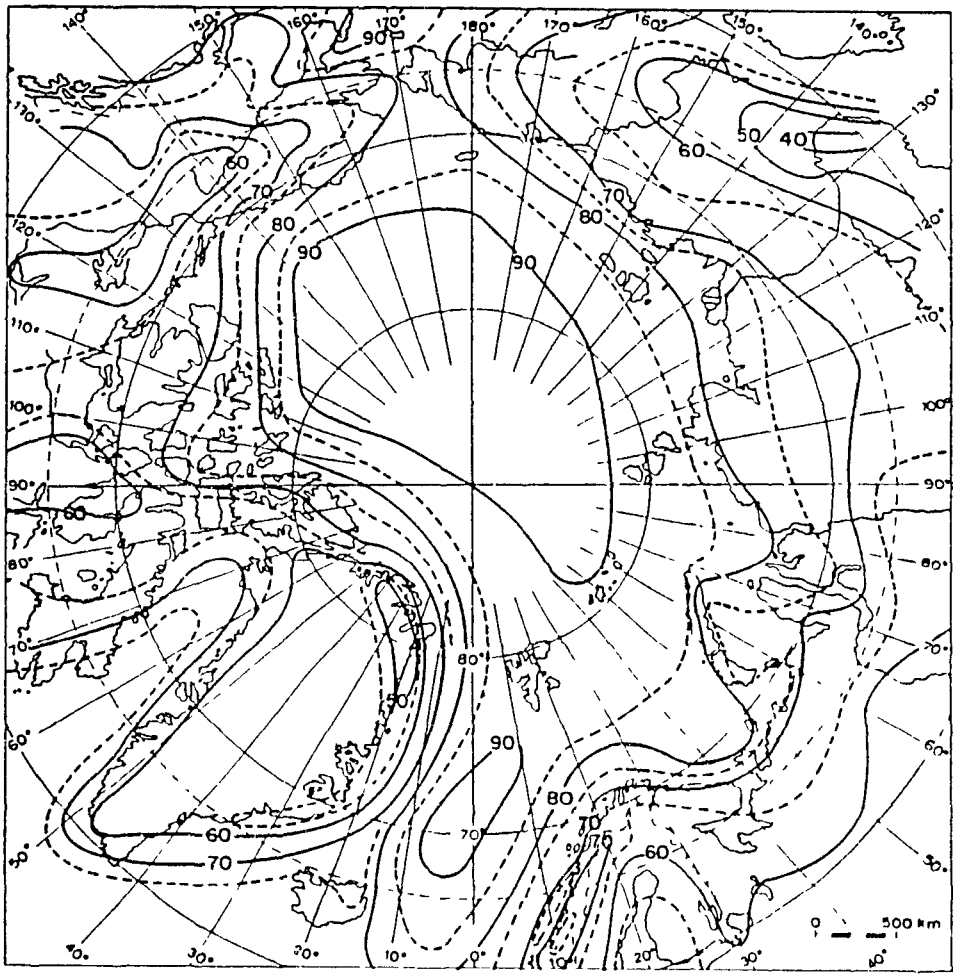

Figure 3.2. Mean cloud amount (%) in July (Vowinckel and Orvig)

The cloud cover is greater in summer than in winter. In Figure 3.2 we present the average cloud cover above the Arctic for the month of July (Vowinckel and Orvig 1970). The most frequent cloud types during the summer are altocumulus and altostratus in the Norwegian Sea, and stratus in the Polar Ocean. Clouds in the Polar Ocean are uniform, and extend as large sheets over much wider areas than other clouds. The water content of these clouds shows a profound decrease from the coast towards the Pole (Vowinckel and Orvig, 1970).

3.2 Identification of Clouds above Arctic Regions

The Arctic region provides an unfavorable situation for the identification of clouds. This is less so during the summer when the snow and ice melt, but the increase in the variety of the surface types that are encountered weakens this advantage.

The effort to identify clouds above the Arctic region is concentrated in the following two directions:

a) correct identification of the surface conditions;

b) organisation of the information extracted by the various channels of the AVHRR in order to optimize the detectability of clouds for the particular surface conditions that were previously identified.

During the Arctic summer, large surface areas have temperatures that are very close to $0^{o}C$, and therefore clouds would have to have temperatures considerably colder than the surface in order to be fully glaciated. Water drops inside clouds are strong reflectors in channel 3, while ocean- and ice-covered surfaces have very low reflectivity in

this channel (Raschke 1987). This difference in reflectivities makes the identification of low and medium clouds above ice and ocean background possible (Kidder and Wu 1984; Tanaka et al. 1984; Raschke 1987).

The plot R_2-R_1 can be used for the identification of clouds that are not necessarily low, but are relatively thick in the sense that they exhibit R_2-R_1 values moderately negative or close to 0 when above ice background, and have R_2 reflectivities higher than around 0.3, regardless of the underlying surface. In this plot, land, ocean, and ice covered surfaces have characteristic signatures, as we shall see in section 3.21. If ice surfaces are not present in the scene, then the required R_2 reflectivities for the cloud identification are even lower. The use of an R_2-R_1 plot for cloud identification does not require any a priori assumptions concerning the cloud microphysics, the cloud top temperature, or the altitude of the cloud.

Cirrus clouds may be poor reflectors in channels 1 and 2. They are also poor reflectors in channel 3, because they are fully glaciated. But as they are much colder than the surface and provided that they are not very thin, have large emissivities, so channel 4 can be used for their identification.

In principle, the whole procedure can be thought of as a three-step process. If a pixel is found cloudy by any of the three processes, it will be assumed to be overcast. Otherwise it will be cloud free.

Section 3.21 will explain how channels 1 and 2 are used.

Section 3.22 will examine the influence of atmospheric water vapor on the IR channels.

Section 3.23 will discuss the role and the limitations of channel 3.

Section 3.24 is concerned with channel 4 and channel 5.

3.21 Clouds and Underlying Surfaces: Plot R_2-R_1

The diagram composed by R_2-R_1 as vertical axis and R_2 as horizontal axis has been used in order to distinguish between vegetated land, water, and clouds (Sakellariou and Leighton 1988). It has been found that vegetated land exhibits positive R_2-R_1 values, roughly proportional to R_2 reflectivity. Positive R_2-R_1 values are also expected for bare soils, while for water surfaces the albedo is small, and for solar zenith angle less than about 70 degrees, R_2-R_1 will be small and negative. Theoretical calculations (Welch at al. 1984) and observations (Twomey and Cocks 1982) yield that thick clouds would be expected to be characterized by small negative values of R_2-R_1, much smaller than those of snow in absolute magnitude (Arking 1986), but with R_2 larger than those of water.

Snow- or ice-covered surfaces should be distinguished by R_2-R_1 values that are less than the corresponding values for clouds, and by their large R_2 reflectivity. Measurements taken from NOAA6 and presented by Dozier et al. (1981) show that R_2-R_1 values can be as small as -0.2 for R_2 = 0.7 above snow covered ice surface. His theoretical calculations presented in the form of the R_2-R_1 plot in Figure 3.3 suggest that R_2-R_1 is always less than -0.06 above snow. Also R_2-R_1 decreases with increasing grain radii, and this implies that it is possible to distinguish bare ice from clouds on the basis of their reflectivities in channels 1 and 2. This was pointed out by Arking

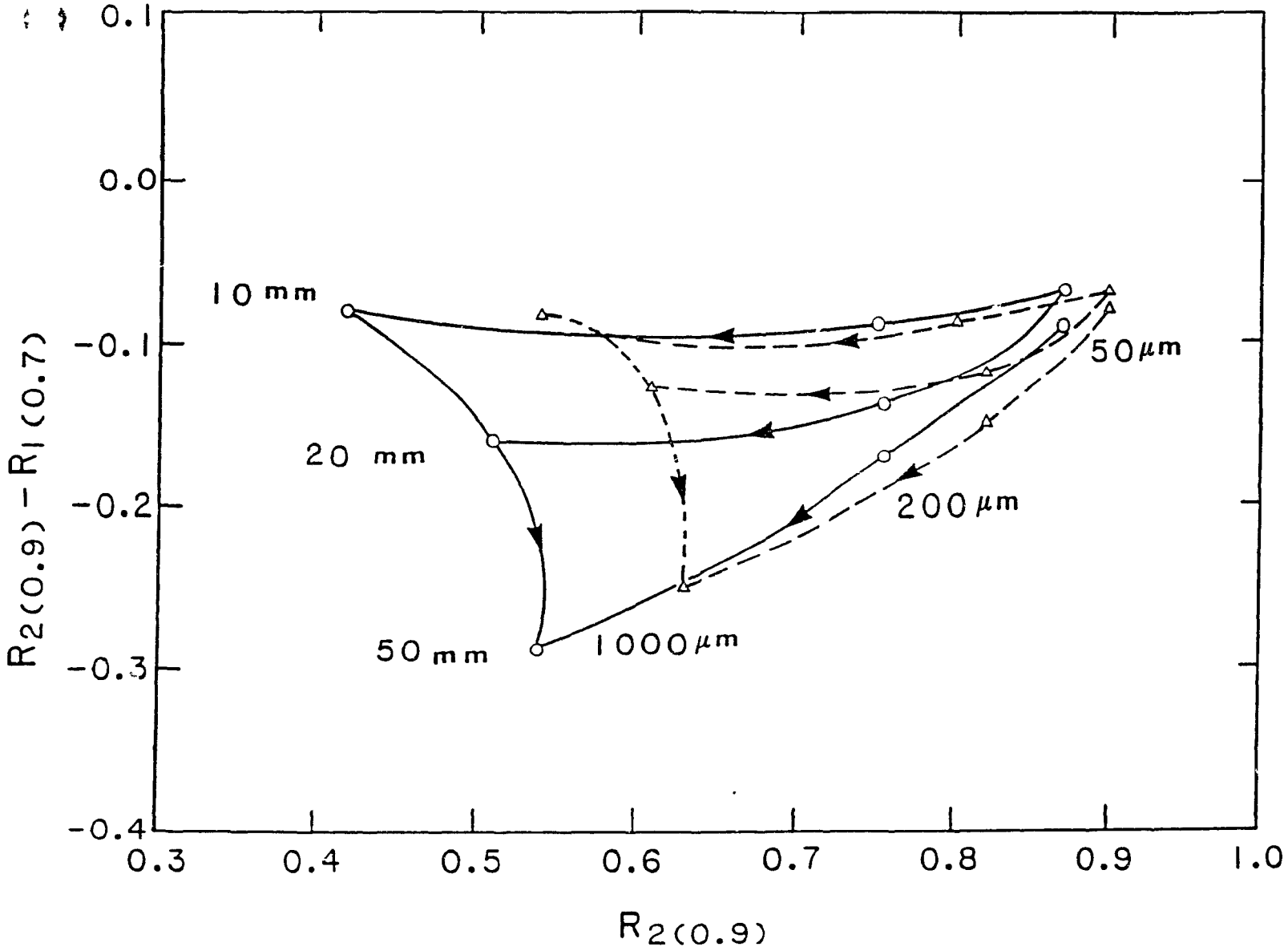

Figure 3.3. Differences in 0.7 and 0.9μm reflectivity, as a function of 0.9μm reflectivity for different snow grain radius (50μm, 200μm and 1000μm) or snow water equivalence (10mm, 20mm and 50 mm) and for solar zenith angles 30^{o} (o) and 60^{o} (Δ).

(1987). According to Raschke (1987) the R_2-R_1 values range from -0.03 to -0.07 for clouds, from -0.11 to -0.15 for sea-ice, from -0.06 to -0.15 for clouds above sea-ice, and from -0.09 to -0.15 for snow-covered surfaces.

In Figure 3.4, the letters C, T, S and I, show schematically the expected position of pixels covered by coniferous forest (C), tundra vegetation (T), sea or lake (S), and ice (I). The arrows show how these pixels change position: C→C', T→T', I→I' as a result of a snowfall, and S→S' as a result of freezing water. The distance T→T' is much greater than C→C', the reason being that coniferous forest has a much greater surface roughness than tundra vegetation, and therefore the same amount of snowfall results in much less snow fraction for the coniferous forest (Briegleb and Ramanathan 1982).

Observed areas composed by different surface types exhibit a mixture of characteristics of each particular type. In the case of only two different types, the outgoing radiance I will be

$$I = (1-f)I_1 + fI_2 \tag{3.1}$$

where f is the fraction of the pixel covered by surface type 2 with radiance I_2, and I_1 is the outgoing radiance from surface type 1. In the plot R_2-R_1 when type 1 represents land, and type 2 represents ice, it is possible to mistake a cloud-free pixel for a pixel covered by cloud. The same thing may happen if one or both of these two surface types contain a snow fraction as well. Help from channels 3, 4 and 5 will be needed in order to resolve the situation.

To show how the appearance of the R_2-R_1 plot changes drastically

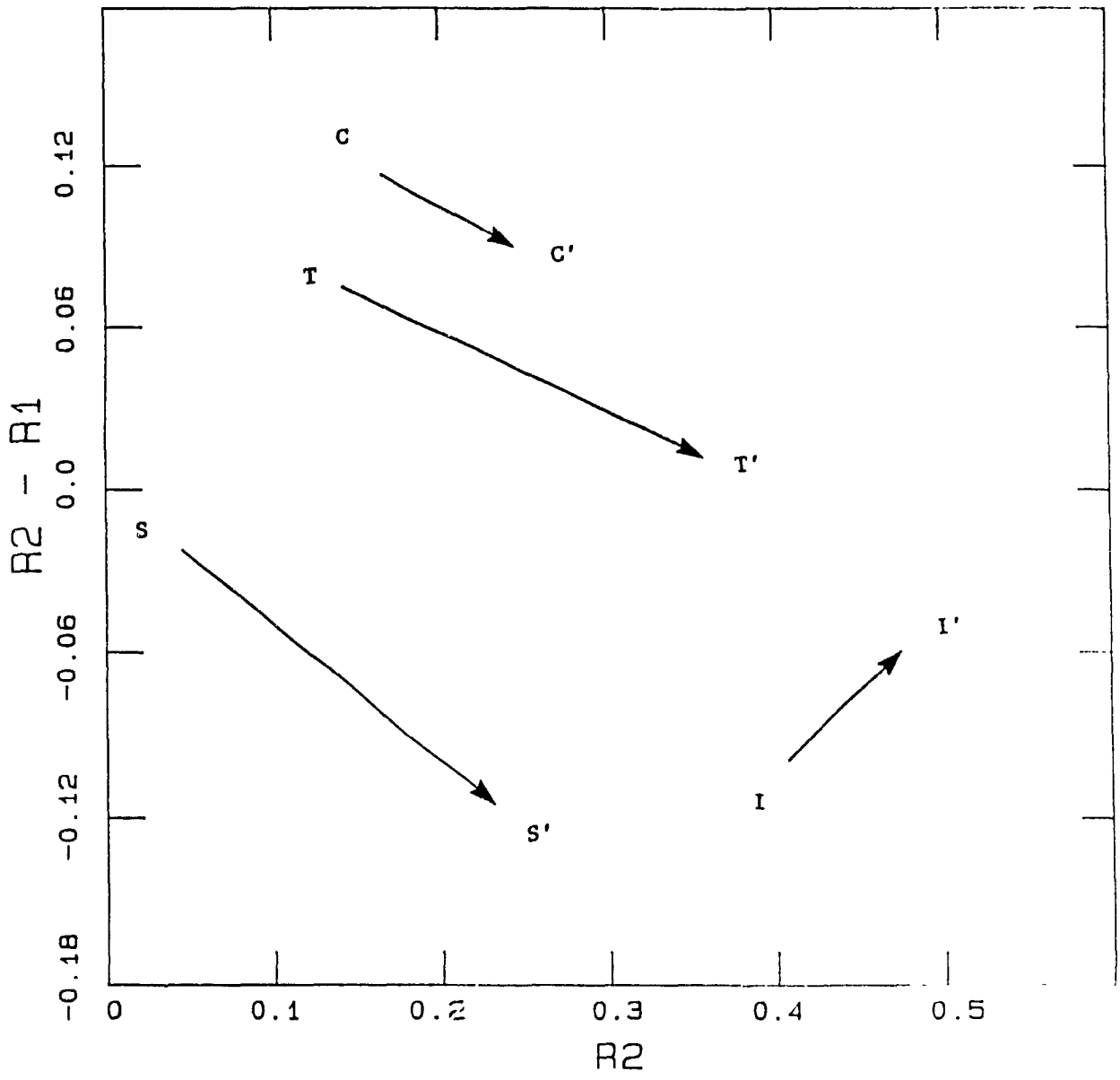

Figure 3.4. Schematic presentation of the effect of snowfall on coniferous forest (C), tundra (T), sea-ice (I) and of the formation of ice on a water covered surface (S).

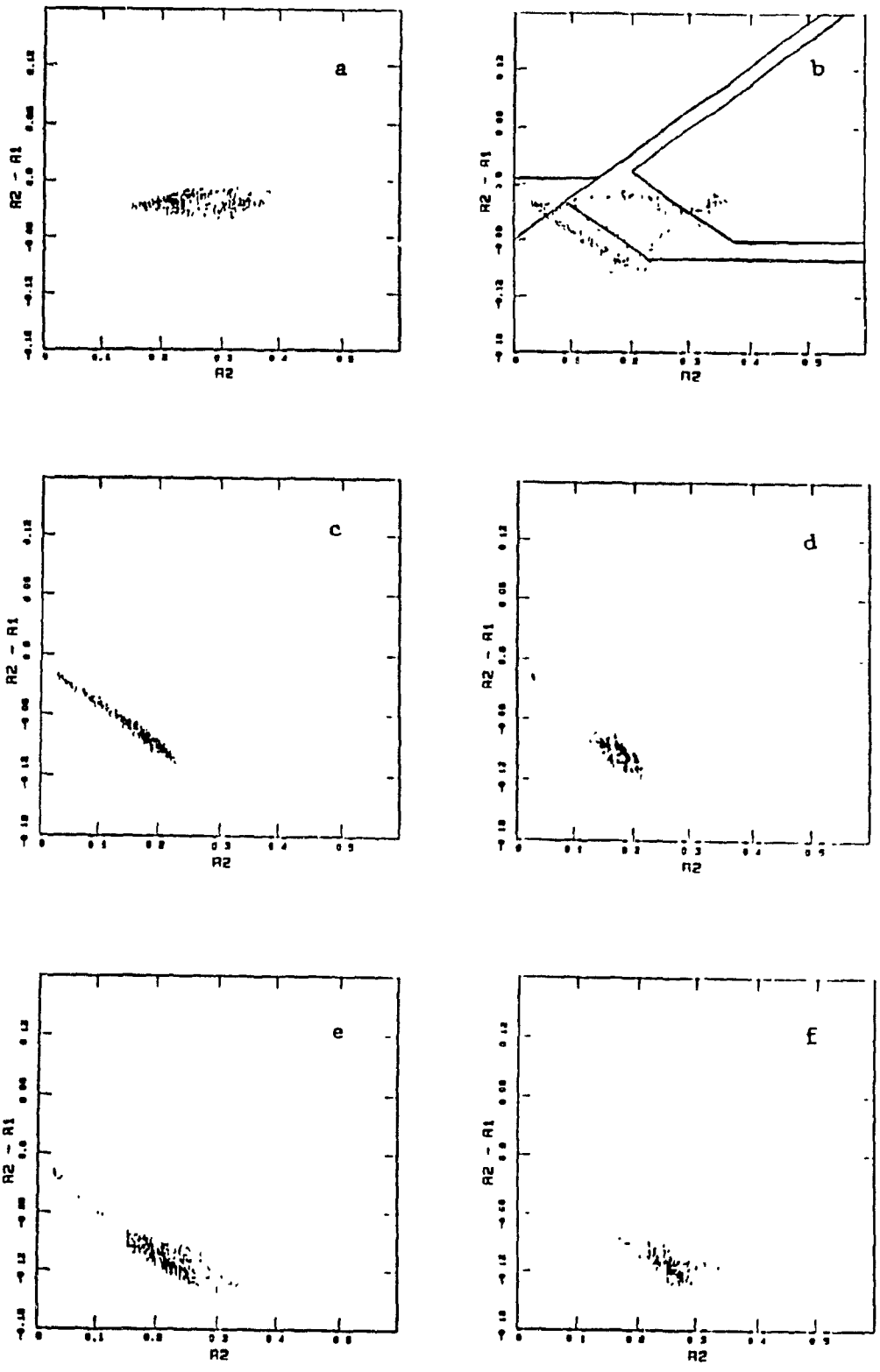

Figure 3.5.

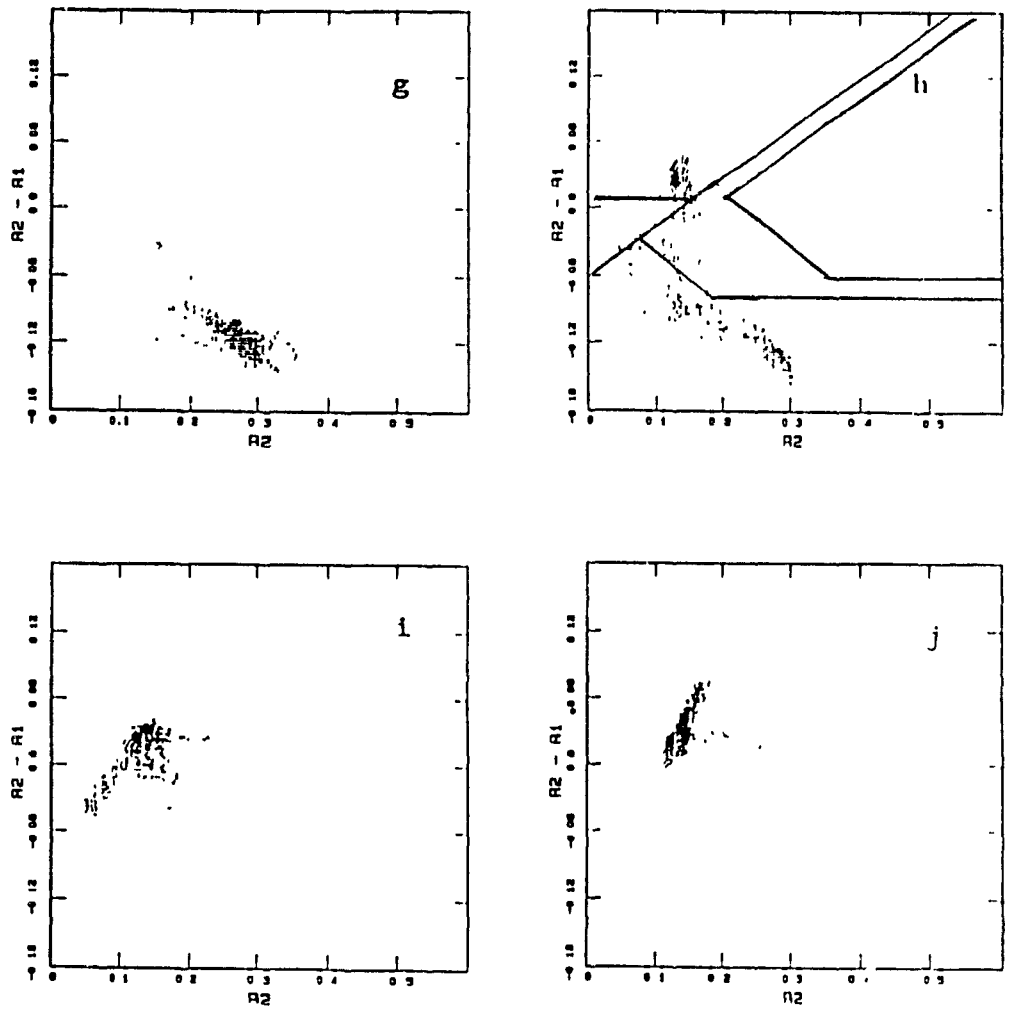

Figure 3.5. R_2-R_1 plots for ten data sets 140X140 km^2 each along the satellite scan direction. The exact location of each data set is indicated in Figure 3.6. The underlying surface change from sea and sea-ice (a), to land (j).

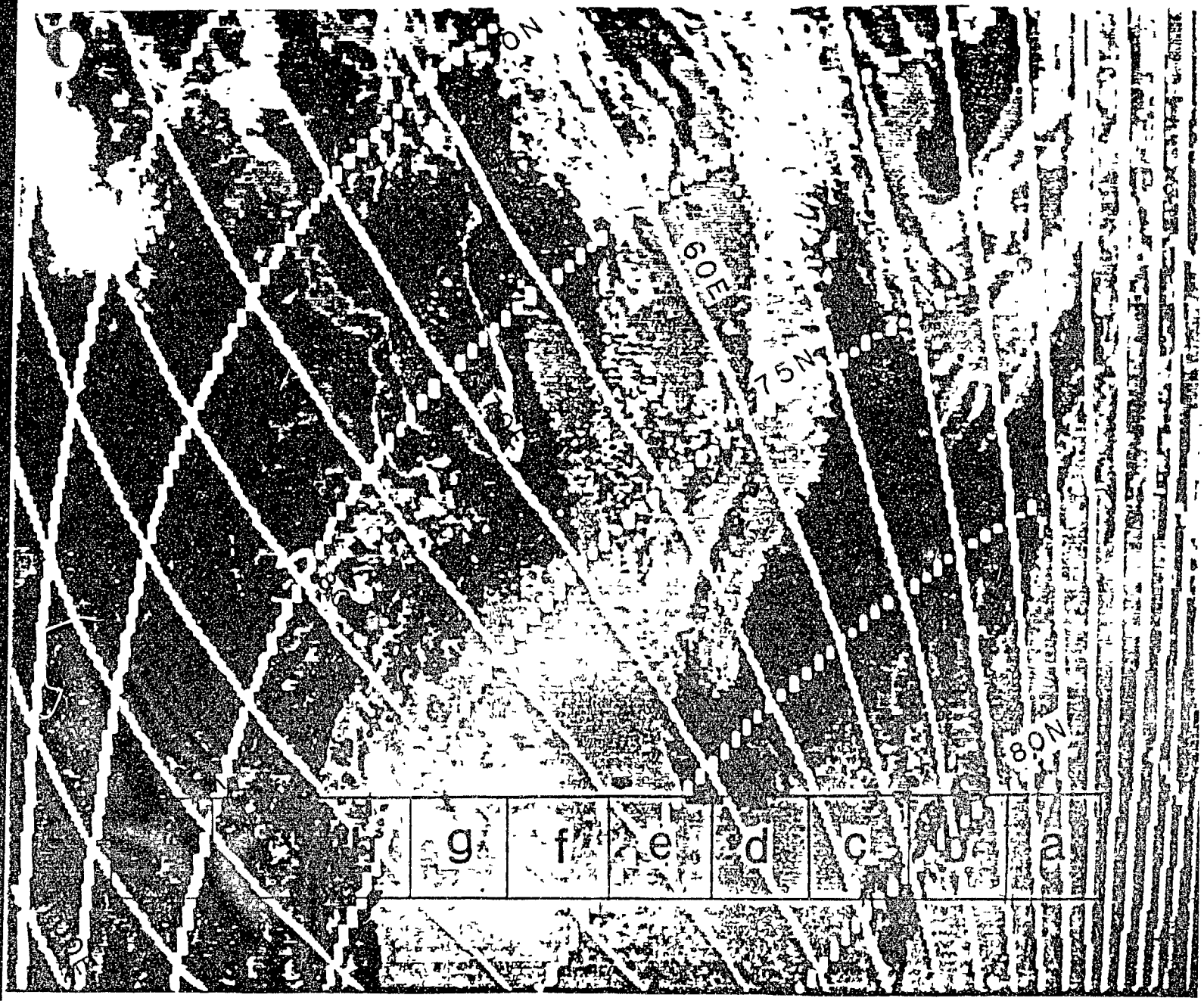

Figure 3.6. Visible image of part of the 1st orbit of July 1, 1984. The squares with the letter inside, denote the exact position of the data set named with the same letter in Figure 3.5.

as we proceed from cloud covered areas towards a mixture of ocean and ice, and finally land, we present a sequence of ten such plots (Figures 3.5a, to 3.5j). These plots correspond to a sequence of ten scenes, 34 X 34 pixels each. The total area covered extends from the Arctic ocean to Siberia, and its visible image is presented in Figure 3.6. The areas covered by the various data sets that were used in order to create the plots presented in Figures 3.5a to 3.5j are also marked in Figure 3.6.

The data were taken by the NOAA7 satellite during its first orbit of July 1, 1984. The orbit was analysed both manually and automatically, and both analyses agree that a cloud band is present in the data set used in Figure 3.5a. As we go southeastward, in Figures 3.5c, 3.5d, 3.5e, 3.5f and 3.5g, we have mostly sea-ice covered pixels. In Figures 3.5i, and 3.5j, we are over Siberia, and we notice the presence of a cluster of pixels with positive R_2-R_1 that identifies land.

The data used in Figure 3.5b are from a scene between that of the cloud-covered scene of Figure 3.5a and the mostly cloud-free scene consisting of ocean and sea-ice of Figure 3 5c. Therefore in Figure 3.5b, we have some overcast pixels, and some cloud-free pixels composed of ocean or ice, and partly cloudy pixels. A visual comparison between Figures 3.5a and 3.5c, and Figure 3.5b enables us to detect the various types of pixels in Figure 3.5b. The set of line segments that exists in Figures 3.5b, and 3.5h, will be explained in section 3.31.

The data used in Figure 3.5h are from a scene between one composed primarily of sea-ice (Figure 3.5g), and one composed of land-covered pixels (Figure 3 5i). Therefore Figure 3.5h contains land and sea-ice covered pixels, and pixels containing fractions of both as well. Again

a visual comparison between Figures 3.5g and 3.5i, and Figure 3.5h, yields the identification of the surface types that are present in Figure 3.5h. Very few pixels in Figure 3.5h have reflectivity characteristics that tend towards those exhibited by water-covered pixels. This is consistent with the fact that the Siberian coast around the area where the data were taken is surrounded by fast ice.

Sea-ice can exhibit a large range of reflectivities depending mainly on its age, its thickness, and the air trapped in the interior of the ice. In Figures 3.7a and 3.7b, we present R_2-R_1 plots that correspond to a region of thick sea-ice (Figure 3.7a), and to a region where clouds above thick sea-ice exist (Figure 3.7b). We notice that despite the fact that the sea-ice now has higher R_2 reflectivity than in Figure 3.5g, the presence of clouds in Figure 3.7b is well marked.

3.22 Atmospheric Effects at the Infrared Channels

The last three channels of the AVHRR are centered at 3.7, 10.8, and 12 μm. The 10.8 and 12 μm channels detect emitted radiation whereas the 3.7 μm channel detects both emitted and reflected solar radiation. All radiances obtained by the satellite at these channels contain some contributions from the atmosphere other than those due to clouds, and these are collectively known as the atmospheric effect. This effect depends on the atmospheric structure and varies with time and location. It is the primary obstacle to accurate surface temperature measurements by the AVHRR (Tanaka et al. 1984). It also weakens and obscures characteristic surface signatures that may be used for the surface-cloud

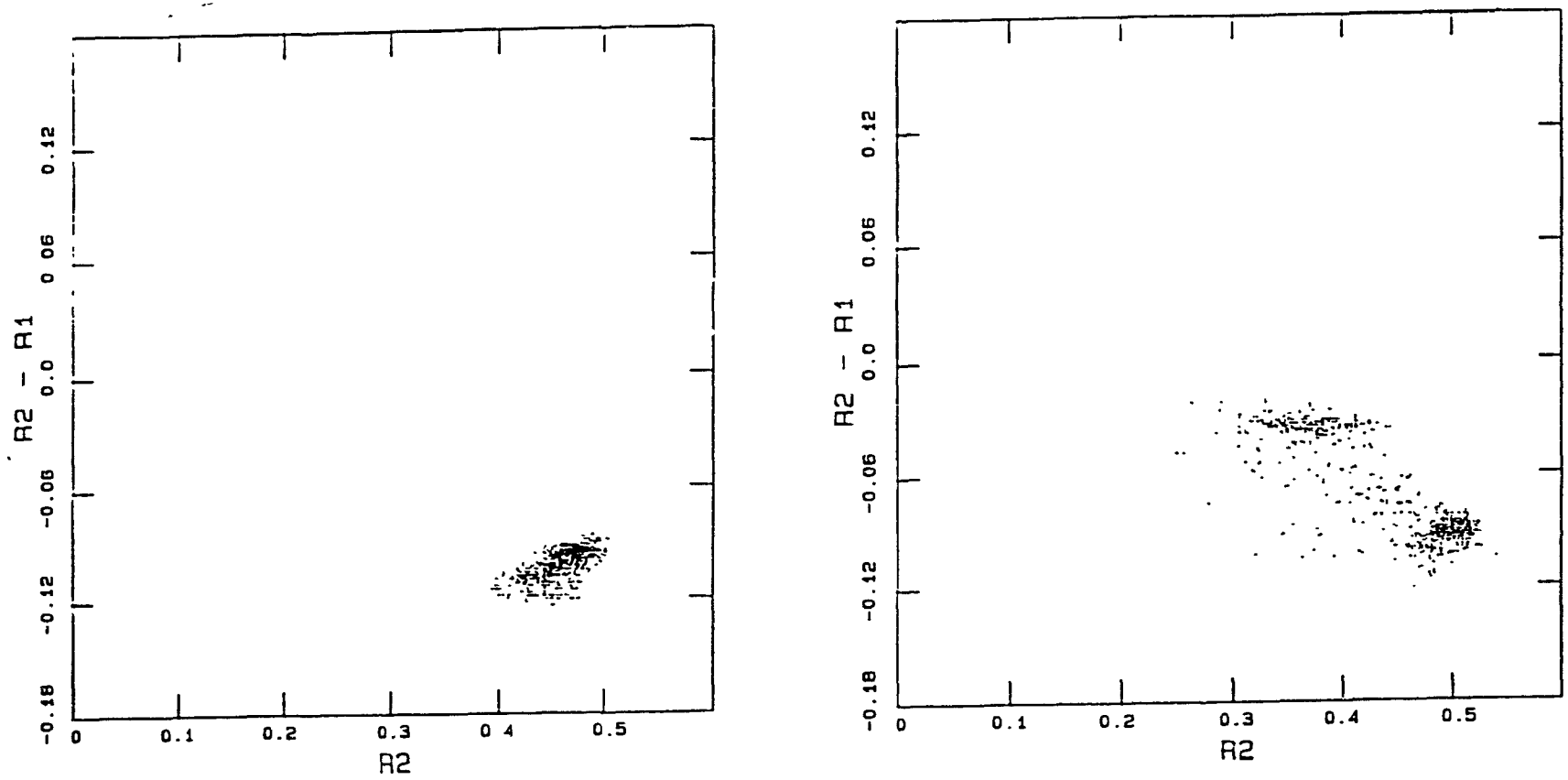

Figure 3.7. R_2-R_1 plots for a) sea-ice under thin clouds, b) sea-ice under thick clouds.

separation (e.g., differences among radiative temperatures obtained by different IR channels).

This effect is dominated by water vapor in the troposphere that exhibits high temporal and spatial variability.

Takashima and Takayama (1986) reported the atmospheric transmittance decreases with increasing channel number, and takes maximum values for radiation in channel 3. Tanaka et al. (1985) have also reported that the influence of water vapor on the transmittance is greatest in channel 5, and smallest in channel 3.

The total radiation received at the satellite is the sum of the reflected solar radiation, the radiation emitted by the earth's surface, and the radiation emitted by the atmosphere. For channels 4 and 5, the first term is neglected.

In the following sections we will see how this discussion applies to particular channels.

3.23 Channel 3

This channel lies in the tail of the incoming solar radiation spectrum, and in the shortwave edge of the Planck function for terrestrial temperatures. Consequently, during the night it senses only emitted radiation but both emitted and reflected radiation during the daytime. This channel was used in several studies that proved its usefulness in identifying low-level water clouds from their high 3.7 μm reflectivity. We briefly list some of these studies and their main findings.

Measured radiance is very sensitive to the phase of the cloud particles and to their average radius Arking and Childs (1985). They found that the 3.7 μm reflectivity of clouds increases with decreasing particle sizes, and that for the same particle size, reflectivity is greater for water clouds than for ice clouds. Knottenberg and Raschke (1982) subtracted the emitted part of the radiation to distinguish between water and ice clouds on the basis of their channel 3 reflectivity, using simple but unspecified assumptions. Bell and Wong (1981) found that the 3.7 μm radiative temperature of some clouds is higher than that of the sea, due to higher albedo at 3.7 μm. Tanaka et al. (1984) used the difference between the 3.7 μm and 11 μm brightness temperatures to distinguish between clouds and underlying sea or sea-ice above the Antarctic. While clouds had large brightness temperature differences (up to 45 K), difference values above sea or snow were close to zero in daytime data.

Contrast between low clouds and snow cover radiative temperature in daytime 3.7 μm data was observed by Kidder and Wu (1984) over central United States. Channel 3 reflectance was used by Allen et al. (1988) in order to distinguish between snow and clouds. They observed 2 to 4% reflectance for snow, and not less than 8% reflectance for water clouds. It should be mentioned though, that they did not take into account absorption and emission from the atmosphere, and therefore their actual reflectance values may not be truly representative of snow and clouds.

The ability to use the channel 3 reflectivity to identify low water clouds with temperature very close to that of the underlying surface makes this channel particularly useful. Because we are inter-

ested in reflected solar radiation, emitted radiation must be subtracted. Emitted radiance from a black body with temperature varying from 240 to 290 K, sensed by the satellite sensor at channels 3 and 4, was estimated. The radiances were calculated by multiplying the Planck function with the normalized response function of the radiometer, and summing over all wavelength intervals of the particular channel. A polynomial fit between 3.7 and 11 μm radiances calculated for different temperatures yields:

$$I3 = 6.841*10^{-4} - 8.851*10^{-5}I_4 + 5.6828*10^{-6}I_4^{\,2} + 4.2377*10^{-7}I_4^{\,3} - 3.0380*10^{-10}I_4^{\,4} \qquad (3.2)$$

where I_3 and I_4 refer to the radiances in channel 3 and 4 respectively. The I_4 values are derived by applying the calibration coefficients to the measured count numbers by the radiometer. It is assumed that the output of each AVHRR infrared channel count is proportional to input radiance. But as non-linearities exist, an error in the I_4 estimations is introduced. According to Brown et al. (1985) this error in channel 4 yields a difference between observed and calculated temperatures that does not exceed 0.75 K at 235 K temperature, and for the temperature range 235 to 287 K the error is even less, with 0 K at 287 K temperature. In terms of curve fitting, Equation 3.2 is accurate, but in addition to the non-linearities, we must note some other limitations as well when trying to apply this equation.

1) The emitted radiation at channel 4 reaching the satellite, also includes emission and absorption from the atmosphere. Con-

sequently, we have sources emitting at temperatures other than the surface temperature.

2) The emissivity of natural bodies at 3.7 and at 11 μm may not be the same, and may be less than 1. For water and ice surfaces though, the black-body assumption seems reasonable (less than 2% albedo; Raschke et al. 1987).

3) The reflected solar radiation at 3.7 μm from very dark natural surfaces (sea or ice) is a small part of the total radiance received at the satellite, and errors introduced by poor estimation of the emitted radiation at that wavelength may lead to large percentage albedo errors.

The transmittance in channel 5 is smaller than in channel 4, and hence using its radiance in order to remove the emitted part of the radiation in channel 3 would deteriorate the albedo estimation.

Selection of an appropriate threshold in channel 3 in order to distinguish clouds from the underlying surface is further complicated by cloud albedos that are higher around the cloud edge than in the cloud interior (Coakley and Davies 1986). Broken cloud fields also reflect more radiation than extensive and unbroken ones (Coakley and Davies 1986). Errors also arise from the fact that by setting a threshold, we do not allow for partially filled fields of view (Coakley and Bretherton 1982).

In the present study, we use a threshold of 4% albedo at 3.7 μm based on empirical considerations. This means that we observed the changes in the analysed cloud field as we progressively lowered the channel 3 threshold, and chose the threshold value that would produce, on average, the most reasonable cloud fields. For example, at thre-

shold values lower than 2%, the cloud amount increased disproportionately and the large-scale cloud patterns were obscured. Water clouds exhibit albedos largely exceeding our threshold, but ice clouds may escape detection (Allen et al. 1988; Raschke et al. 1987). To show the effect of the selected channel 3 threshold on cloud contaminated scenes, we present in Figures 3.8a and 3.8b the same data sets as in Figures 3.5b and 3.5e respectively, but all pixels that exceeded the aforementioned threshold have been excluded from Figures 3.8a and 3.8b. In Figure 3.8a, almost all pixels that are associated with the presence of cloud in Figure 3.5b have been omitted. Differences between Figures 3.5e where the presence of cloudy pixels is not marked in the R_2-R_1 plot, and Figure 3.8b are much less significant than those between Figures 3.5b and 3.8a. It yields that the selected threshold and the R_2-R_1 plot are in close agreement regarding the cloud contaminated pixels.

3.24 Channels 4 and 5

Channel 4 of the AVHRR/1 on board the first NOAA satellites had a central wavelength at 11 μm and covered a range from 10.5 to 11.5 μm (Lauritson et al 1979). It was replaced in more recent spacecraft (NOAA7 included) by two channels: one (number 4) that covers on average the 10.3 to 11.3 wavelength interval, and another (number 5) targeted towards the 11.5 to 12 5 μm interval. This modification was intended to further enhance the sea-surface measurement in the tropics (Barnes and Smallwood 1982).

The new configuration known as the split channel adds confidence

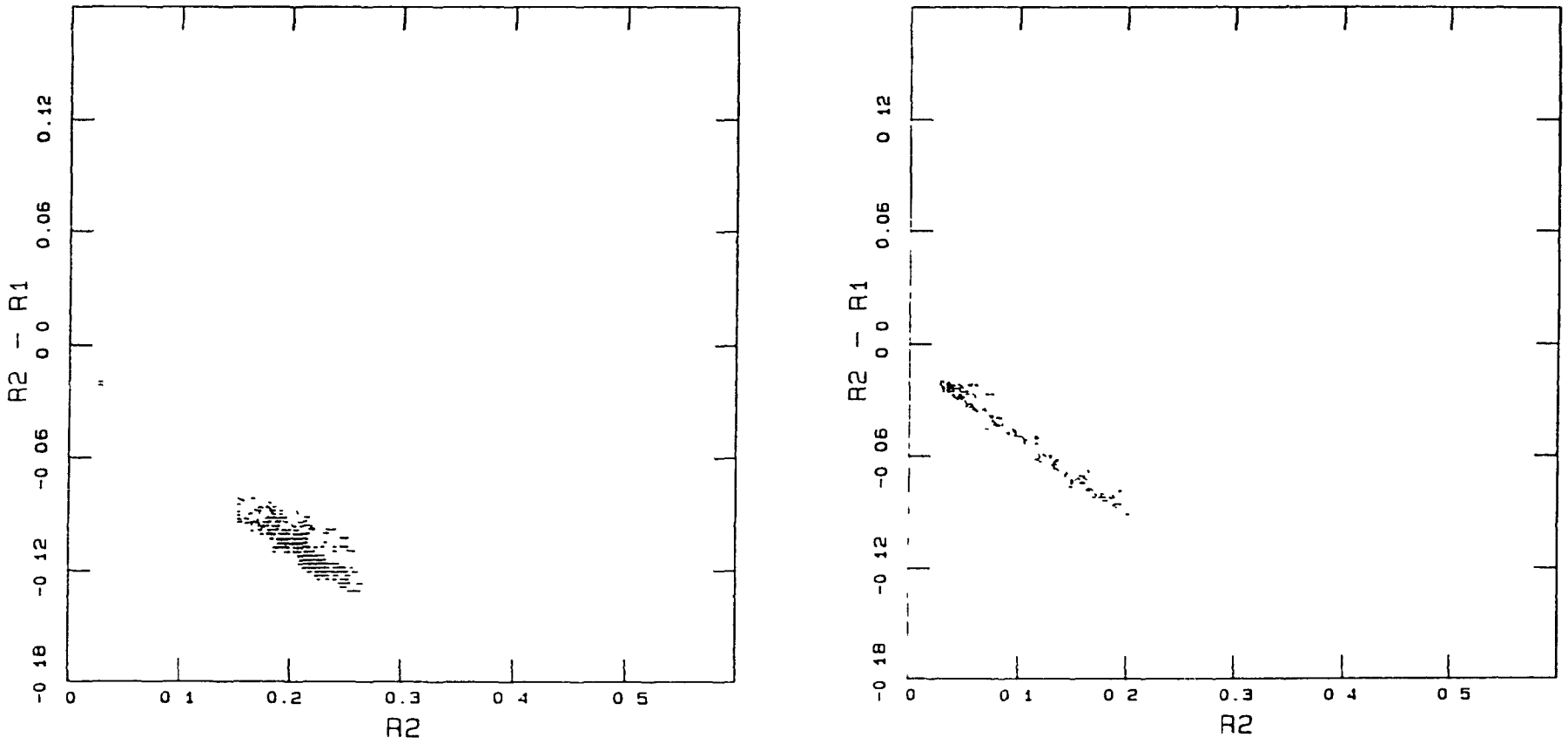

Figure 38 Pixels with channel 3 reflectivity less than 4%, for the data sets presented a) in Figures 3 5b and b) 3 5e

in removing the radiant contributions from water vapor when determining the sea- surface temperature. We will mention shortly some of its applications as far as cloud detection and cloud characteristics are concerned; subsequently, we will present the essential information that is required when trying to employ the split channel for the same purposes.

Inoue (1985) used the split channel for the retrieval of cloud temperature and emissivity for semi-transparent cirrus clouds above ocean. Semi-transparent cirrus brightness temperature difference between channel 4 and channel 5 (T_4-T_5) was considerably higher than the observed differences above ocean and thick clouds. The same observation combined with the channel 4 brightness temperature improved the detection of convective rainfall areas imbedded in a larger cloud field (Inoue 1987) Yamanouchi et al. (1985) detected thin clouds above the Antarctic as they exhibited T_4-T_5 values larger than the underlying surface, and they also mentioned that all clouds may not be detected that way (e.g., if they have the same temperature as the surface). The same authors also presented information on how the T_4-T_5 varies as a function of temperature and viewing angle (Yamanouchi et al.1987).

The split channel yields the aforementioned results by making use of the T_4-T_5 values. These values contain contributions from a variety of factors that are listed below.

1) Atmospheric Effect. Water vapor absorbs and emits more at 12 than at 11 μm. Consequently channel 5 receives larger contributions from the atmosphere than channel 4, and finally we have T_4-T_5 other than zero. The atmospheric effect becomes less significant in the polar

regions, especially during the polar winter, because the atmosphere cannot sustain large amounts of water vapor. The example of mid-latitude winter atmosphere in Section 3.22 gives a T_4-T_5 value of 0.7 K for the satellite overhead. The value increases with increasing satellite zenith angle.

2) Response to the Presence of Clouds. Emission and transmission properties of clouds differ in the two wavelengths of the split window Olesen and Grasl (1985) found that their models of stratus, cumulus and cirrus clouds absorb more strongly at 12 than at 11 μm. Liou (1974) has shown that the optical properties of his model cirrus cloud composed of ice cylinders varied between 8-11 μm, and 11.5-12 μm. Inoue (1985) has derived an empirical relationship between the effective emissivity at channel 5, E_5, and the effective emissivity at channel 4, E_4, for semitransparent cirrus.

$$E_5 = 1 - (1-E_4)^{1.08} \qquad (3.3)$$

This implies that E_5 is greater than E_4. This is not the case for thick clouds. Thick clouds have a T_4-T_5 of almost zero because they are optically thick and the amount of water vapor above the cloud top is limited. But as they become progressively thinner towards their edges, T_4-T_5 may provide the tool for the cloud edge detection. Yamanouchi et al. (1985) have reported the detection of the cloud edge of high clouds, using T_4-T_5 values.

3) Temperature Dependence. A strong temperature dependence of T_4-T_5 with temperature for clear skies and snow-covered surface was

noticed by Yamanouchi et al. (1985). Yamanouchi et al. (1987b), tentatively attributed this dependence to the temperature dependence of the snow emissivity rather than to the non-linearity error of the AVHRR sensors. But variation of the snow emissivity with temperature is still considered to some extent uncertain (Yamanouchi et al. 1987b). The temperature variation of T_4-T_5 for a snow surface at nadir ranges from -2K at T_4 = 195K to 0 at T_4 = 230K, and reaches a maximum of about 1K at T_4 = 270 K (Yamanouchi et al. 1987b).

4) Non-Linearity Errors of AVHRR Sensors. The calibration procedure is based on a linear fit between two measurements. The first measurement is of an internal target at a temperature close to 288 K and the second is of the cold space at a temperature close to 3 K. Channels 4 and 5 are not linear, and so there is need for correction for these non-linearities. The temperature difference due to the non-linearity of the sensors for NOAA7 is generally opposite to the differences due to the temperature dependence. Its value 0.8K at T = 205 K, decreases with increasing temperature. It does not exceed absolute 0 3 K from 225 to 295 K. At warmer temperatures, its absolute value increases again, reaching 0.39 at 310.1 K measured temperature, and 15°C internal target temperature.

For the range of temperature values that are associated with snow, ice or ocean surfaces during the polar summer, this error is small relative to the others.

5) Viewing Angle Dependence. The effect of viewing angle on the infrared brightness temperature of snow has been examined by Dozier and Warren (1982). An opaque or semi-infinite medium does not transmit incident radiation. Therefore, directional emissivity and direc-

tional hemispherical reflectance are connected with the following equation:

$$E(\lambda,\mu) = 1 - R(\lambda,\mu) \tag{3.4}$$

The viewing angle $\theta=\arccos(\mu)$ is the angle from the vertical. Reflectance increases with increasing angle for snow covered surfaces (Warren 1982; Fig.15), and hence the emissivity decreases This results in a brightness temperature T_B, that is smaller than the actual temperature T. The difference over snow-covered surfaces can be expressed by the following formula proposed by Dozier and Warren (1982):

$$T_B - T = (C_0 - C_1\mu)/(1+D_1\mu) \tag{3.5}$$

Values of the coefficients C_0, C_1 and D_1 for NOAA7 AVHRR IR channels were also presented by the same authors. Yamanouchi et al. (1985; 1987b) compared T_4-T_5 values derived from NOAA7 Local Area Coverage data taken above snow-covered surfaces, with values calculated theoretically from (3.5). Observations and theory agreed that the viewing angle dependence increases with increasing viewing angle and decreasing radiative temperature. They also found that the data show this effect more strongly than is expected by the theory. It should be mentioned though, that their viewing angle estimation does not account for the Earth's curvature and so it differs from Dozier and Warren's viewing angle definition. Accounting for the Earth's curvature would bring theory and observation into closer agreement.

The viewing angle dependence problem becomes more severe over

mountainous areas, were local slopes combined with the satellite scan angle may result in even larger viewing angles. In this case the orientation of the slope along the scan line also becomes important.

6) Dependence on the Nature of the Surface. Emissivity variation with wavelength in the 10-12 μm interval may also give rise to T_4-T_5 value other than zero. Spectral emissivity curves from 7 to 13 μm show such dependences (Infrared Handbook p.3-92 to 3-95). There is no general rule concerning this dependence, except that drastic emissivity changes occur for some types of rocks. Water and ice also exhibit differences in emissivity in the split channel. For surface temperature 272 K these differences may produce a T_4-T_5 difference of 0.2 and 2.1 K for water and ice respectively (Wannamaker 1984).

The above discussion suggests that the use of T_4-T_5 to identify clouds above a certain location is subject to a large number of errors. Some of them may be avoided by using existing parameterization schemes (Yamanouchi et al. 1987b), but errors associated with the actual atmospheric structure and surface composition cannot be avoided. For that reason, the split channel will have a rather limited use in our algorithm. Its main task will be to improve the detection of cloud-free pixels. For this purpose any nominally cloud-free pixel with T_4-T_5 value exceeding a certain threshold will be excluded from initial calculations of average cloud-free channel-2 and channel-4 radiances. It will be declared cloud-free at a subsequent step if its corresponding radiances in these channels are close to the already estimated cloud-free radiances.

3.3 Description of the Algorithm

The R_2-R_1 plot is the first step in our effort to automatically classify the pixels. We obtain the reflectivity values from the satellite data. They contain one count number from 0 to 1023 per channel per pixel, and information concerning longitude, latitude and solar zenith angle for every eighth pixel across a scan line. We apply the calibration coefficients of the relevant channel to the corresponding count number and normalize the reflectance by the cosine of the solar zenith angle Normalizing the reflectivity by the solar zenithian angle becomes necessary at the present stage of the work because of the extended polar areas that will be analysed and the variation of the solar zenithian angle along the satellite orbit. Particularly large changes in solar zenith angle occur when the satellite starts the descending part of its orbit, the 'night pass".

Using this plot we tentatively assign pixels to one of the five following classes.

1) cloud-free land;

2) cloud-free ocean;

3) pixels covered by thick clouds, in the sense that these pixels have high reflectivities and R_2-R_1 values greater than -0.06;

4) ice-covered pixels that may also have a cloud fraction by thin cloud; and

5) pixels that do not belong to any of the above classes.

In subsequent tests, pixels belonging to classes 1, 2 and 4 may be attributed to classes 3 or 5, and pixels belonging to class 5 can be attributed to class 3 or 4. This initial classification is achieved by

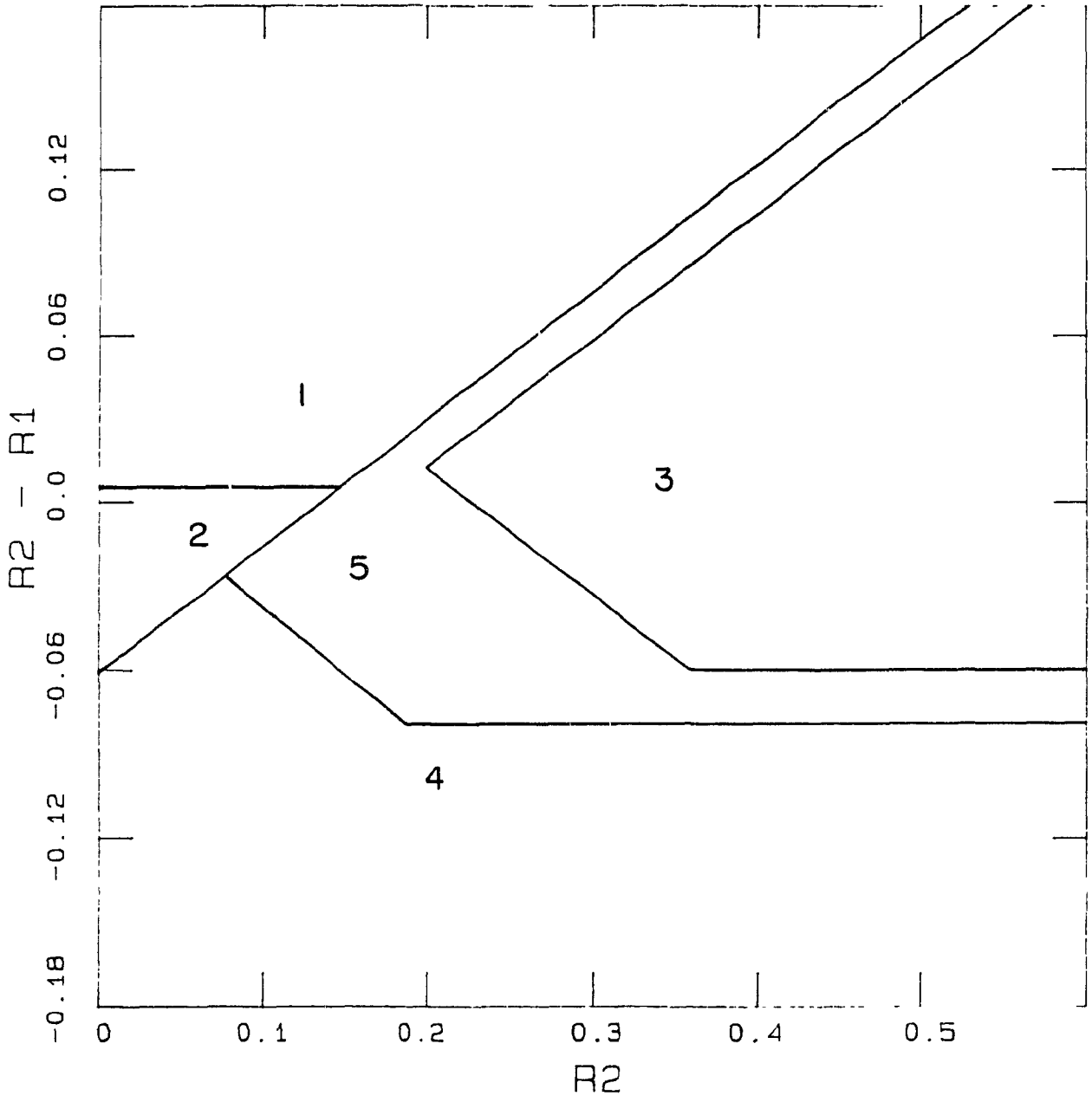

Figure 3.9. Lines separating the five classes of pixels in the R_2-R_1 plot.

separating the R_2-R_1 plot into the five domains presented in Fig. 3.9. According to the discussion in section 3.2, clouds can be distinguished from underlying surfaces by the R_2-R_1 plot. The reflectivity values of the boundaries that were used for the separation of the aforementioned five domains were obtained after some experimentation. Figures 3.5b and 3.5h serve as an example of how these boundaries can separate the five classes of pixels, and also how we were guided by the data in order to select these boundaries.

By comparing the present use of the R_2-R_1 plot to the previous one in section 2.3, we find that:

1) The present form of the R_2-R_1 plot can accommodate ice and snow covered surfaces, and therefore it can be thought of as an improvement and expansion of the previous form.

2) The line that separates pixels belonging to classes 1 and 2 from the rest in the present form is similar to a typical line formed by cloud-free pixels in the R_2-R_1 plot of the previous form adapted to higher latitudes. The slope of the line has been changed from 0 70 to 0.45 because it is influenced by chlorophyll absorption. Chlorophyll absorbs in channel 1, and vigorous vegetation increases the slope of the line. On the average, the density of the vegetation decreases poleward and so the slope has to decrease as well. The change of the intercept of the line from -0.03 to -0.06 is intended to avoid misclassification of clear pixels composed of a large water fraction and a small ice fraction as cloudy.

This line is expressed by the equation:

$$R_2 - R_1 = -0.06 + 0.45R_2 \qquad (3.6)$$

Stratiform clouds will be well removed from this line and so cloud amount estimations of stratiform cloud fields will be insensitive to the actual position of the line. Partially cloud-covered pixels will be closer to the line and may result in greater uncertainties in cloud amount estimates.

As stratiform clouds are the most common cloud type in the arctic during the summer, the resultant error in the total number of cloudy pixels above arctic regions is expected to be small, and our total cloud fraction estimation should be insensitive to the actual values of the constants used in Eq. 3.6.

The land-water boundary has been set at R_2-R_1 slightly above 0 (0.005). This value is kept constant in our program, and despite the fact that in reality land-water boundaries express R_2-R_1 values that are influenced by the solar zenith angle and land and water characteristics, it gave a good description of land-water boundaries in the satellite pictures over extended areas. Again pixels that are likely to be misclassified by the land-water boundary are those close to the boundary, as they are likely to contain large fractions of both land and water. As demonstrated by Kondratyev (1969) and supported by Figures 3.5b, 3.5h, 3.5i and 3.5j water can be easily separated from land by an R_2-R_1 threshold, provided that the solar elevation angle is greater than about 20^{o} .

Region 4 is separated from region 2 by the aforementioned line, and from region 5 by the line segments that are expressed by

$$R_2-R_1 = 0.005 - 0.45R_2 \qquad (3.7)$$

for R_2 reflectivities ranging between $0.072 < R_2 < 0.19$, and by

$$R_2 - R_1 = -0.08 \qquad (3.8)$$

for R_2 reflectivities greater than 0.19.

The first line segment is tilted because for the given range of R_2 and R_2-R_1 reflectivities, the cloud-free pixels are usually composed of various fractions of water and ice. We have already seen that ice-free water has R_2 reflectivities around 0.02 and R_2-R_1 values close to zero, while sea-ice has large R_2 reflectivities and R_2-R_1 values less than -0.06. Pixels covered by a mixture of water and ice are placed in intermediate positions between the extremes of completely ice-free water and completely water-free ice, and this creates the afore-mentioned tilt. All examined R_2-R_1 plots for clear skies where evidence from sea-ice analysis charts indicated that the background is composed of water and ice showed this pattern. Figures 3.5c, 3.5d and 3.5e are typical examples of such plots.

The second line segment is equivalent to a threshold. For R_2 reflectivities greater than 0.19, the cloud-free pixels are composed mainly or exclusively of ice. As ice may have R_2-R_1 values much lower than our threshold, (Section 3.21) thin or broken cloud above ice surface may escape detection at the present step, and they will be filtered out at subsequent steps.

Region 3 is separated from region 5 by:

a) a line parallel to the cloud-free pixels line for land and water surfaces, but with a buffer or uncertain region. This line is

expressed by the following equation:

$$R_2-R_1 = -0.08 + 0.45R_2, \text{ for } R_2>0.2 \quad (3.9)$$

b) a line parallel to the threshold of region 4, but with a buffer. This line is expressed by:

$$R_2-R_1 = -0.06, \text{ for } R_2>0.355 \quad (3.10)$$

c) a tilted line segment with the purpose of excluding cloud-free pixels composed of ice and land from region 3. Cloud-free pixels above land, exhibit small R_2 reflectivities (0.1 to 0.2) and positive R_2-R_1 differences, while ice covered pixels may have considerably larger R_2 reflectivities and their R_2-R_1 differences are negative. Cloud-free pixels composed of land and ice have intermediate reflectivity values, and as their R_2 reflectivity may increase with increasing ice fraction, they may tilt towards increasing R_2 reflectivities, and decreasing R_2-R_1 differences. These pixels should not be classified accidentally as cloudy, and the tilted line segment serves this purpose. Its equation is:

$$R_2-R_1 = 0.10 - 0.45R_2, \text{ for } 0.355>R_2>0.2 \quad (3.11)$$

Special attention should be paid to the lower boundary of region 3. Assigning pixels to class 3 is an irreversible process, in the sense that once a pixel is designated as being cloudy, that designation is not changed. Therefore, that boundary should not be exceeded by re-

flectivities resulting from small grain snow-covered surfaces, or ice- and snow-covered surfaces that are exposed to low solar elevation angles. As we see from Figure 3.3, according to the calculations of Dozier et al. (1982), cloud-free snow- or ice-covered surfaces do not exceed that boundary.

Region 3 does not necessarily include all cloudy pixels. It includes only those cloudy pixels that can be unambiguously distinguished from those that are cloud-free by their R_2 and R_1 reflectivities. Therefore, the exact location of the boundaries of region 3 is not critical, provided that we do not misclassify cloud-free pixels as being cloudy.

Pixels that are assigned to class 5 are those which do not belong to any of the above 4 classes. They form the transition region between classes 1, 2 and 4, and class 3.

As we have mentioned in section 3.2, cloudy pixels are assigned by any one of three different processes. So far, we have examined an initial classification of pixels, based only on their R_2 and R_1 values. Channel 4 will contribute to this initial classification of cloudy pixels by assigning all non-cloudy pixels with 11 μm radiances less than 53 $mWm^{-2}cmSR^{-1}$ as being cloudy. This radiance corresponds to a brightness temperature of around $-16^{o}C$. All surface observations report surface temperatures considerably higher during the data collection period. The coldest surface temperatures over the Arctic region occur in the interior of Greenland, where the average surface temperature for the month of July is no lower than $-11^{o}C$ (L. Gates 1973).

Channel 3 adds to the cloudy pixels all pixels inside regions 2

and 4 with reflectance greater than 4% in that channel. Pixels initially assigned to class 5 with R_2-R_1 less than zero are assumed to have background radiances coming from water and ice surfaces rather than land, and hence are subjected to the same threshold test in channel 3.

Finally we calculate the total number of pixels assigned to the various classes and the average 11 μm radiance for each particular class. This is our first step towards the cloud fraction estimation. Subsequent tests will use the information obtained in the present section to further resolve the situation.

3.31 Underlying Surface and Further Analysis

The analysis described in the previous section may, and often will reveal, that not all classes are present in a particular scene. In practice, if a particular class contains less than 1% of the total number of pixels in the scene, that class is treated as being absent.

When a particular class is not present, then the area assigned to the cloudy pixels in the R_2-R_1 plot (Region 3) can be expanded, because the misclassification danger diminishes. Also, the channel 4 threshold used in section 3.3 can be increased if ice covered surface (class 4) is not present, because cloud-free pixels will have brightness temperatures considerably higher than -19°C. We need therefore to explicitly take into account the underlying surface types occurring in each scene, and to develop routines that will use this information. The program should be able to decide which routine

performs best under the situation detected in section 3.3, and to call that routine automatically.

Three routines are used for that purpose:

Routine #1 is used when no ice is present (No pixels in region 4).

Routine #2 is used when ice is present, but not land (pixels in region 4, but not in region 1).

Routine #3 is used when land and ice are present.

As the number of pixels per data set increases, the complexity of the situations encountered increases. In the case of a single data set that encompasses a whole satellite orbit, the underlying surface will almost always contain land, ocean and ice, the most unfavourable situation. We wish to have an adequately large data set, but to avoid complex situations by dividing the satellite orbit into small areas, we have chosen data sets composed of 34 X 34 pixels. They cover an area of approximately 140 X 140 square kilometers, the number of pixels along the scan line corresponding to almost 1/12 of the whole scan line.

The general procedure is as follows Groups of thirty-four scan lines are divided into twelve data sets of 34 X 34 pixels. Every data set is examined separately, and the appropriate algorithm for the data set analysis is called. The results are stored in the computer for further use (creation of a false colour image, or calculation of cloudy and cloud-free radiances and cloud fraction). When all twelve data sets have been examined we advance to the next thirty-four scan lines and continue until we examine the whole image.

Sections 3.32, 3.33, and 3.34 describe Routines 1, 2 and 3 respectively.

3.32 ROUTINE #1

This routine is called when land and or water is present in the scene but ice is not. By assuming that ice is not present, we may expand the area assigned to cloudy pixels in Figure 3.9. This is achieved by extending the line that separates region 3 from region 5, from R_2=0.2 back to R_2=0.0 for all R_2 value. It is now parallel to the line that separates classes 1 and 2 from class 5, from the beginning of the X axis, displaced by 0.02 reflectivity downwards. The discussion in section 3 21 concerning equation 3.6 of that section is also appropriate here, when trying to examine the sensitivity of the cloud fraction estimations to the constants of the present equation.

In the absence of ice due to warmer surface temperatures, the threshold in channel 4 used to distinguish clear and cloudy pixels can be raised from $53mWm^{-2}cmSR^{-1}$ to $67mWm^{-2}cmSR^{-1}$, corresponding to a brightness temperature of -4 K.

Pixels belonging to classes 1 and 2 that succesfully pass that threshold test are assumed to be cloud-free. Those that fail are assumed to be cloudy. Pixels belonging to class 5 with 11 μm radiance less than the threshold value are also assumed to be cloudy. This threshold has an impact on identification of cirrus clouds because even though they exhibit low reflectivities, they also have low 11 μm radiances.

A flowchart of this routine, is also presented in Figure 3.11, and the corresponding R_2-R_1 plot is represented in Figure 3.10

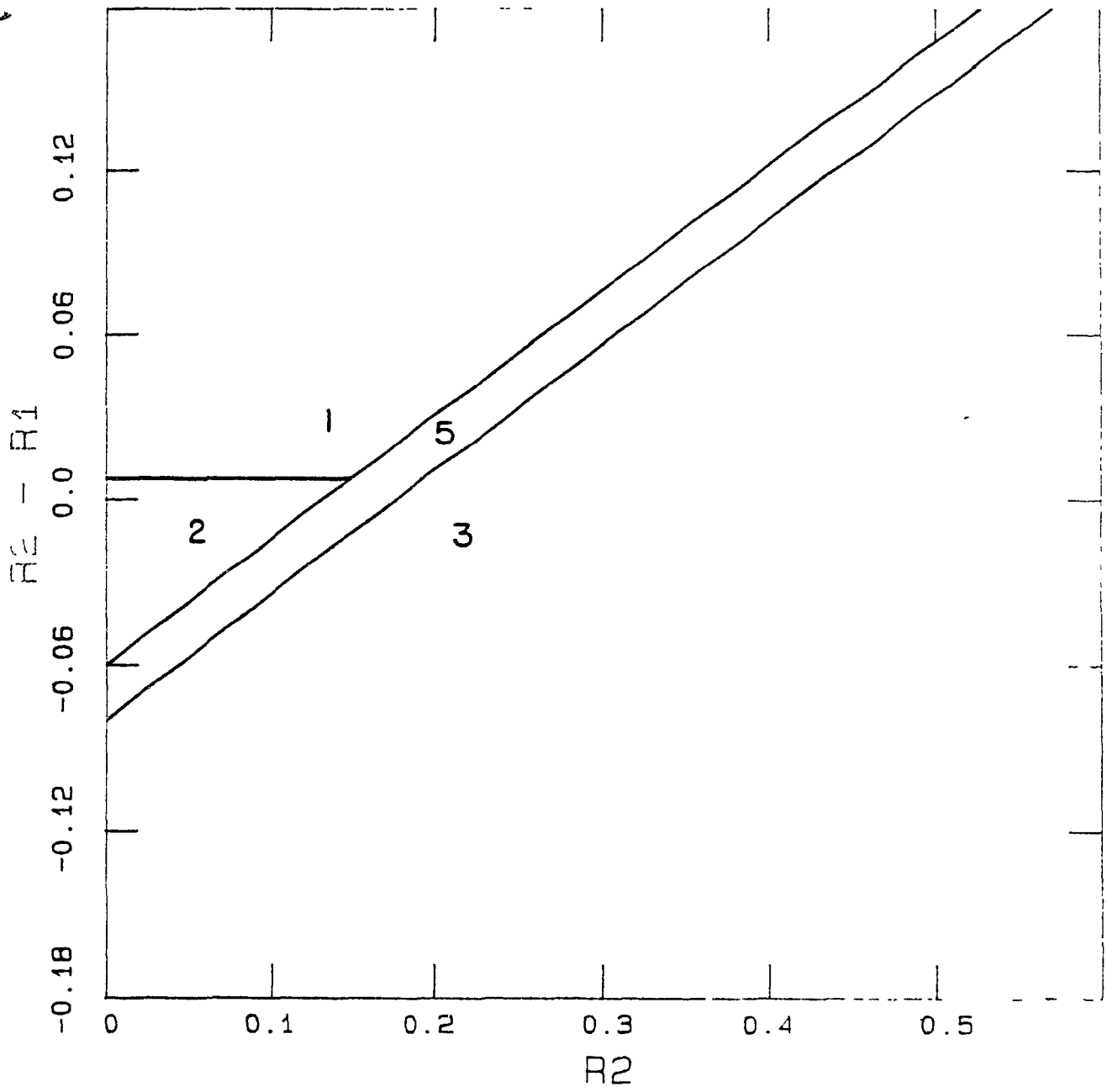

Figure 3.10. Lines separating the various classes of pixels in the R_2-R_1 plot, when Routine #1 is called.

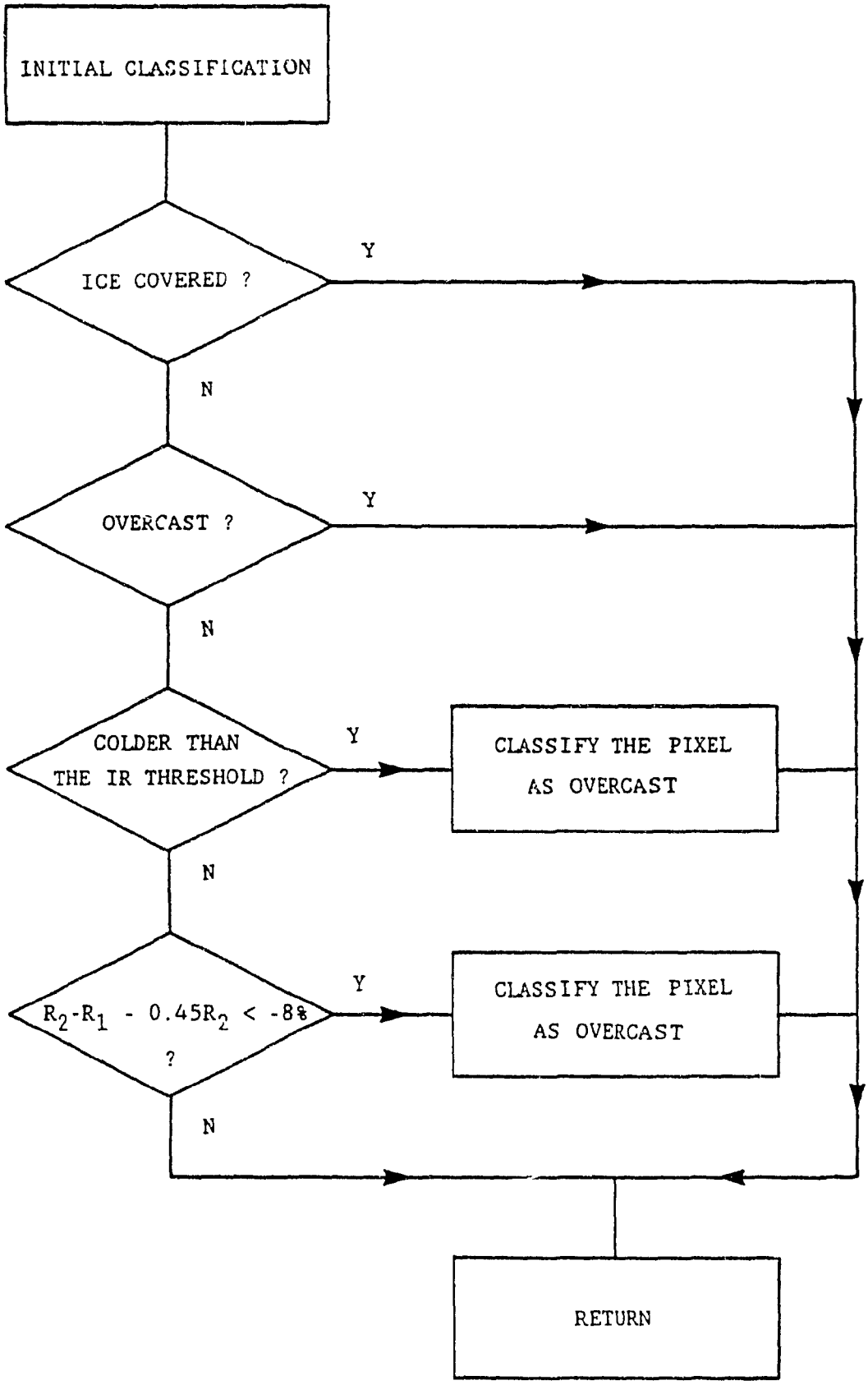

Figure 3.11. Flowchart corresponding to Routine 1.

3.33 ROUTINE #2

This routine deals with clouds above sea and sea-ice. Due to the absence of land and land-ice combinations, we neglect the possibility that cloud-free pixels associated with large R_2 reflectivities and also having R_2-R_1 values similar to those of overcast pixels may exist. This enables us to expand the region for class 3 in the R_2-R_1 plot by assigning all pixels within:

$$R_2-R_1 + 0.45R_2 > 0.04 \quad \text{for } R_2 < 0.22 \tag{3.11}$$

$$\text{and } R_2-R_1 > -0.06 \qquad \text{for } R_2 > 0.22 \tag{3.12}$$

as being overcast (Figure 3.13).

Not all overcast pixels will necessarily have been included in this boundary. Subsequent tests will reexamine the non-overcast pixels.

In order to facilitate the detection of the remaining cloudy pixels, we group all the pixels that have not been found overcast to this point into two sets. Set A is composed of pixels with $R_2-R_1 \geq -0.06$. We consider that these pixels contain mainly ice-free water. Set B is composed of pixels with $R_2-R_1 < -0.06$, and we consider the radiative properties in this set to be dominated by the presence of ice. We will search for the existence of cloudy pixels first in set A, and afterwards in set B.

Although this new separation seems to be inconsistent with the previous boundary between water and ice covered pixels (Figure 3.10), it should be noted that pixels composed of water and ice are spread in regions 2 and 4 as well. This is caused by the variable water and ice fraction and the variable optical properties of the ice in the pixels. Therefore by regrouping the pixels this way, we may include in group A some pixels belonging to class 4, but these pixels also contain a water fraction, as the other pixels of the group do. Finally, all pixels in group A share more or less similar surface properties.

For set A, a cloudy pixel will be detected on the basis of its R_2 reflectivity and/or its 11 μm radiance. All nominally cloud-free pixels for which $T_4 - T_5 < 1K$ yield the average cloud-free channel 2 reflectance, R_2', and channel 4 radiance, I_4'. The corresponding radiances of all non-overcast pixels will be compared to the average cloud-free radiances and a particular pixel will be declared overcast if one of the following holds:

$$R_2 > R_2' + 0.06 \quad \text{or} \quad I_4 < I_4' - 4\text{mWm}^{-2}\text{cmSR}^{-1}$$

The pixel will be declared cloud-free, if it is not overcast, and if its radiances satisfy the following two conditions.

$$R_2 < R_2' + 0.04 \quad \text{and} \quad I_4 > I_4' - 2\text{mWm}^{-2}\text{cmSR}^{-1}$$

Otherwise the pixel will be declared uncertain

For set B, a cloudy pixel will be detected on the basis of its 11μm radiance only, because clouds and ice are both strong reflectors

on this channel and therefore no conclusions can be easily reached on the basis of the R_2 reflectivity. Again, all nominally cloud-free pixels in set B with $T_4-T_5 < 1K$ yield the average cloud free 11μm radiance I_4'.

The 11 μm radiances of all non-overcast pixels will be compared to the average cloud-free 11 μm radiance of set B, and a particular pixel will be assumed to be overcast if its 11 μm radiance I_4 satisfies the following condition:

$$I_4 < I_4' - 4\text{mWm}^{-2}\text{cmSR}^{-1}$$

A pixel will be declared cloud free if:

$$I_4 > I_4' - 2\text{mWm}^{-2}\text{cmSR}^{-1}$$

and otherwise it will be declared uncertain.

The value of the threshold in T_4-T_5 is not crucial to our results because the final decision for pixel classification is based on a threshold in channel 2 or channel 4. If these thresholds correspond to radiances very close to those of the underlying surface, it is possible to mistake some cloud-free pixels as cloudy. If they differ too much from the cloud-free radiances, some thin (channel 2 threshold) or some warm (channel 4 threshold) clouds may escape detection. The present thresholds were chosen after some experimentation in order to minimize these errors and produce cloud fields that look realistic on the basis of the corresponding visible and infrared satellite pictures.

If clouds have temperatures similar to or greater than the surface

temperature, all uncertain pixels belonging to set B are declared cloud- free. The reason is that clouds with temperatures close to the underlying surface should reflect at 3.7 μm, and therefore should have been already detected by channel 3.

A flowchart of routine 2 is presented in Figure 3.13, and the corresponding R_2-R_1 plot is represented in Figure 3.12.

3.34 ROUTINE #3

This routine deals with the most difficult situation, namely scenes containing both land and ice. The very varied surface may have a large range in surface temperature, the sea and sea-ice likely having temperatures close to $0^{o}C$ while the land surfaces may be significantly warmer. Land surfaces alone may have non-uniform temperatures as a result of varying topography and surface type. Similarly, the reflected solar radiation from such a background may also be highly variable (Figure 3.5h). The variation in the clear-sky radiances precludes the setting of fixed thresholds as a satisfactory means of distinguishing clear and overcast pixels. To alleviate tne problem we will divide the 34X34 pixel scenes into more homogeneous sub-scenes in a manner similar to that used in chapter 2. The essence of the procedure will be to set a variable threshold in I_4 for each sub-scene.

The procedure can only work if the cloudy pixels are on average colder than the clear-sky pixels. To determine this, the first step in tne routine is to compare the average value of I_4 for the pixels in region 3 of the R_2-R_1 plot with the average of those in region 4

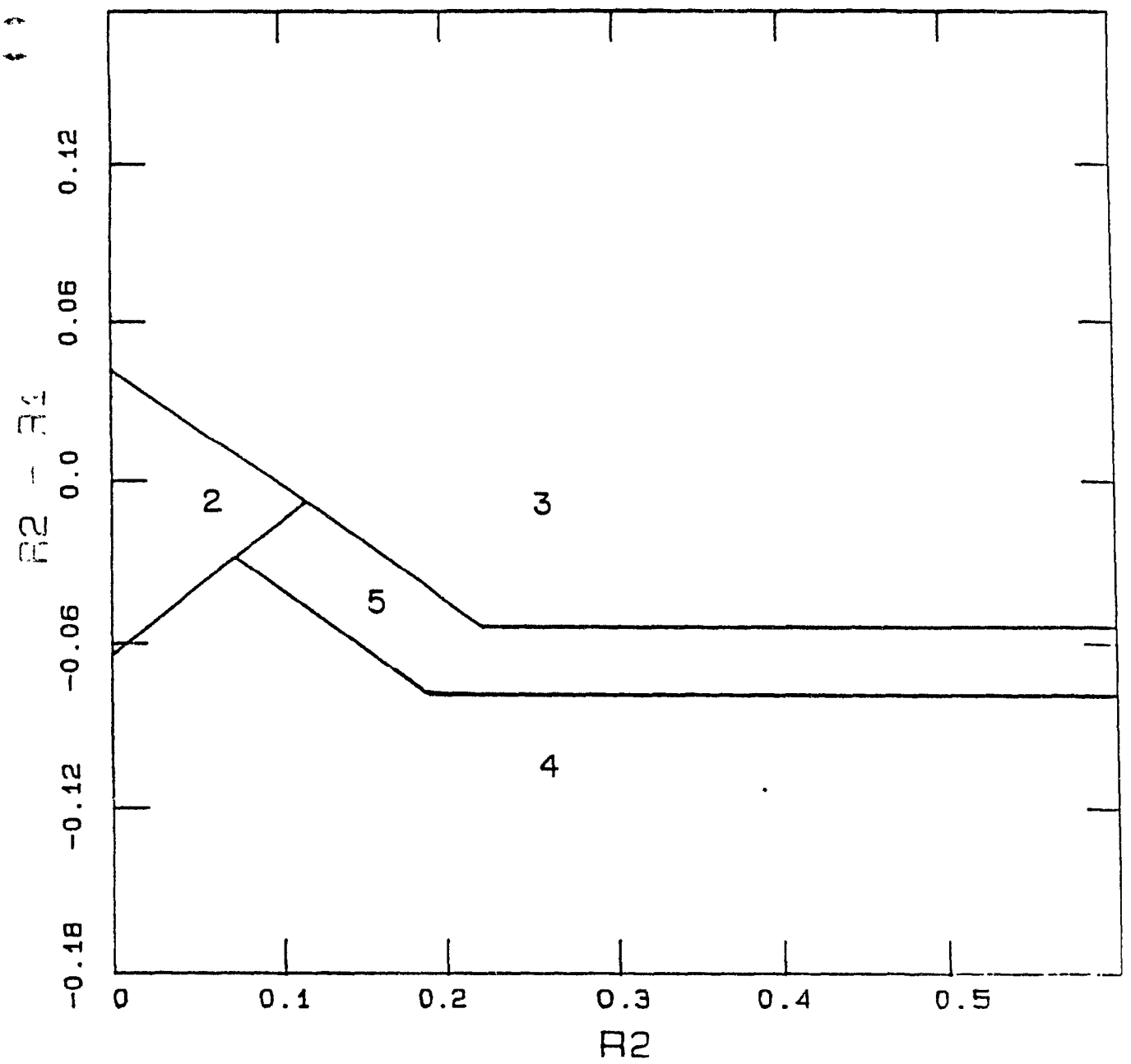

Figure 3.12. Lines separating the various classes of pixels in the R_2-R_1 plot when Routine #2 is called.

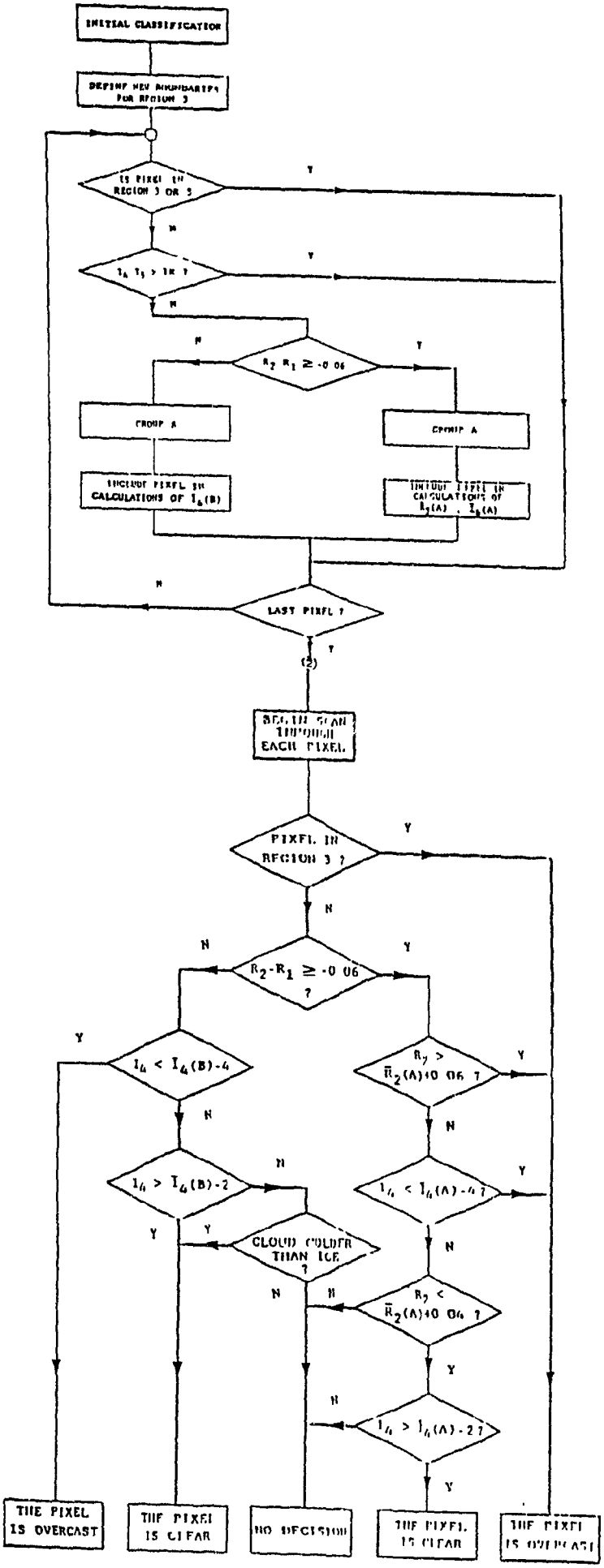

Figure 3.13. Flowchart corresponding to Routine 2.

(Figure 3.9). If the average value for the pixels so far identified as being cloudy is less than the value for the nominally clear pixels, the next step in the routine is invoked. If this is not so but there are more water covered pixels (region 2) than land covered pixels (region 1), routine 2 is suitable for further analysis with the influence of the land being neglected; otherwise, the initial guess is retained as the best estimate.

The pixels that need particular attention at this point are those in the relatively large region 5 of the R_2-R_1 plot which are classified as being uncertain, and those in region 4 which consist of ice and snow surfaces under either clear skies or thin or partial cloud cover. Figure 3.15a shows an example of the R_2-R_1 plot for a scene consisting of clouds, land, ice and some water.

Pixels in region 4 that are most likely not cloud contaminated are identified by requiring that their brightness temperatures in channels 4 and 5 differ by less than $1^{o}K$ (see section 3.24). All these pixels yield the average 11 μm radiance for cloud-free, ice covered pixels, I_4'. Although it is assumed that stratus and altostratus have been eliminated by the threshold in I_3 described in section 3.23, it is still possible that pixels containing thick cold clouds might have escaped detection. To avoid such pixels being included in the next step, all pixels that are so-far identified as being clear are subjected to a threshold in I_4 equal to I_4'- $5mWm^{-2}cmSR^{-1}$ (~.5K).

The remaining pixels are now grouped into sub-groups on the basis of their R_2-R_1 values, each sub-group containing pixels with R_2-R_1 values differing by less than 0.01. The significance of grouping

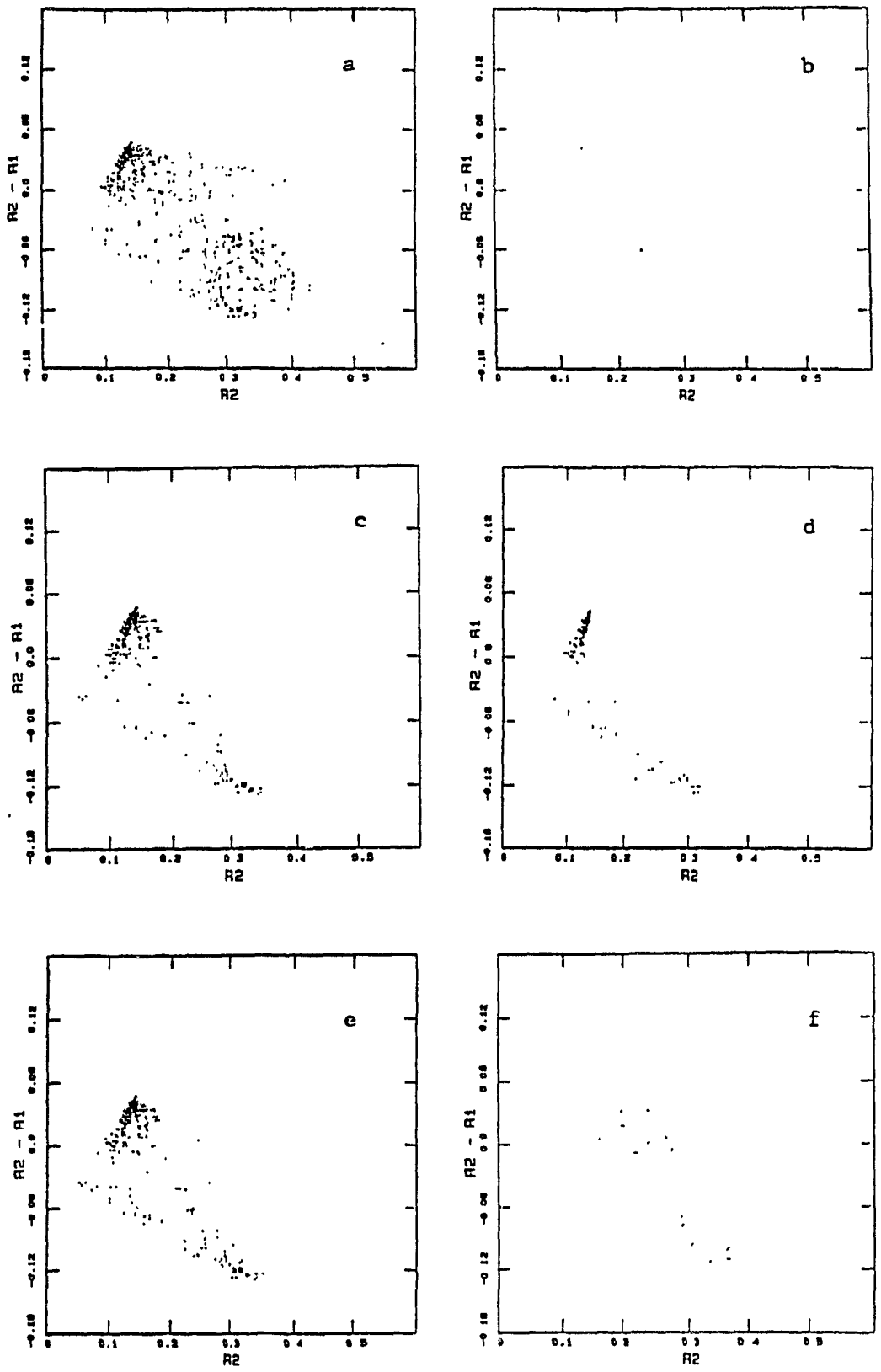

Figure 3.14. R_2-R_1 plot for a data set containing: (a) all the pixels; (b) selected cloud-free pixels that have minimum T_4-T_5 value inside a layer; (c) cloud-free pixels on the basis of their 11μm radiances; (d) cloud-free pixels on the basis of their R_2 reflectivities; (e) all cloud-free pixels contained in c and d; (f) all pixels that were found to be overcast.

pixels in this way is that each sub-group will be more homogeneous, the largest values of R_2-R_1 corresponding to land, the smallest to ice, and intermediate values to varying combinations of land, water and ice. To the extent that this is true, one would expect that the mean channel 4 radiance of each subgroup should decrease with decreasing R_2-R_1. That this does indeed happen is illustrated in Figures 3.15, in which the mean values of I_4 in each layer are plotted against R_2-R_1 for three different cloud-free coastal scenes with surfaces containing a mixture of land and ice.

Because these sub-groups contain a much more homogeneous background than the whole scene, we assume that variations in T_4-T_5 for pixels inside the subgroup are due to the presence of small cloud amounts. The fact that the clouds are colder than the surface implies that cloud contaminated pixels exhibit larger T_4-T_5 values than completely cloud-free ones. We therefore assume that for every subgroup, the pixel with the minimum T_4-T_5 value is cloud-free.

We also assume that these cloud-free pixels are composed of varying mixtures of land and ice, and therefore require that their 11 μm radiances satisfy:

$$I_{4,i-1} \geq I_{4,i} \geq I_{4,i+1} \tag{3.12}$$

for every layer, where the subscript i labels the sub-groups according to their R_2-R_1 value with increasing values of i corresponding to decreasing values of R_2-R_1. The purpose of this requirement is to avoid characterizing the 11 μm radiance of the cloud free pixels in a layer by the radiance of a pixel that is much warmer or colder than

that of the average cloud free pixels composed of land and ice. For example, there may be a case where the selected cloud-free pixel is colder than the average cloud-free pixel in the layer if it receives less solar radiant energy as a result of local topography. Alternatively, the selected pixel may be warmer than the average cloud-free pixel in the particular layer, possibly as a result of a large open water fraction in the pixel. If, for a subgroup i inequality (3.12) does not hold, then the selected cloud free pixel in this subgroup is replaced by the cloud-free pixel in subgroup i + 1. In our example the selected cloud free pixels are indicated in Figure 3.14b.

One should expect that more than one cloud-free pixel will exist in every subgroup and that they may be a few degrees colder or warmer than the pixel already selected to characterize the layer. We accept as cloud free all pixels that have:

a) 11 μm radiance greater than the 11 μm radiance of the selected pixel - $3mWm^{-2}SR^{-1}$ (~-3K); and

b) T_4-T_5 less than the T_4-T_5 value of the selected pixel plus $+1.2^{o}K$.

They are presented in Figure 3.14c.

All pixels with 11 μm radiance less than the 11 μm radiance of the selected pixel minus $6mWm^{-2}cmSR^{-1}$ (~-6K) are assumed to be overcast, and the rest are uncertain.

The average R_2 reflectivity of all the cloud-free pixels in each layer selected up to this point, $R_{2,i}'$, is calculated. Finally all uncertain pixels in a particular layer with channel 2 reflectance less than $R_{2,i}'$, are also assumed to be cloud-free provided that they also satisfy requirement (b) of the previous step. They are presented in

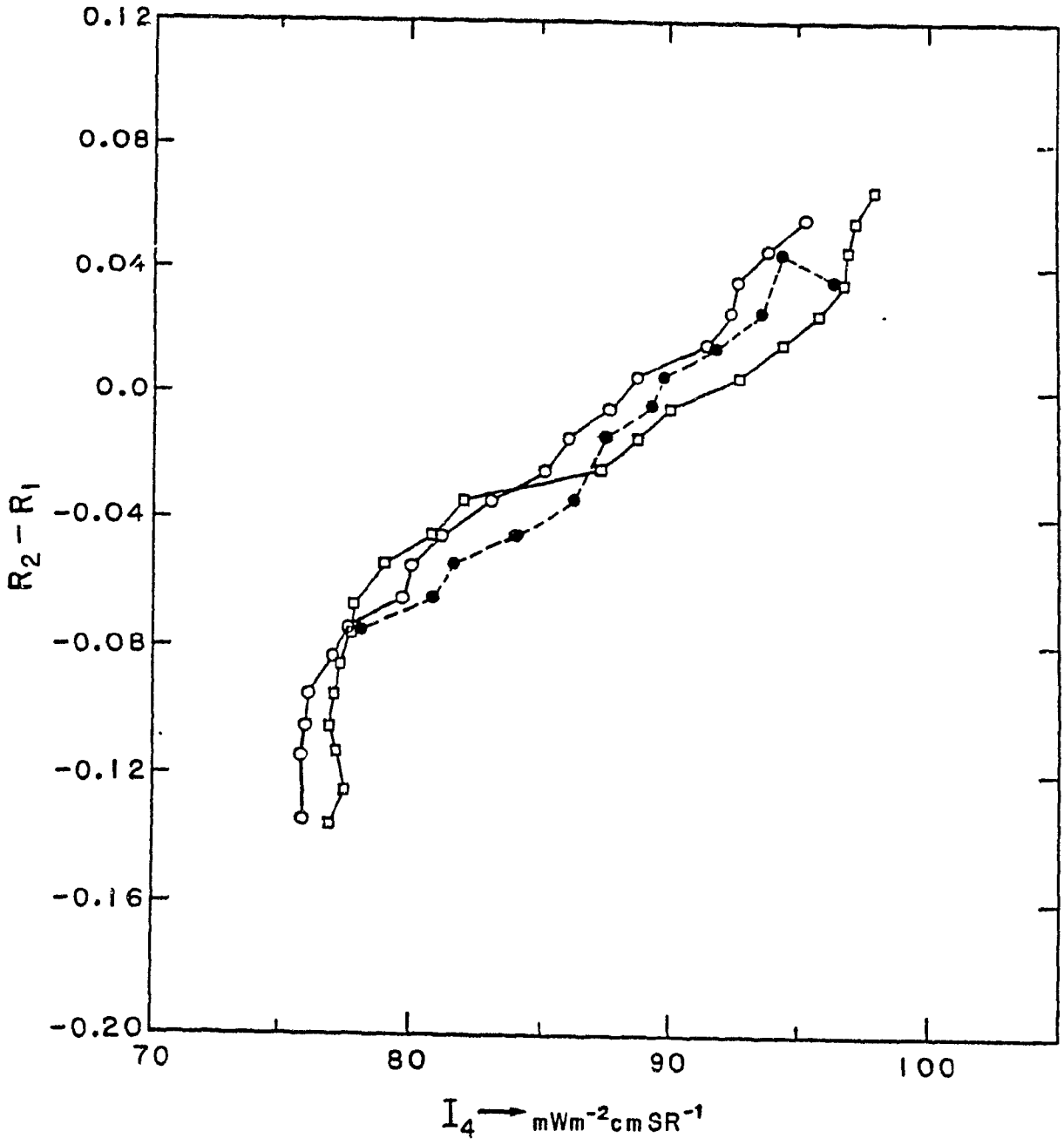

Figure 3.15. Average cloud-free 11 m radiance for layers with different R_2-R_1 values and for three different data sets.

Figure 3.14d. Pixels not specifically identified as being cloud-free (Figure 3.14e) or cloudy (Figure 3.14f) remain classified as uncertain. A flow chart of the complete routine is given in Figure 3.16.

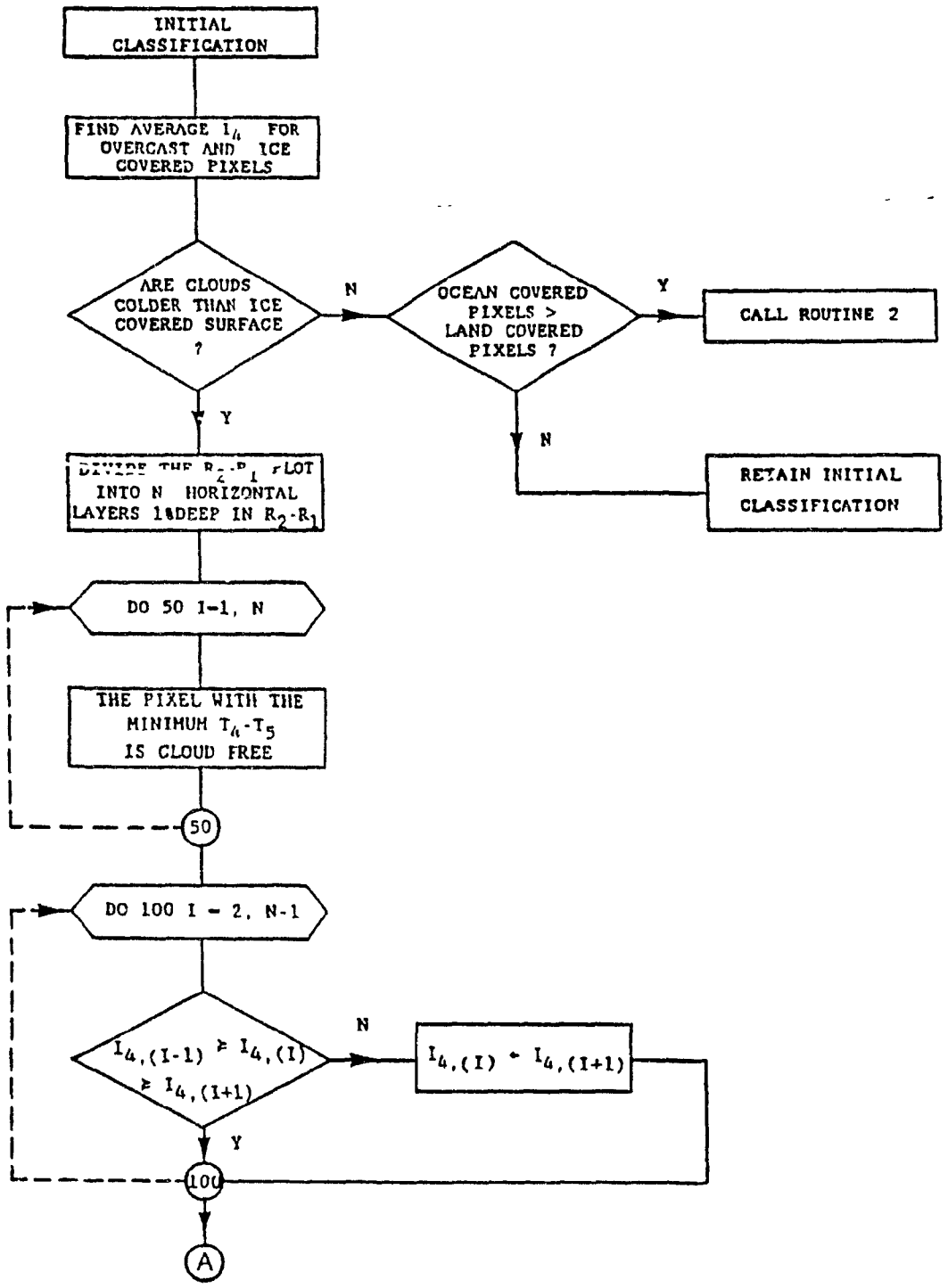
INITIAL CLASSIFICATION
FIND AVERAGE I_4 FOR OVERCAST AND ICE COVERED PIXELS
ARE CLOUDS COLDER THAN ICE COVERED SURFACE ?
N
OCEAN COVERED PIXELS > LAND COVERED PIXELS ?
Y
CALL ROUTINE 2
Y
N
RETAIN INITIAL CLASSIFICATION
INTO N HORIZONTAL LAYERS 1°DEEP IN R_2-R_1
DO 50 I=1, N
THE PIXEL WITH THE MINIMUM T_4-T_5 IS CLOUD FREE
50
DO 100 I = 2, N-1
$I_{4,(I-1)} \geq I_{4,(I)} \geq I_{4,(I+1)}$
N
$I_{4,(I)} \leftarrow I_{4,(I+1)}$
Y
100
A

Figure 3.16.

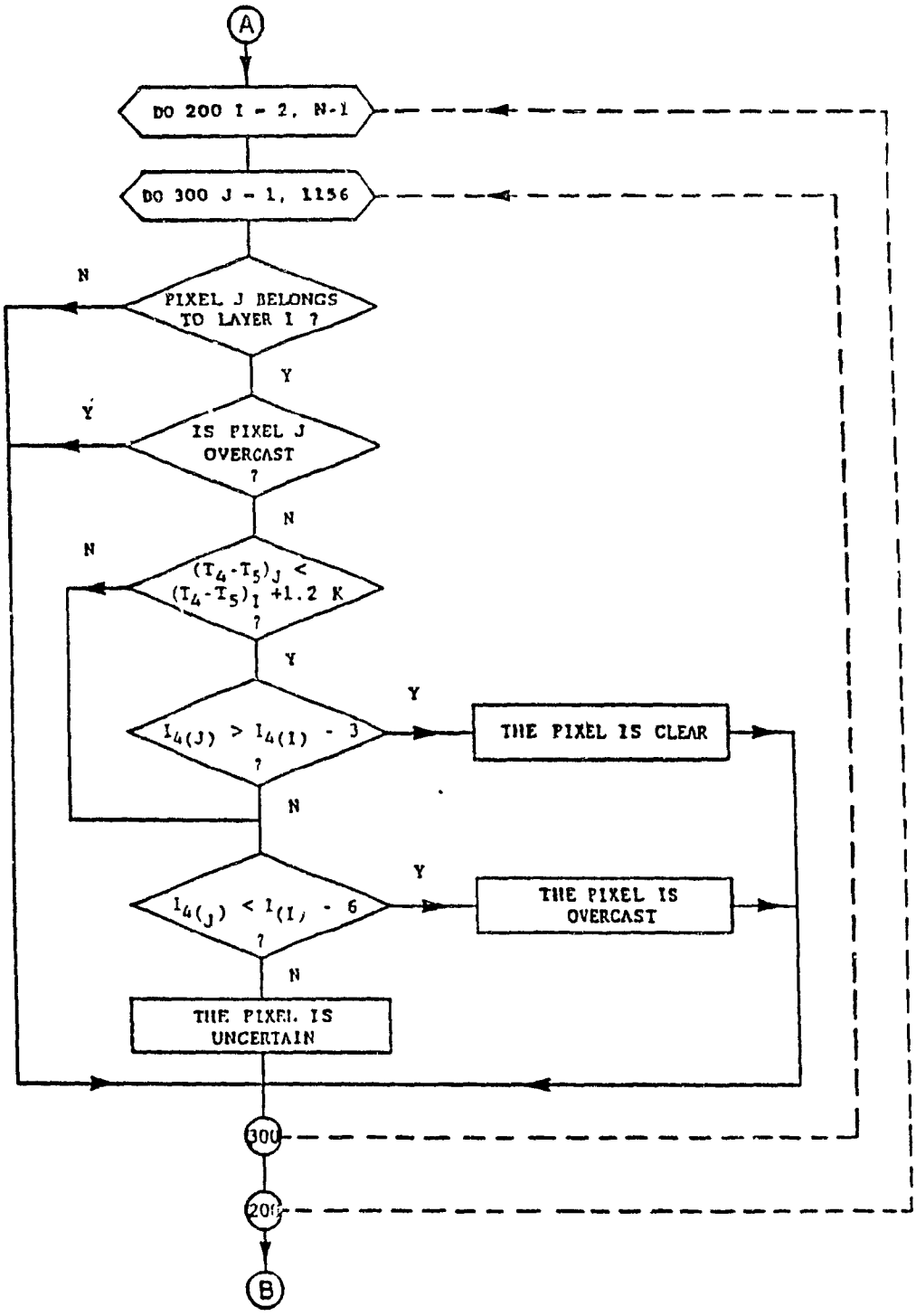
A
DO 200 I = 2, N-1
DO 300 J = 1, 1156
PIXEL J BELONGS TO LAYER I ?
N
Y
IS PIXEL J OVERCAST ?
Y
N
$(T_4-T_5)_J < (T_4-T_5)_I + 1.2$ K ?
N
Y
$I_{4(J)} > I_{4(1)} - 3$?
Y
THE PIXEL IS CLEAR
N
$I_{4(J)} < I_{(I)} - 6$?
Y
THE PIXEL IS OVERCAST
N
THE PIXEL IS UNCERTAIN
300
200
B

Figure 3.16.

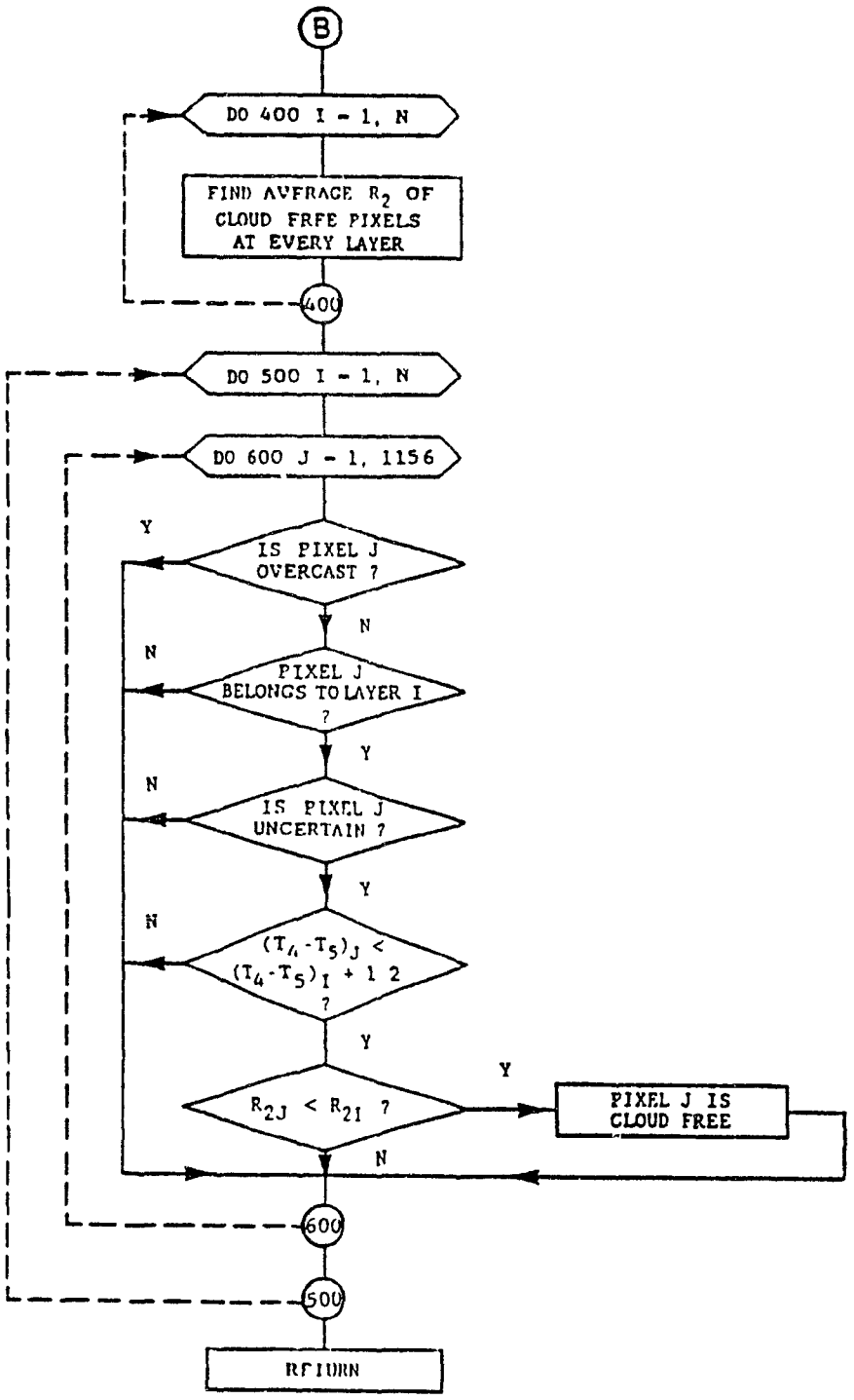

Figure 3.16. Flowchart corresponding to Routine 3.

CHAPTER 4

4.1 Validation of the Algorithm

The algorithm was mainly trained using data taken during the first orbit of July 1, 1984. The validation followed the training of the algorithm as an independent process. Both GAC and LAC data were used from various satellite orbits. At this point, it is worth recalling from section 1.3 the problems associated with the validation of an algorithm for cloud detection. These problems are more severe in the high latitudes due to the sparcity of surface observations. We therefore rely on a number of tests, explained below, to assess the algorithm's capability of producing accurate analyses of cloud fields over the Arctic.

It is expected that the algorithm should be able to:

a) produce large scale cloud fields that are in general in good agreement with the corresponding synoptic characteristics;

b) explain persistent radiative characteristics above a certain location as either clouds or ice, regardless of the changing satellite and solar angles;

c) recognize geographic boundaries, and correctly identify the nature of the surface under clear skies. While this is not directly connected to the cloud field, it adds confidence in the performance of the algorithm and it should be taken into account,

d) give results that, when compared to manual analyses based on satellite pictures, synoptic weather maps and surface observations

show good agreement; and

e) be performed on both GAC and LAC data, and be insensitive to the resolution degradation from LAC to GAC. Manual analysis based on the LAC data, and any other available evidence should give results similar to those obtained by the automatic analysis regardless of the type (GAC or LAC) of the data used

Regarding (a), retrieved cloud patterns should vary smoothly and realistically and in particular should not show discontinuities at the boundaries of the 34 X 34 pixel analysis regions A typical scene contains more than 100 such regions and covers a sufficiently large area that the nature of the surface and cloud will exhibit significant variation. Since different analysis regions will use different cloud detection routines depending on the nature of the underlying surface, there is a possibility of generating discontinuities in the analysed cloud field at the boundaries of the analysis regions.

When developing the algorithm, we tried to avoid the appearance of these discontinuities as much as possible by tuning the various thresholds of the algorithm. But it is impossible to eliminate them entirely because certain types of clouds that can be detected above a certain background in a particular data set may escape detection in an adjacent data set due to different surface conditions. For example, warm stratus above ice that continues into a data set where land is also included may escape detection in the data set that contains land and may produce a discontinuity in the cloud field at the data sets boundary. In general these discontinuities do not appear more often than once or twice in an analysed cloud field, except when the solar zenith angle becomes very low in the descending part of the orbit, when

they appear more frequently.

An example of the comparison between the synoptic situation and the cloud field that was created by the algorithm follows. Figure 4.1 presents the synoptic situation over the Arctic region for July 1, 1984, at 00 GMT. Data taken above the Arctic by the NOAA7 satellite during its first orbit of the same day, at around 01:30'GMT were analysed by the algorithm, and the results are presented in Figure 4 2 in the form of an a false colour image composed of individual pixels. The same results were averaged in terms of cloud fraction on a 2.5° X 2.5° longitude, latitude grid. From these averaged values, we generate smoothed isolines that correspond to cloud fractions of 0.2, 0.5, and 0.8. In Figure 4.3, we present these isolines, on an orthographic projection map, centered at 80°E, 75°N, along with the Arctic geography.

When Figure 4.3 is compared to Figure 4.1, we notice the presence of a cloud band close to Obskaja Guba (70°E, 70°N) that corresponds to a front on the synoptic map. A cloudy area westwards of Novaya Zemlya (60°E, 75°N) is associated with an approaching low pressure system centered at around (40°E, 70°N) on the synoptic map. The cloudy area in Figure 4.3 which extends from Novaya Zemlya to Franz Zoseph Land (60°E, 80°N), to Severnaya Zemlya (100°E,80°N), and from Severnaya Zemlya southwards to the Siberian Coast, corresponds to the warm front that starts from the aforementioned low pressure system (40°E, 70°N), and crosses the Siberian coast at around the Taymyr Peninsula (110°E, 75°N). This front has been displaced northwards in Figure 4.3. This displacement looks reasonable, taking into account the existence of the high pressure system over central Siberia. The existence of this

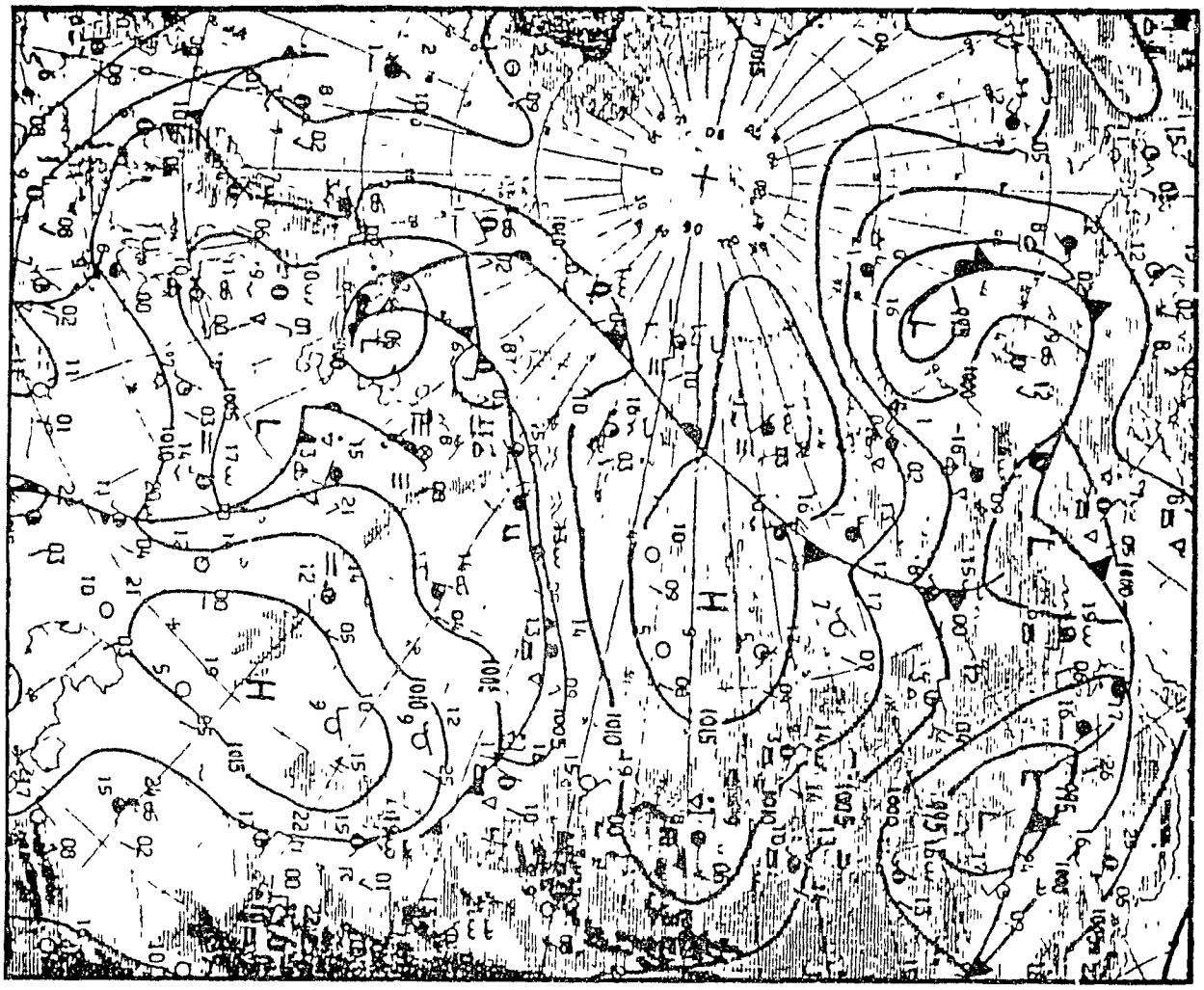

Figure 4.1. Synoptic map for July 1, 1984 of 00 GMT.

Figure 4.2 Automatic analysis of the cloud field based on data selected during the 1st orbit of July 1, 1984. Red represents clouds, yellow ice, green land, and blue water.

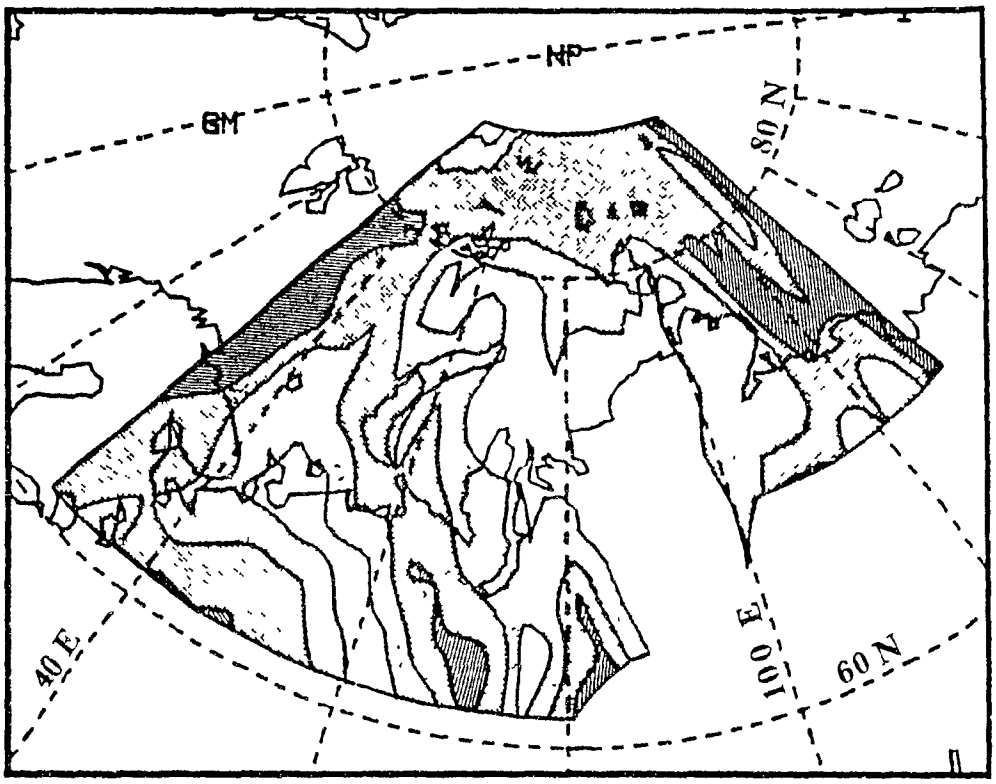

Figure 4.3. Isolines of cloud cover averaged over 2.5X2.5 latitude longitude cells, on a polar orthographic projection. White areas correspond to cloud fraction from 0.0 to 0.2, light grey to cloud fraction from 0.2 to 0.5, dark grey from 0.5 to 0.8, and the darkest shade corresponds to cloud fractions greater than 0.8.

system is evident in the automatic analysis by the low cloudiness area from eastwards of Obskaya Guba (80^{o}E, 70^{o}N) to the Taymyr Peninsula (105^{o}E, 70^{o}N).

All the automatically analysed satellite orbits produced cloud fields consistent with the corresponding synoptic cituation.

To check the ability of the algorithm to satisfy requirement (b), we look for some well recognised geographical features in the absence of considerable cloud cover as denoted by surface observations and prevailing synoptic anticyclonic conditions. These features can be, for example, Iceland and its ice caps, Spitsbergen Island or the area around Obskaja Guba. We noticed that the algorithm assigned the same surface type over a specific location during subsequent satellite orbits, regardless of the changing solar and satellite viewing angle, with the exception of very low solar elevation angles. In this exceptional case, land surfaces which necessarily appear dark are interpreted as water surfaces due to their very low R_2 and R_2-R_1 values and similarly, bergy water may be interpreted as ice-free water, or as sea-ice. Small changes in cloud fraction from orbit to orbit were not considered to discredit the algorithm.

Geographical boundaries between water, ice and land were also properly identified, provided that the solar elevation angle was high enough, a condition that was met throughout the whole ascending part of the satellite orbit, and the northern section of the descending part of the orbit. The area around Obskaja Guba has a distinct shape, and a complicated land water boundary. A sea-ice analysis chart, valid for the end of the June 1984 period, shows that part of the area is covered by fast ice (Figure 4.4). It is therefore an interesting testing area.

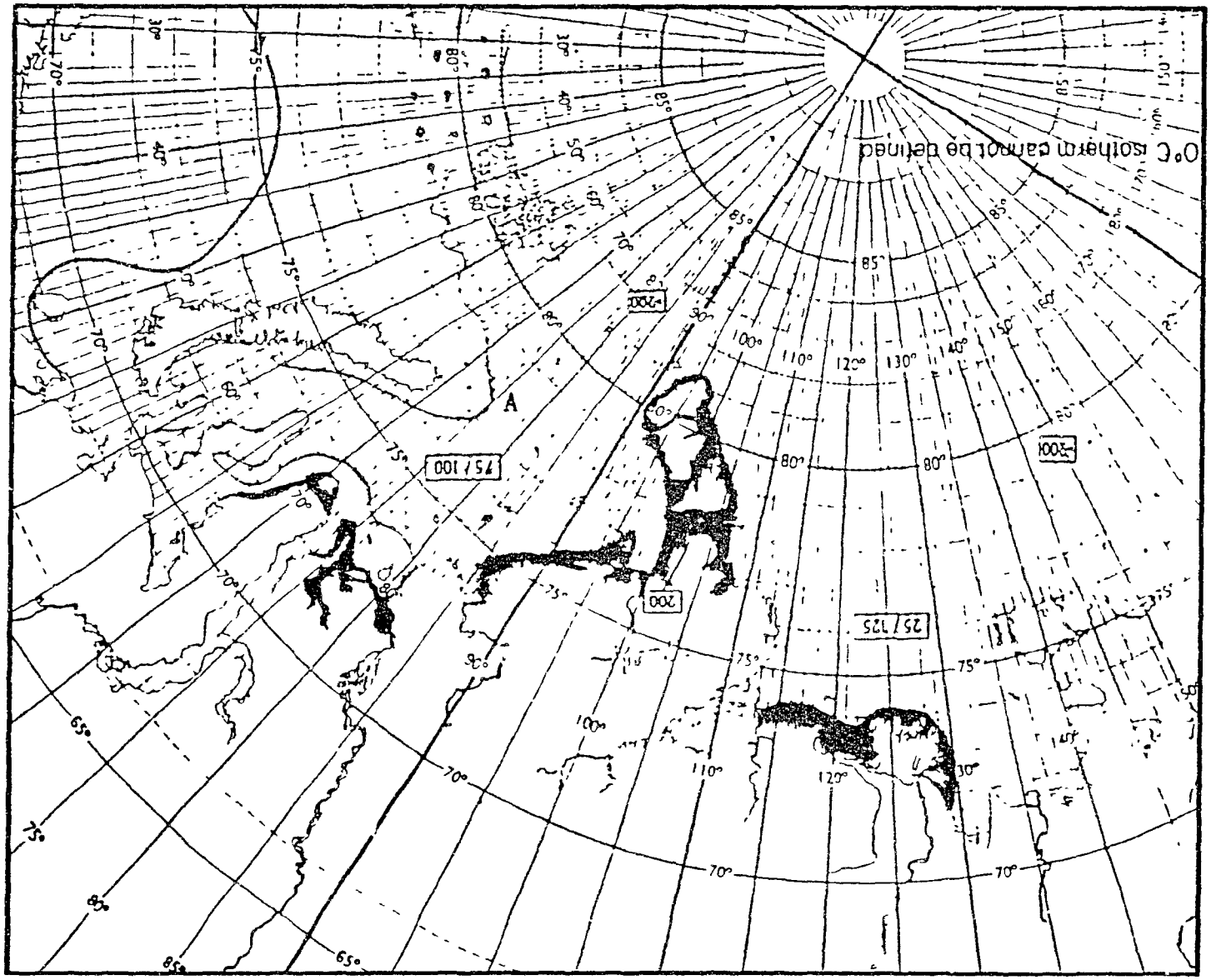

Figure 4.4. Sea-ice analysis chart valid for the end of June 1984 period. Very dark surfaces correspond to fast ice. Maximum extent of sea-ice, is marked by line (A).

Looking at Figure 4.2, we notice that land-water boundary is properly identified. Ice is also located in these areas where the sea-ice analysis chart indicates fast ice. The presence of ice was also found inside O.G., but as we have already mentioned in Section 3.33 the algorithm assigned as sea-ice, areas with even a small ice fraction by using a fixed boundary in the R_2-R_1 plot. One consequence is that we cannot distinguish between small and large ice fraction, or fast ice. But as our effort is directed towards cloud identification, we did not attempt to obtain a more precise ice estimation Subsequent satellite orbits also succeeded in obtaining the proper surface identification above the aforementioned area. The present test, as well a number of similar tests display the ability of the algorithm to sense the surface type correctly.

To check requirement d, a manual analysis of the cloud field was performed using the same satellite data that were also used in the automatic analysis. From the recorded radiance values, we created black and white satellite images corresponding to channels 1 and 4 on a high resolution graphics terminal. The images were photographed, and enlargements of the pictures were made available to an independent analyst. Ten different grey shades could be distinguished resulting in a resolution of about 4% albedo for the visible, and about $4mWm^{-2}cmSR^{-1}$ (~4K) for the IR image. The independent analyst also used information concerning the synoptic situation, surface conditions and climatology.

We consider that the most important additional advantage in the manual analysis is the ability of the human eye to understand and interpret textural features. The most important disadvantage is the restriction to two of the five AVHRR channels. To give a typical

example of how the manual and the automatic analysis compare, we present in Figure 4.5 the manual analysis that corresponds to the automatic one previously presented in Figure 4.2.

Comparison of Figures 4.2 and 4.5 yields that the main cloud features are common in both analyses. The cloud structure in the automatic analysis is more detailed than the cloud structure in the manual analysis. This is expected because the automatic analysis is performed on a pixel by pixel basis while the observer looks at more gross characteristics.

The major differences between the two cloud field analyses are:

i) a cloud band at the most eastward section of the analysed part of the orbit that does not exist on the manual analysis;

ii) considerably lower cloud amounts above Siberia in the automatic analysis, than on the manual analysis;

iii) a cloud band southwards of Novaya Zemlya that does not exist in the manual analysis; and

iv) small cloud amounts between the two major cloud systems, above the European part of the USSR, that are not present in the automatic analysis.

The most serious difference among all these is the first one. The cloud band in question was detected in the automatic analysis by channel 3. But this band has no signature in the IR image, something that is possible but not usual for a whole cloud band. To help resolve the situation, we created IR images with increased resolution in terms of grey shades per radiance for radiance values close to those of the cloud band and the underlying surface, and compressed resolution everywhere else. In this way we selectively increased the resolution at

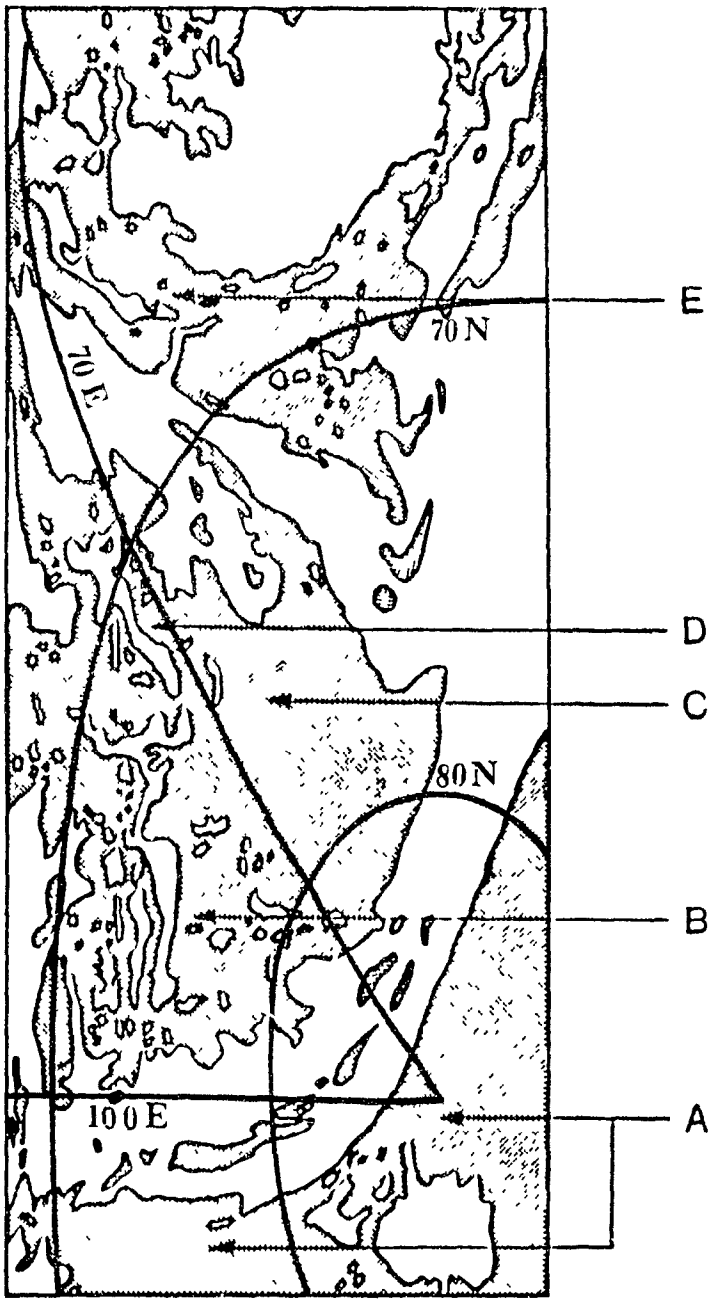

Figure 4.5. Manual analysis of the satellite orbit whose automatic analysis is present in Figure 4.2. Clouds are white, surface is dark.

around the value of our interest, to $1mWm^{-2}cmSR^{-1}$ or to around 1K degree in terms of temperature. In Figure 4.6, we present the new IR image. The IR signature of the low cloud with temperatures slightly colder than the underlying surface is now evident, and we believe that this confirms that the automatic analysis was indeed correct. Additional evidence that the manual analysis is likely to be wrong at this point, is provided by the comparison between the visible and infrared images of the eastward part of the first satellite orbit of July 1 1984 (Figure 4.7), and the first satellite orbit of July 2, 1984 (Figure 4.8). Significant changes in the images around the area of interest ($140^{o}E$, $80^{o}N$) are observed from one day to the next which suggests the presence of clouds in one or both images. The manual analysis does not find clouds in either case, while the automatic analysis shows clouds in July 1, 1984 and clear-skies in July 2, 1984.

We followed the same procedure in order to resolve the second difference. It was found that southwards of Novaya Zemlya, temperatures are warmer and reflectivities higher than those of the open sea (Figure 4.9, and 4.10). Thi' also favors the automatic analysis.

It is somewhat more difficult to come to a conclusion concerning the cloud field differences above Siberia because the land is a less uniformly radiating medium than sea and sea-ice.

In case (iv) it appears that the automatic analysis failed to detect relatively thin and warm clouds above land.

From the overall comparison in the present example, and in other examples as well, we found that the automatic and the manual analyses were in good agreement. For most of the cases where the two analyses disagreed, the automatic analysis seems more likely to be correct.

Figure 4.6. Infrared image of the eastward part of the satellite orbit whose manual and automatic analyses are present in Figures 4.4, and 4.2 respectively. The temperature resolution per grey shade is ~1K from ~-10°C to ~0°C.

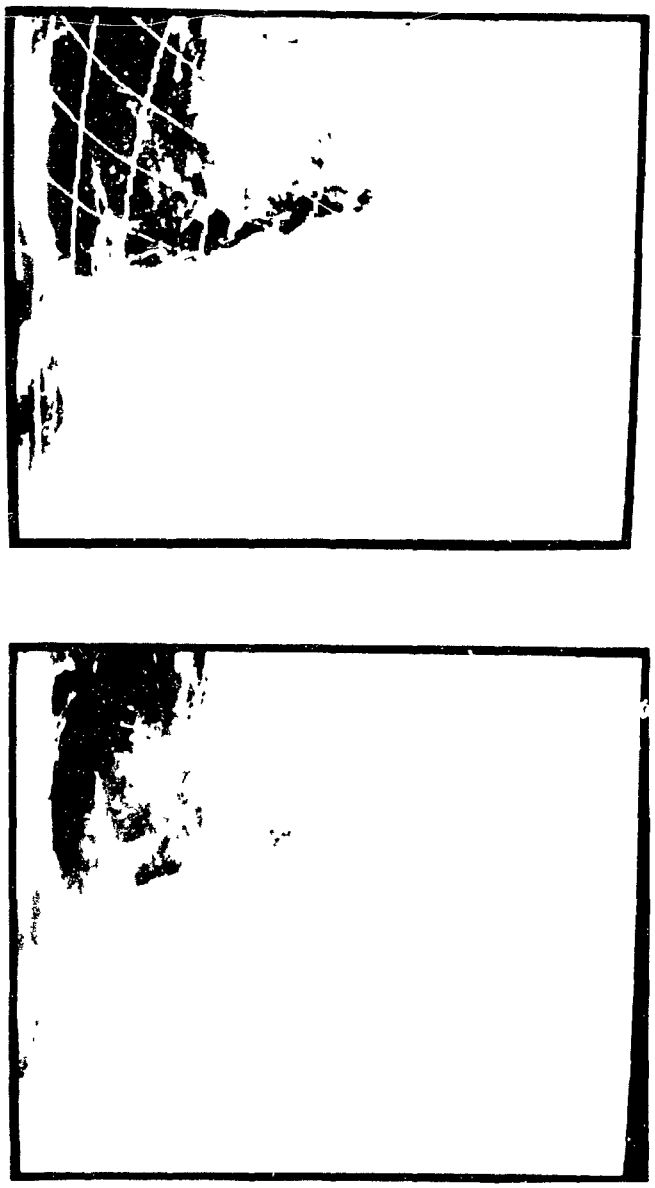

Figure 4.7. Visible (a) and infrared (b) image of the eastward part of the first orbit of July 1, 1984.

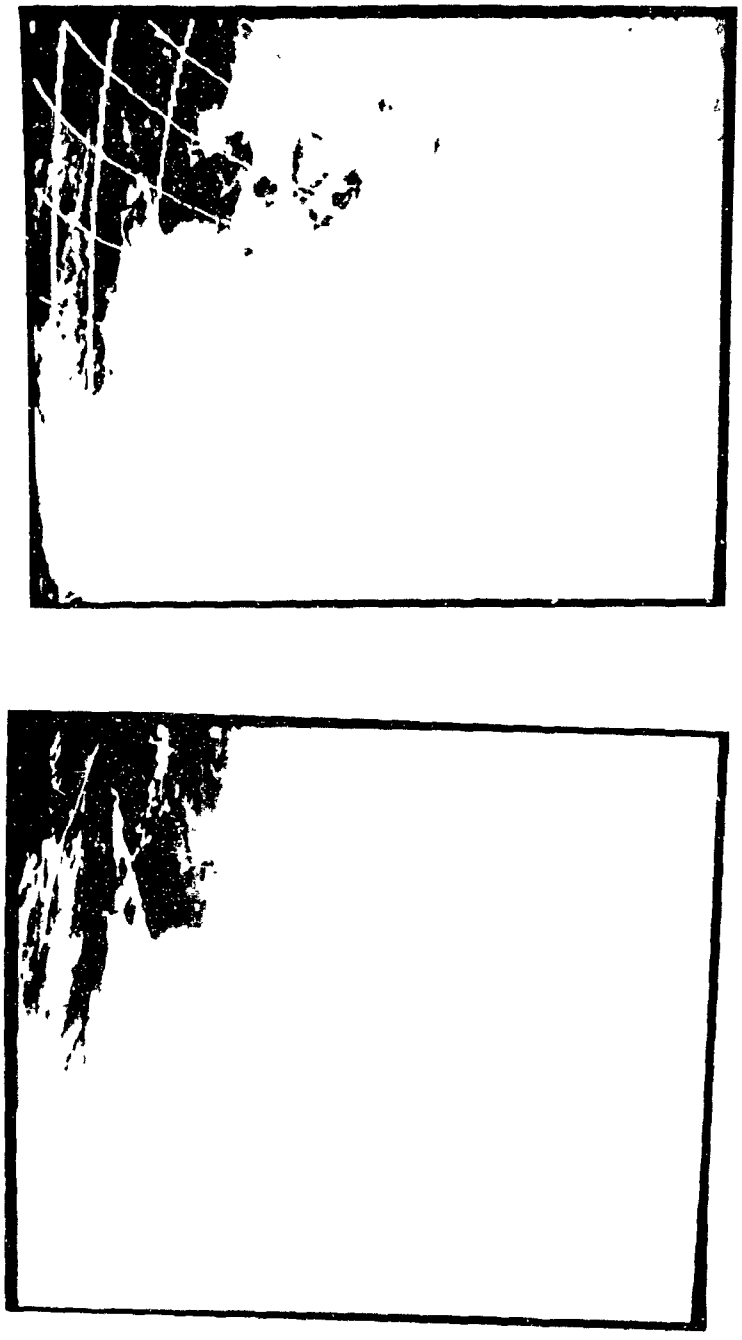

Figure 4.8. Same as Figure 4.7, but for the first orbit of July 2, 1984.

Figure 4.9. Visible image of the area around Novaya Zemlya. Longitude and Latitude lines are also present.

Figure 4.10. Infrared image of the same area as in Figure 4.10 with increased resolution (~1K/grey shade) around $0^{o}C$.

Surface observations are consistent with both analyses. They are sparse and they do not provide adequate additional information over areas where manual and automatic analyses disagree.

High resolution LAC data were available for another satellite orbit. To examine the differences between the cloud field analysis derived by the present algorithm when GAC data and when LAC data are used, we compared the two automatic analyses for the same satellite orbit above an area that covered the region from Iceland to the eastern part of Greenland. A manual analysis by an independent analyst based on satellite images produced from the same LAC data was also available. The VIS and IR images that were used by the independent analyst, after being enlarged, are presented in Figures 4.11 and 4.12. These Figures illustrate the importance of high spatial resolution data for recognition of the surface structure. Existence of well recognisable surface structure greatly facilitates the recognition of clouds in a manual analysis. This analysis is shown in Figure 4.13, where white corresponds to cloudy areas, and black corresponds to cloud free areas. The automatic analysis based on the LAC data is shown in Figure 4.14. Comparing the manual to the automatic analysis, we notice that:

1) In the lower part the general agreement is good. The two most important differences occur in:

a) The mountainous area of Iceland, where the cloud amount is found to be larger in the automatic analysis than in the manual. The extra cloud amount in the automatic analysis is associated with the threshold in channel 2, and the possibility of a stratus cloud or fog located at around the ice caps cannot be ruled out. The automatic analysis shows thin cloud belts surrounding all ice caps on the

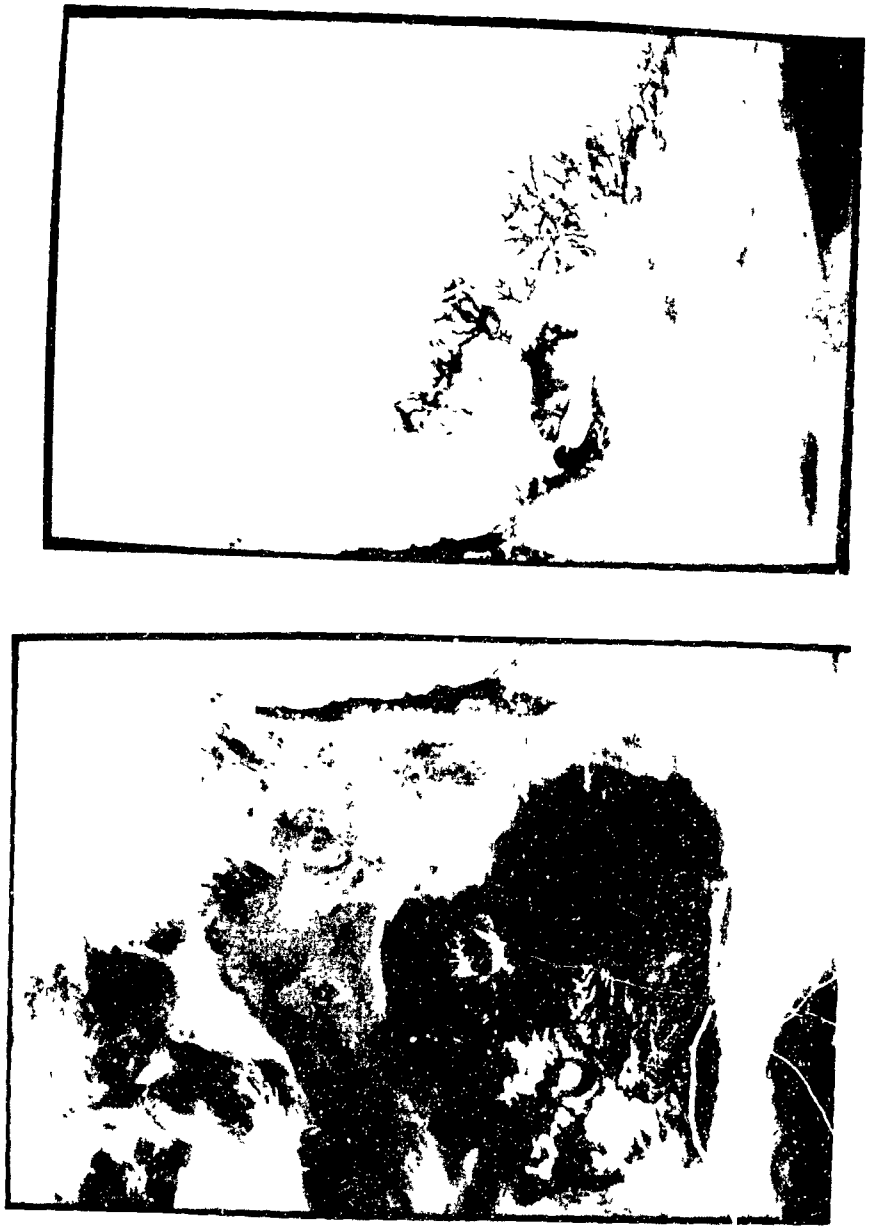

Figure 4.11. Visible image of the area around Iceland (lower part) and the Eastern part of Greenland (upper part) from LAC data. High reflectivity values, correspond to lighter shades. There is a ~5% reflectivity increase per grey shade.

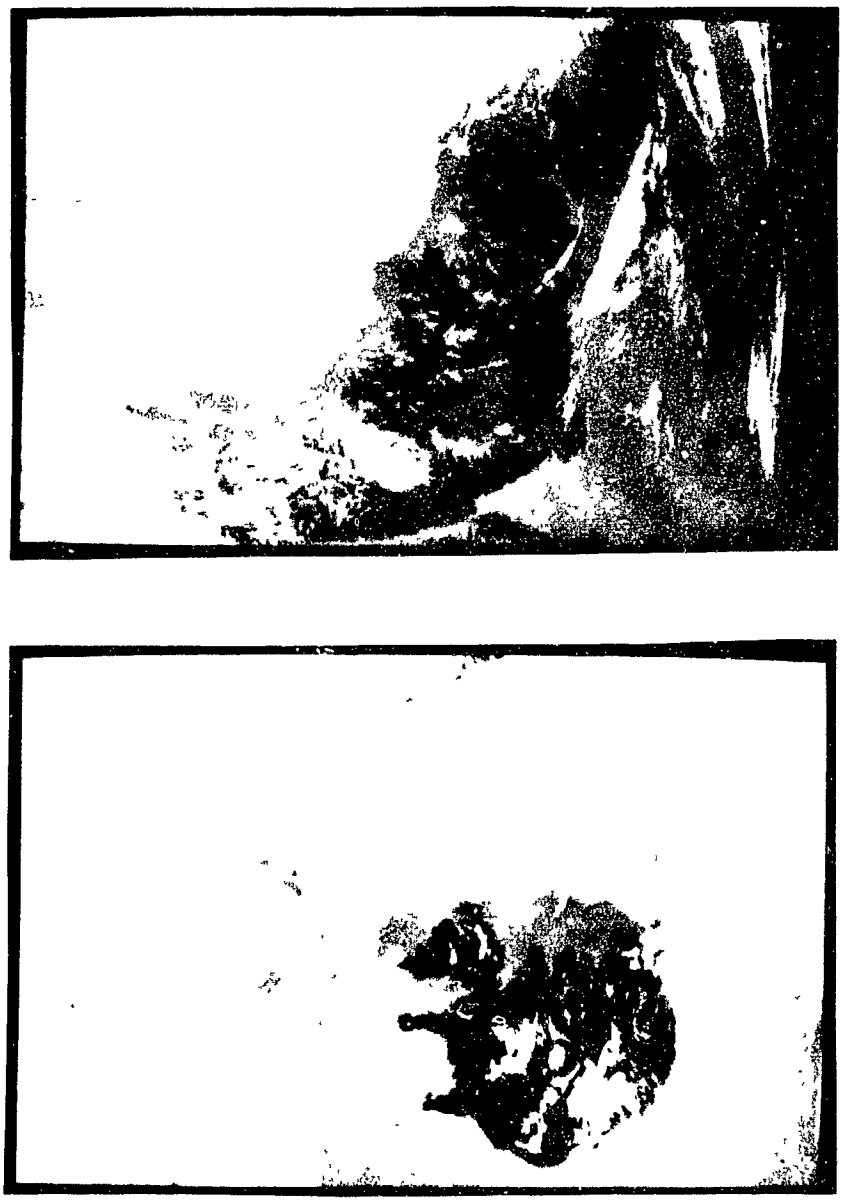

Figure 4.12. Infrared image of the same area as in Figure 4.11. Lighter shades correspond to correspond to colder temperatures. The scale is $4mWcmm^{-2}SR^{-1}$ per grey shade.

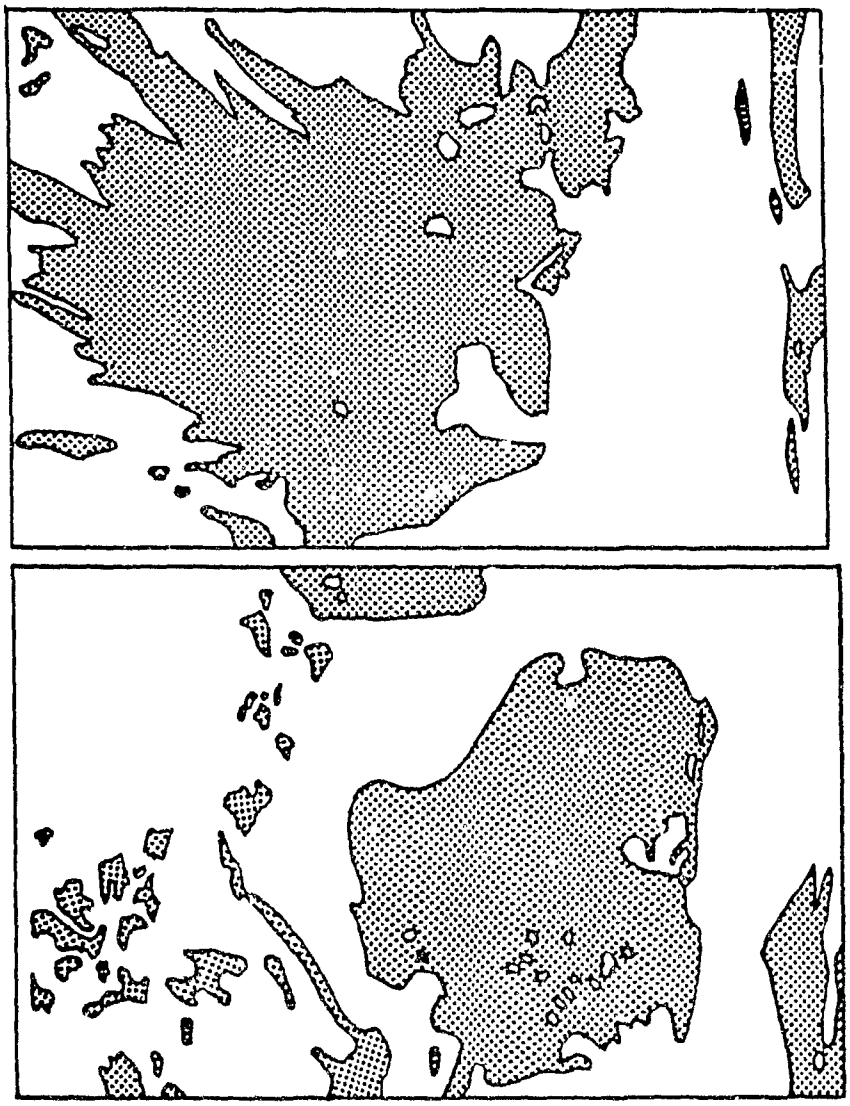

Figure 4.13. Manual analysis of cloud cover for the scene presented in Figures 4.11, 4.12. Clouds are white, surface black.

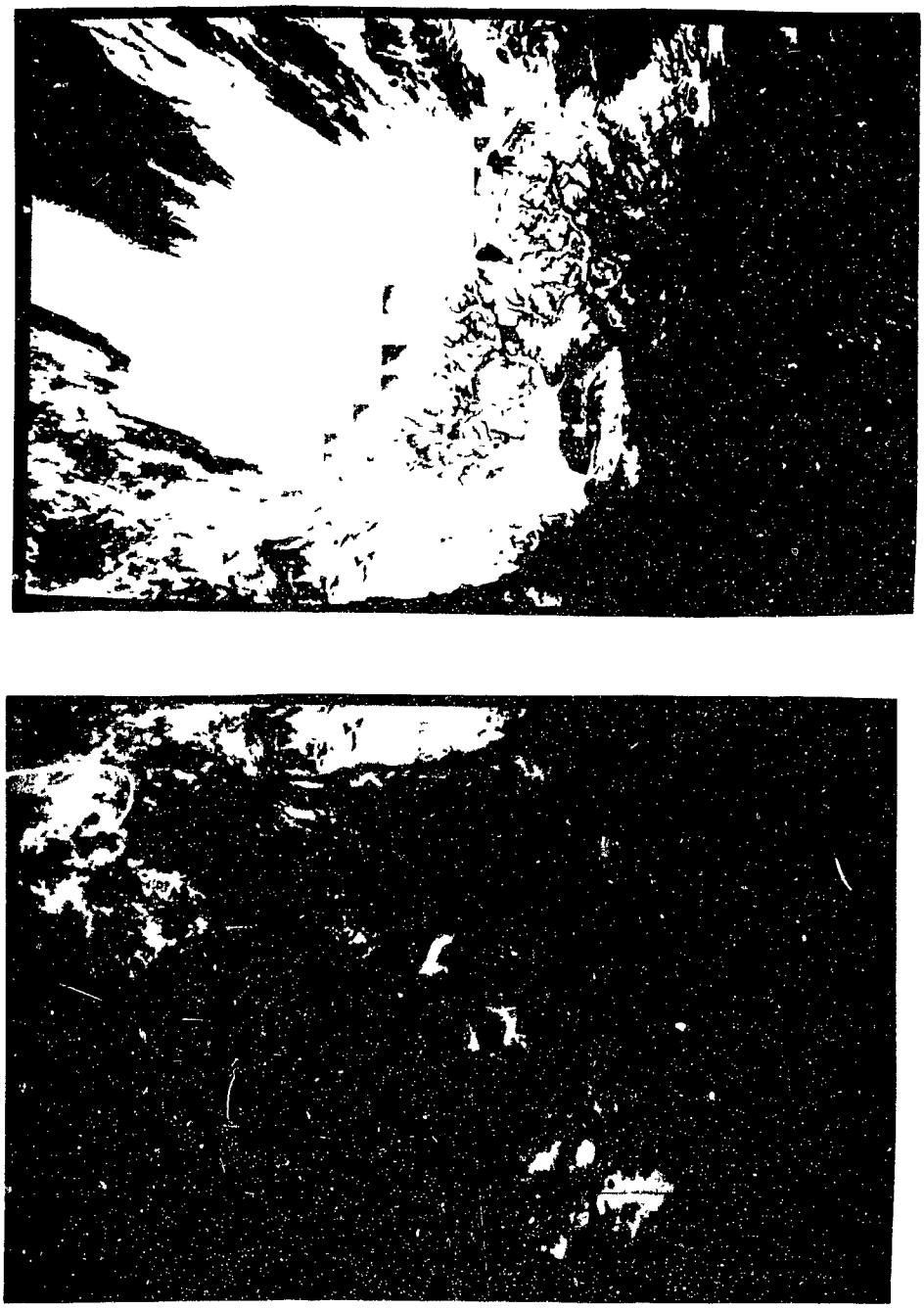

Figure 4.14 Automatic analysis of the same orbit as in Figures 4.11, 4.12, 4.13. Red corresponds to clouds, yellow to ice, green to land, blue to ocean, grey to undecided pixels. Long horizontal lines correspond to scan lines with bad data.

island.

b) The vicinity of Greenland, where the automatic analysis finds a broken cloud field, with sea and sea-ice below, while the manual analysis shows solid cloudiness. The sea-ice analysis chart indicates that very open ice (1/10, to 3/10), and open ice (4/10 to 6/10) exist between Greenland and Iceland. As a result we do not have any obvious answer to the question which of the two analyses is closer to the actual cloud field.

2) In the upper part of the figures, we also notice generally good agreement. The most important differences occur in:

a) The southern part of Greenland where we have a continuation of the disagreement that we discussed in 1b).

b) In the numerous fjords of Greenland, westwards of Scoresbysund where cloud around the sea-land interface is found by the automatic, but not by the manual analysis. It is either ice in fjords or cloud (fog). It is unlikely to be distinguished in either visible or infrared images, but it is most likely fog on the basis of channel-3 analysis.

c) In the area of the Scoresbysund ($22^{o}W$, $72^{o}N$), on the east coast of Greenland, where the manual analysis assumes the existence of a low stratus on the basis of the IR image The automatic analysis, is capable of identifying low water clouds, from their high channel 3 reflectivity and by failing to do so in the present case, it is implied, that this particularly low cloud has also low 3.7 μm reflectivity. We consider this a contradiction, and we assume that the automatic analysis is correct.

d) In the eastward part, where the cloud free area above

ocean that exists in the manual analysis has been greatly restricted in the automatic analysis, as a result of relatively large channel 3 reflectivity.

The automatic analysis based on GAC data above the same area is shown in Figure 4.15. Figures 4.15 and 4.14 give almost identical cloud fields above the same region, with the exception of the area west of Scoresbysund. The averaging process that creates the GAC from the LAC data has destroyed the structure of the complex cloud around the coast and it survives only as a small number of scattered cloudy pixels.

At this point it is worth comparing the cloud fields produced by the present method to the cloud fields obtained by other algorithms. Of the various groups working on the same problem, only E. Ebert (1987) has published results. Her method of analysis includes two basic steps:

i) A pattern recognition method is used for the cloud and surface type identification; and

ii) on the basis of the information obtained in the previous step, the optimal channel is chosen, and the hybrid histogram-spatial coherence method is employed for the cloud fraction estimation and the extraction of cloud-free and cloudy radiances.

Her results include both manual and automatic analysis of specific satellite orbits, as well as the average cloud fraction above the Arctic for July 1, 1984, derived by the automatic analysis of all satellite orbits of NOAA7 during that day.

In Figure 4.16, we present the manual and the automatic analysis of Ebert, and the automatic analysis derived by the present algorithm

Figure 4.15. Automatic analysis applied to the GAC data of 4.11

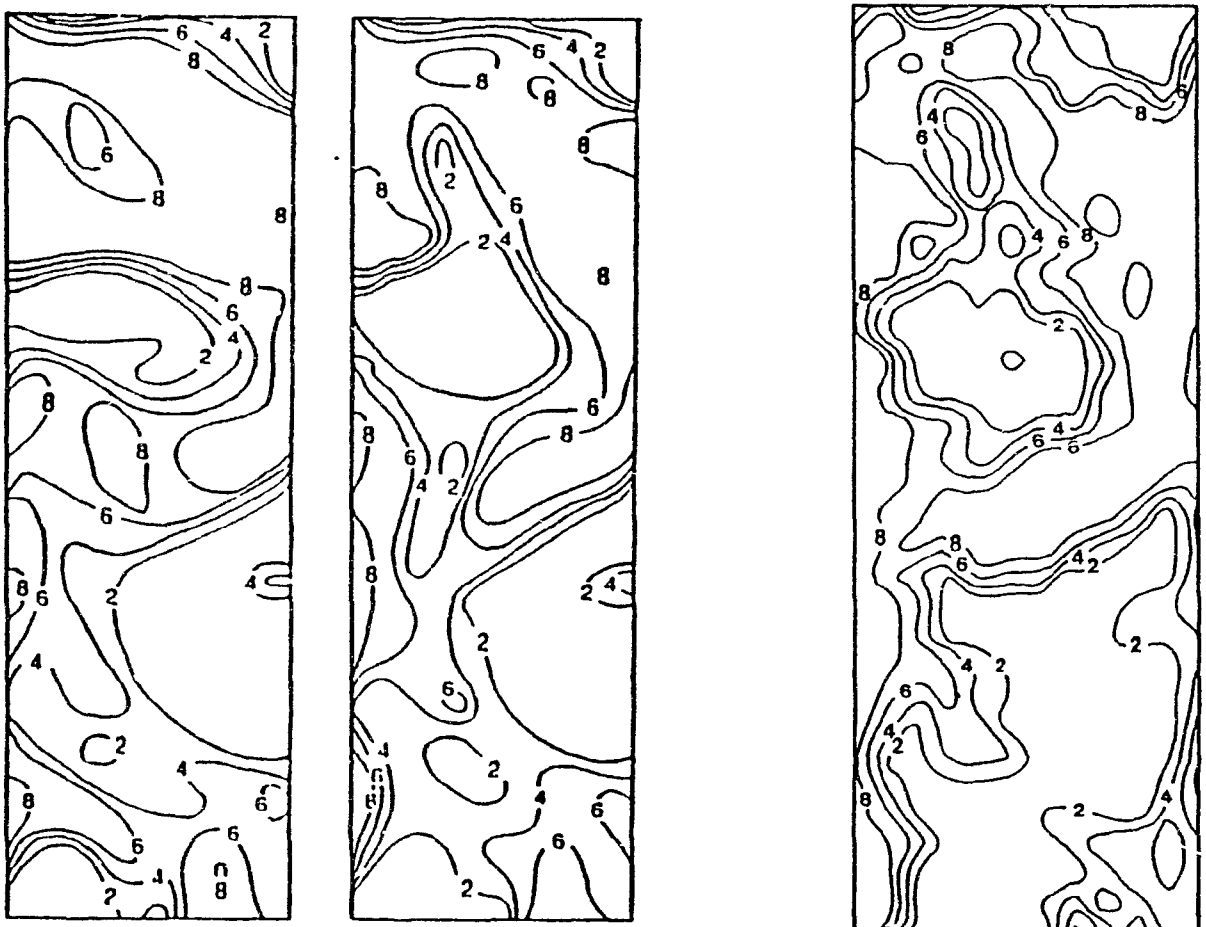

A B C

Figure 4.16. a) Manual and b)automatic analysis of Ebert (1987); c) automatic analysis derived by the present algorithm for the satellite data taken during the first orbit (=00:33' GMT) of July 5, 1984.

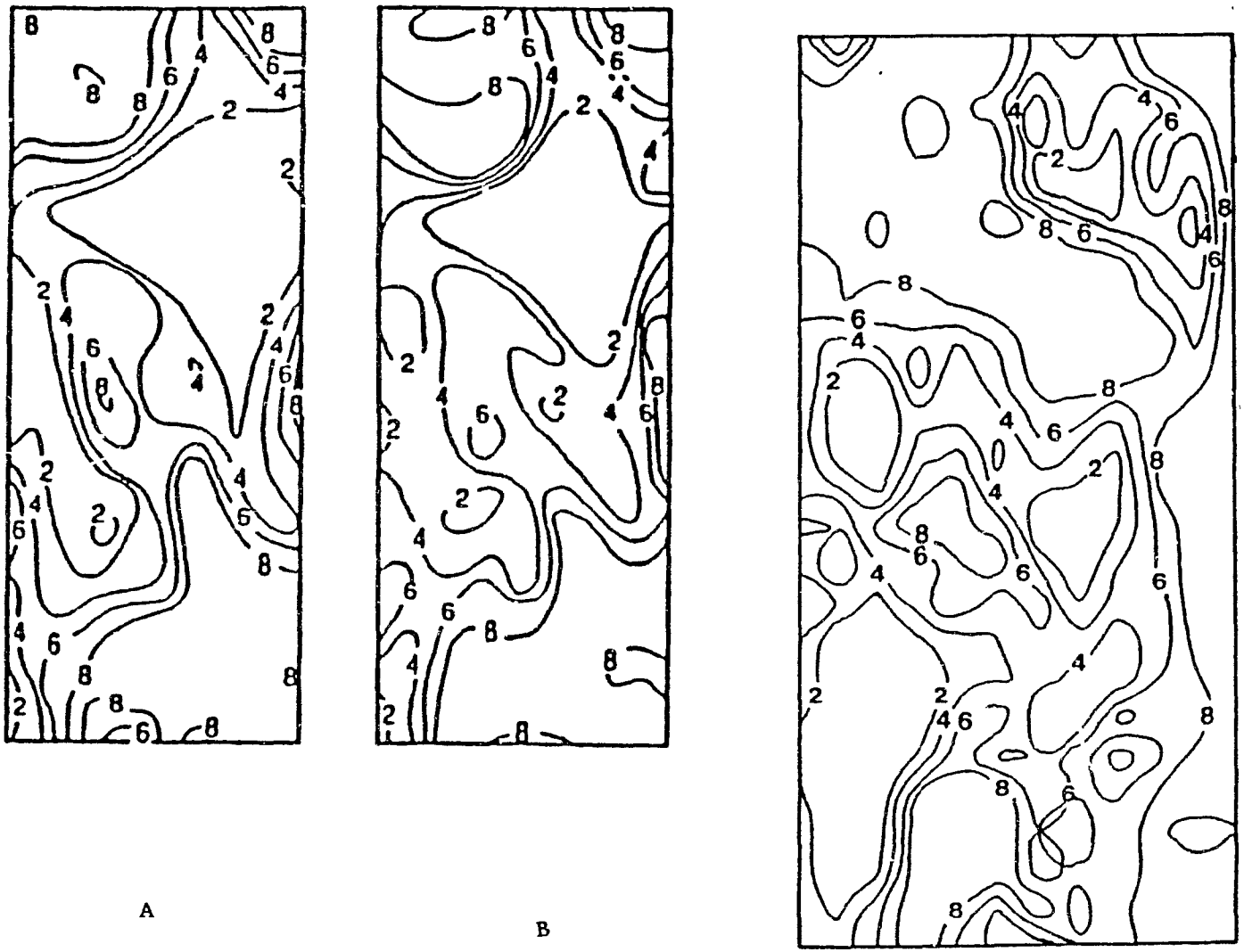

A B C

Figure 4.17. Same as in Figure 4.14, but for satellite data taken during the sixth orbit (≈09:05' GMT) of the same day.

of the first NOAA7 orbit of July 5, 1984. The area covered extends from the Arctic Ocean southwestwards to the Siberian interior. Comparing the analyses, we see that in the upper (northeastward) part of the Figure 4.16 the two automatic analyses agree but they disagree with the manual analysis In the middle part, the present algorithm gives results that are closer to the manual analysis than Ebert's automatic analysis. In the lower (westward) part of the Figure, the two automatic analyses exhibit similar cloud features, not always in accordance with the manual analysis. The present algorithm exhibits larger areas with limited (<0.2) cloudiness, than the automatic and the manual analysis presented by Ebert, and more structured cloud field.

In Figure 4.17 we present manual and automatic analyses, as in Figure 4.16, but now the satellite data were taken at around 09:05 GMT (6^{th} orbit) during the same day. The area covered extends from the northern part of Greenland to the Davis Straight. The data were taken during the descending part of the satellite orbit, and therefore the solar zenith angle is lower than in the previous case. We believe that cloud-free snow covered areas in the Greenland interior have been misclassified by the present algorithm as overcast this being the major disagreement between the present analysis and that presented by Ebert. The reason for this misclassification lies in the combination of snow-covered surfaces with the low solar zenith angles. It causes the R_2-R_1 values of cloud-free surfaces to be raised above the threshold of -0.06 in R_2-R_1 that separates cloudy from undecided pixels in the R_2-R_1 plot. One should also notice that this data was used as a training set by Ebert, while the present algorithm uses fixed thresholds for all backgrounds and solar zenith angles without any kind of adjustment.

If we compare the cloud field above the whole Arctic from all the satellite orbits during July 1, 1984 obtained by the present algorithm to the cloud field published by Ebert, we see that low (<0.2) cloudiness and high cloudiness (<0.8) areas are very well correlated. In Figure 4.18 we present the low cloud amount areas obtained by both analyses and in Figure 4.19 the high cloud amount areas. In these Figures we see that the area covered by heavy cloudiness (>0.8) is larger in the present analysis. This may be due to the use of thresholds in almost all channels of the AVHRR by the present algorithm, while Ebert uses only the "optimum" channel for the determination of cloud amount.

It seems likely that limiting the cloud detection to an "optimum" channel will tend to preferentialy select the dominant cloud type while other existing clouds with different optical properties may be less readily detected. If two cloud types with extremely different properties such as cirrus and stratus exist in a scene, it is possible that making use of one channel may lead to a cloud amount underestimation.

4.2 The Present Algorithm and the Antarctic Environment

As has already been mentioned (Section 4.1), problems are encountered when the solar elevation angle is low above the Greenland interior. These problems were tentatively attributed to the presence of small grain radii ice particles on the surface as the average surface temperature during the month of July is less than -10°C (Putnis and

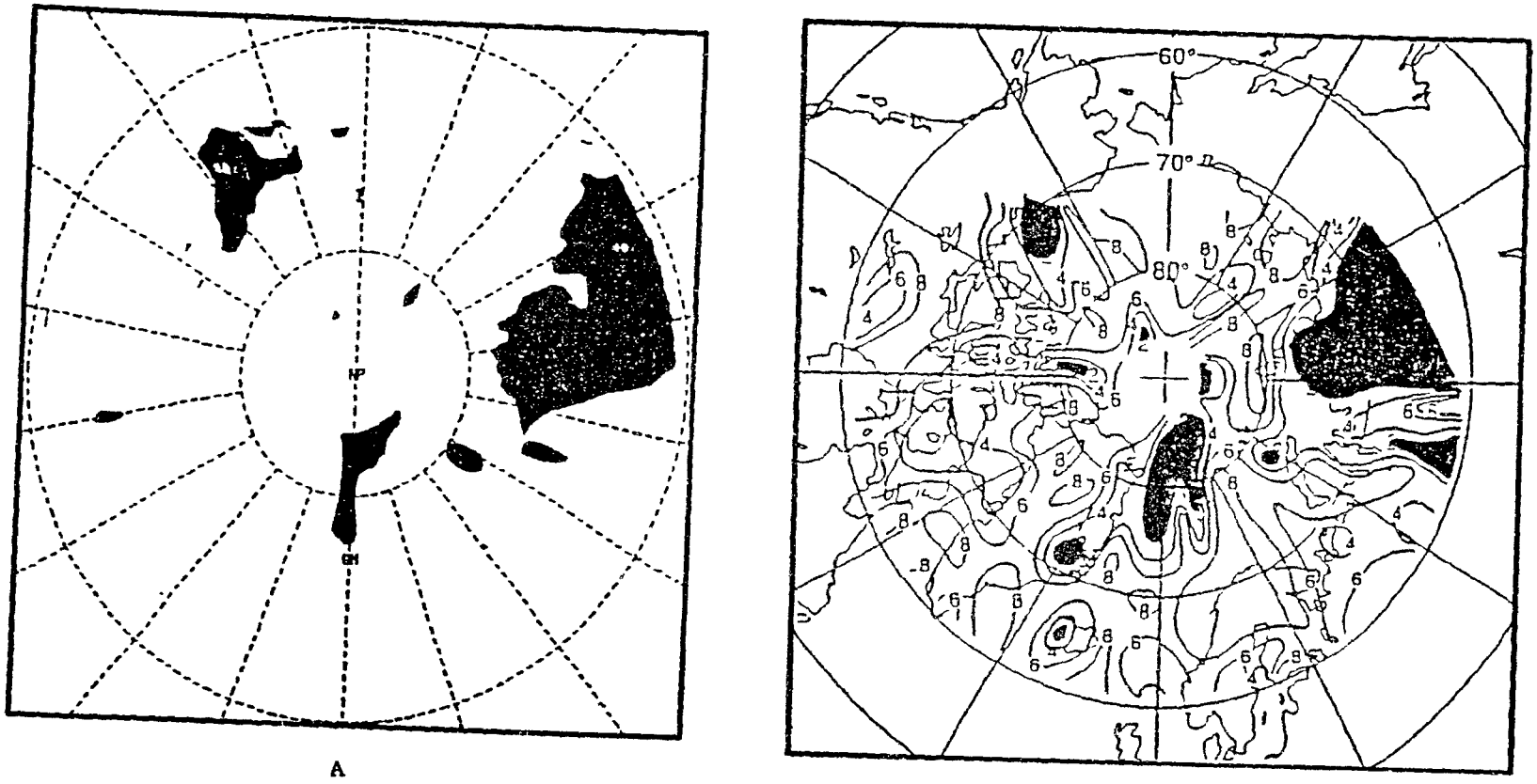

Figure 4.18. Average cloud fraction from all (14) orbits of July 1, 1984. Areas with analysed cloud cover less than 0.2 based on the present algorithm (a), and on Ebert's algorithm (b) are shaded.

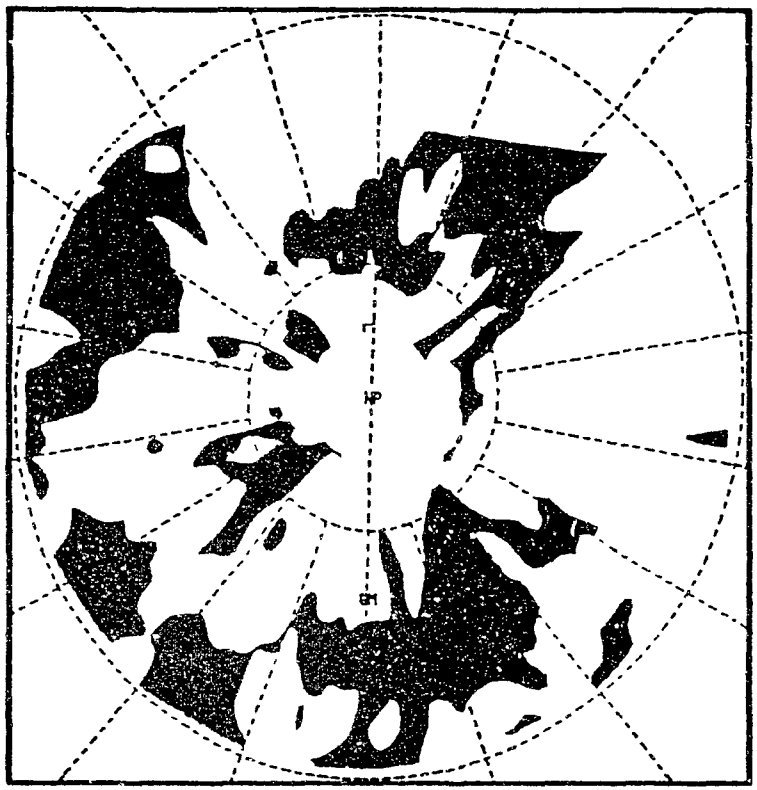

A

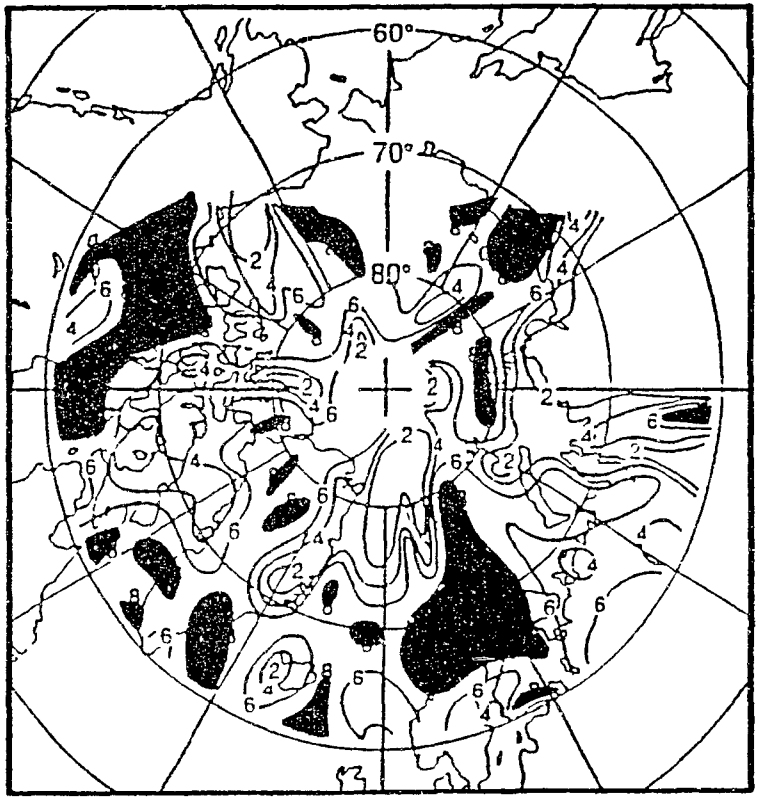

B

Figure 4.19. Same as in Figure 4.16, but for areas with cloud cover greater than 0.8.

Orvig 1970).

Summertime surface temperatures are even less over the Antarctic Plateau. Average temperatures for some stations can be lower than -30°C for the month of January (Schwerdtfeger and Orvig 1970). One should therefore expect that melting events take place only rarely in the Antarctic Plateau, and that the snow grain radii can be even smaller than those of the Greenland interior in July. Consequently, it is difficult to distinguish between thick clouds and snow covered surfaces. It is also relatively rare to find thick clouds above the Antarctic Plateau, because the existing very low surface temperatures and the high altitude do not allow the atmosphere to sustain large amounts of water vapor. Another effect of the low temperatures is that low clouds, with temperature close to the underlying surface, can be completely glaciated, and the 3.9 μm channel may not be used for their identification, as was the case above the Northern Hemisphere.

The present algorithm was developed on the assumptions that thin, low clouds are not completely glaciated, and that high clouds are much colder than the surface.

The prevailing atmospheric conditions on the Antarctic Plateau may violate the aforementioned assumptions, and we expect that analysis of cloud fields above that region by the present algorithm will be met by only limited success.

On the other hand, the present algorithm pays a lot of attention to the presence of land and to land-ice combinations. Over the Northern Hemisphere, where the Arctic Ocean is surrounded by continents, and where a number of islands of considerable size exist in high latitudes, it is essential. But in the Antarctic continent, the ex-

istence of bare land is much more limited and problems arising from the presence of land and from surfaces covered by a mixture of land and ice are much less important.

For these reasons, the present algorithm should undergo a number of modifications in order to be applied over the Antarctic Plateau. Channels 1 and 2, that are so crucial in Northern Hemisphere, now become less important due to the small grain radii snow, to the thinner clouds, and to the sparcity of land. The split channel, that has rather limited use partly because of the atmospheric effect, should be more heavily employed in the Antarctic. Consequently the modified algorithm should rely more on the emitted terrestrial radiation channels than the present algorithm, and the direction of change, is from a "day time algorithm" towards a "night time algorithm".

As far as the large area of sea-ice around the Antarctic Continent is concerned, the present algorithm should not have problems identifying clouds and estimating cloud amounts, because sea-ice does not violate the basic assumptions used for its development.

CHAPTER 5

CONCLUSIONS AND SUGGESTIONS FOR FUTURE WORK

In the present thesis, we have documented:

a) an automated method, capable of separating cloudy from clear pixels above surfaces composed of land and water, where previously proposed techniques have been least reliable; and

b) an automated method for the cloud amount estimation above the Arctic, based partly on the principles used for the separation of cloud-free pixels from cloudy ones, under background composed of land and water.

For both methods, the use of channels 1 and 2 of the AVHRR, in the form of the R_2-R_1 plot, introduced in the present work, is essential for the recognition of the surface and cloud signatures.

The method for the cloud amount estimation is essentially a multiple- threshold method, coupled with some statistical elements used for the estimation of cloud free radiances. All the thresholds are fixed, but some of the cloud-free radiances are calculated separately at every data set, giving flexibility to the algorithm.

A continuous seven-days time interval of AVHRR data taken above the Arctic were analysed. The obtained cloud fields were compared to manual analyses, to the corresponding synoptic situation, and to cloud fields obtained by automatic analysis of the same satellite data, by other investigators with satisfactory results.

The present work can find applications in the following situa-

tions:

1) when separation of cloud-free from cloudy radiances above coastals, and lakeshore regions is needed. There is no latitude limit for this separation. Large parts of Canada, Europe's complicated coastlines, and North-Europe and Scandinavia with the multitude of lakes are among the areas where the present work can be successfully applied,

2) when separation of cloud-free from cloudy radiances above areas containing ice or snow-covered surfaces is needed. High latitudes in the North hemisphere during the summer, and lower latitudes during the winter, are possible application areas; and

3) when cloud amount estimation above the aforementioned areas is needed.

Part of this study was completed with the purpose of contributing to the ISCCP project, and especially to cloud amount estimations above the Arctic.

We consider the present work to avoid the use of extensive numerical computations, requiring rather limited computational effort. Additionally it is not history dependent. Every orbit can be independently analysed.

Its disadvantages arise from the variety of the cloud-free radiances one may encounter above the Arctic, especially when the solar zenith angle is large and the reflected solar radiation channels are less reliable.

It has already been mentioned (Section 4.1) that above the Greenland Plateau, some cloud-free areas are interpreted as cloudy. This happens because snow covered areas under large solar zenith angles exhibit R_2-R_1 values that are interpreted as belonging to clouds.

A large temperature gradient has been observed in data sets that contain areas belonging to the Greenland coastline and areas inside Greenland. In this case, some relatively cold cloud-free radiances can be interpreted as cloudy.

Combinations of land and ice, constitute the most unfavorable background for cloud identification. This situation is quite often encountered over the Canadian Archipelago, which is therefore considered an area where clouds can escape detection easier than elsewhere.

As was mentioned earlier, the part of the algorithm that estimates the cloud amount uses thresholds. Consequently the estimated cloud amounts suffer from all the problems associated with cloud amount estimations, based on threshold methods (Coakley and Bretherton 1982).

Channel three threshold is even more questionable than the rest because at this channel cloud edges reflect more vigorously than cloud interiors (Coakley and Davies 1986). As a result, partly cloudy pixels are more likely to be characterised as overcast than the overcast ones. Fortunately, clouds in high latitudes have large areal extent, and they are usually of the stratiform type, so these problems are partly alleviated.

As far as future work is concerned, it should be noted that the present algorithm for cloud amount estimations includes two logical steps:

1) surface identification, and

2) proper routine for cloud analysis.

Increase in complexity is essential if one tries to avoid the difficulties encountered above the Arctic region. We believe that the present algorithm can be used for the creation of a data base where cloud-free radiances for every 2.5 X 2.5 latitude, longitude cell have been estimated, and that this data base can be used along with solar zenithian angle information, in order to self-tune the thresholds it uses for cloud amount estimation.

Low solar zenith angles appear to favor pattern recognition methods because bumps in the solar reflected radiation field are easily recognized, while cloud detection by thresholds in the same channels may face difficulties. Experimentation with pattern recognition features therefore could be fruitful and some of these features could be incorporated into the algorithm to enhance its cloud detection capabilities when the sun is low in the horizon. In terms of existing cloud types at a particular scene, the algorithm can easily be modified in order to separate high, medium and low clouds, on the basis of their 11 μm radiances. It is also possible to distinguish between water and ice clouds on the basis of their 3.7 μm reflectivity. By including pattern recognition features into the algorithm, even more types of clouds like stratus, broken cumulus, cloud streets, etc. can be distinguished (Garand 1986).

REFERENCES

Allen, R.C., Durkee, P.A., and Wash, C.H., Snow and Low Cloud Discrimination from Multispectral Satellite Measurements, Third Conference on Satellite Meteorology and Oceanography, 383-387, 1988.

Arking, A., Spectral Albedo of Snow, Ice and Clouds: A Short Review, Report of the International Satellite Cloud Climatology Project (ISCCP) Workshop of Cloud Algorithms in the Polar Regions, Appendix C.1, World Climate Research Programme, Report WCP-131, 1987.

Arking, A., and J.D. Childs, Retrieval of Cloud Cover Parameters from Multispectral Satellite Measurements, J. Clim. Appl. Meteor., 24, 322-333, 1985.

Barnes, J.C., and Smallwood M.D., TIROS-N Series, Direct Readout Services, Users Guide, US Department of Commerse, Washington DC, 1982.

Bell, G.J., and Wong, M.C., The Near-infrared Radiation Received by Satellites from Clouds, Monthly Weather Review, 109, 2158-2163, 1981.

Briegleb, B., and Ramanathan, V., Spectral and Diurnal Variations in Clear Sky Planetary Albedo, J. Appl. Meteor., 21, 1160-1171, 1982.

Brown, O.B., Brown, J.W., and Evans, R.H., Calibration of Advanced Very High Resolution Radiometer Infrared Observations, J. Geophys. Res., 90, 11667-11677, 1985.

Coakley, J.A., and Davies, R., The Effect of Cloud Sides on Reflected Solar Radiation as Deduced from Satellite Observations J. Atmos. Sci 43, 1025-1035, 1986.

Coakley, J.A., and Baldwin, D.G., Toward the Objective Analysis of Clouds from Satellite Imagery Data, J. CLim. Appl. Meteorol., 23, 1065-1099, 1984.

Coakley, J.A., and Bretherton, F.P., Cloud Cover from High Resolution Scanner Data: Detecting and Allowing for Partially Filled Fields of View, J. Geophys. Res., 87, 4917-4932, 1982.

Desbois, M., G. Sege, and G. Szejwach, Automatic Classification of Clouds on METEOSAT Imagery: Application to High Level Clouds, J. Appl. Meteorol., 21, 401-412, 1982.

Dozier, J., and Warren, S.G., Effect of Viewing Angle on the Infrared Brightness Temperature of Snow, Water Resources Research, 18, 1424-1434, 1982.

Dozier, J., Schneider, S.R., and McGinnis, D.F., Effect of Grain Size and Snowpack Water Equivalence on Visible and Near-Infrared Satellite Observations of Snow, Water Resources Research, 17, 1213-1221, 1981.

Ebert E., A Pattern Analysis Technique for Classifying and Analyzing Surface and Cloud Types in the Arctic, Report of the International Satellite Cloud Climatology Project (ISCCP) Workshop of Cloud Algorithms in the Polar Regions, Appendix C.3, World Climate Research Programme, Report WCP-131, 1987a.

Ebert, E., A Pattern Recognition Technique for Distinguishing Surface and Cloud Types in the Polar Regions, Journal of Climate and Applied Meteorology, 26, 1412-1427, 1987b.

Ebert, E., Classification and Analysis of Surface and Clouds at High Latitudes from AVHRR Multispectral Satellite Data, Scientific Report #8, Department of Meteorology, University of Wisconsin, 1988.

England, C.F., and G.E. Hunt, A Bispectral Method for the Automatic Determination of Parameters for Use in Imaging Satellite Cloud Retrievals, Int. J. Remote Sens., 6, 1545-1553, 1985.

Garand, L., Automated Recognition of Oceanic Cloud Patterns and its Application to Remote Sensing of Meteorological Parameters, Ph. D. thesis, University of Wisconsin, 231 pp., 1986.

Gates, L., The Simulation of the Arctic Climate with a Global General Circulation Model, Climate of the Arctic, Weller, G. and S. A. Bowling, Ed , 132-142, 1973.

Goodman, A.H., and Henderson-Sellers, A., Cloud Detectior and Analysis: A Review of Recent Progress, Atmospheric Research, 21, 203-228, 1988.

Inoue, T., The Clouds and NOAA-7 AVHRR Split Window, Report of the International Satellite Cloud Climatology Project (ISCCP) Workshop of Cloud Algorithms in the Polar Regions, Appendix C.5, World Climate Research Programme, Report WCP-131, 1987a.

Inoue, T., An Instantaneous Delination of Convective Rainfall Areas Using Split Window Data of NOAA-7 AVHRR, J. Meteorol. Soc. Jpn. 65, 469-480, 1987b.

Inoue, T., On the Temperature and Effective Emissivity Determination of Semi-Transparent Cirrus Clouds by Bi-Spectral Measurements in the 10μm Window Region, J. Meteorol. Soc. Jpn, 63, 88-99, 1985.

Kidder, S.Q., and Wu, H.T., Dramatic Contrast between Low Clouds and Snow Cover in Daytime 3.7μm Imagery, Monthly Weather Review, 112, 2345-2346, 1984

Knottenberg, H., and Raschke, E., On the Discrimination of Water and Ice Clouds in Multispectral AVHRR-Data, Annalen der Meteorologie, 18, 145-146, 1982.

Kondratyev, K. Ya., Radiation in the Atmosphere, 912pp. Academic Orlando, Fla., 1969.

Lauritson, L. et al., Data Extraction and Calibration of Tiros-N/NOAA Radiometers, NOAA Technical Memorandum NESS 107, Washington DC, 1979.

Liou, K.N., On the Radiative Properties of Cirrus in the Window Region and their Influence on Remote Sensing of the Atmosphere, J. Atm. Sc., 31, 522-532, 1974.

Llewellyn-Jones, D.T., P.J. Minnet, R.W. Saunders, and A.M. Zavody, Satellite Multichannel Infrared Measurements of Sea Surface Temperature of the N. E. Atlantic Ocean using AVHRR/2, Q. J. R. Meteorol. Soc., 110, 613-631, 1984

Olesen, F.S., and Grassl, H., Cloud Detection and Classification over Oceans at Night with NOAA7, Int. J. Remote Sensing, 6, 1435, 1985.

Putnis and Orvig, The Climate of Greenland, S. Orvig, Ed., World Survey of Climatology, 14, Elsevier, Amsterdam, p 39, 1970.

Raschke, E., et al., Cloud Analysis of AVHRR Data Measured over the Polar Regions, Report of the International Satellite Cloud Climatology Project (ISCCP) Workshop of Cloud Algorithms in the Polar Regions, Appendix C.6, World Climate Research Programme, Report WCP-131, 1987.

Rossow, W.B., Application of ISCCP Cloud Algorithm to Satellite Observations of the Polar Regions, Report of the International Satellite Cloud Climatology Project (ISCCP) Workshop of Cloud Algorithms in the Polar Regions, Appendix C.7, World Climate Research Programme, Report WCP-131, 1987.

Rossow, W.B , et al., ISCCP Cloud Algorithm Intercomparison, J. Clim. Appl. Meteorol., 24,877-903, 1985.

Sadler et al., Pacific Ocean Cloudiness from Satellite Observations, Tech. Rept. Meteor., Univ. of Hawaii, Honolulu, Hawaii, 1976.

Sakellariou, N.K., and Leighton, H.G., Identification of Cloud-free Pixels in Inhomogenous Surfaces from AVHRR Radiances, J. Geophys. Res., 93, 5287-5293, 1988.

Saunders, R.W., An Automated Scheme for the removal of Cloud Contamination from AVHRR Radiances over Western Europe, Int. J. Remote Sensing, 7, 867-886, 1986.

Schiffer, R.A., and Rossow, W.B., The ISCCP. The first Project of the World Climate Research Programme, Bull. Amer. Meteor. Soc., 64, 779-784, 1983.

Schwertfeger and Orvig, The Climate of the Antarctic, S. Orvig, Ed., World Survey of Climatology, 14, Elsevier, Amsterdam, p. 39, 1970.

Scorer, R.S., Sunny Greenland, Quart. J. Roy. Meteor. Soc., 114, 3-29, 1988.

Simmer, C.E., E. Rashke, and E. Ruprecht, A Method for the Determination of Cloud Properties from Two-dimensional Histograms, Ann. Meteorol., 18, 130-132, 1982.

Takashima, T., and Takayama, Y., Sea Surface Measurements from Space Allowing for the Effect of the Stratospheric Aerosols. Papers in Meteorology and Geophysics, 31, 193, 1986.

Tanaka, S., Yamanouchi, T., and Kawagouchi, S., Extraction of Sea Ice Area Using AVHRR Data of NOAA Satellite, Proceedings of the sixth Symposium on Polar Meteorology and Glaciology 197-206, 1984.

Telegadas, K., and London, J., A Physical Model of Northern Hemisphere Troposphere for Winter and Summer, New York Univ. Sci. Rept. 1, Contract AF 19(122), New York, N. Y., 1954:

Twomey, S., and T. Cocks, Spectral reflectance of Clouds in the Near-infrared: Comparisons of Measurements and Calculations, J. Meteorol. Soc. Jpn., 60, 583-592, 1982.

Vowinckel, E., and S. Orvig, The Climate of the North Polar Basin. Climates of the Polar Regions. S. Orvig, Ed., World Survey of Climatology, 14, Elsevier, Amsterdam, pp.144, 1970.

Wannamaker, B., Operational Compression of AVHRR Data, Int. Rep. MSRB-85-6, 20 pp., Atmos. Environ Serv., Toronto, Ontario, Canada, 1985.

Wannamaker, B., Satellite Visible and Infrared Sea-Ice Mapping: Considerations on Techniques, Int. Rep. MSRB-84-9, 14 pp., Atmos. Environ. Serv., Toronto, Ontario, Canada, 1984.

Warren, S.G., Optical Properties of Snow, Reviews of Geophysics and Space Physics, 1, 67-89, 1982.

Welch, R.M., S.K. Cox, and J.M Davis, Solar Radiation and Clouds, AMS Meteorol. Monogr., 17, 39, 1-96, 1980.

Wiscombe, W.J., R.M. Welch and W.D. Hall, The effects of very Large Drops on Cloud Absorption, 1, Parcel models, J. Atmos. Sci., 41, 1336-1355, 1984.

Wolfe, W.L., and Zissis, G.J., The Infrared Handbook, p.3-92 to 3-95, Office of Naval Research, Department of the Navy, Washington DC, 1978.

Yamanouchi, T., Suzuki, K., Kawaguchi, S., Discrimination of Polar Clouds from AVHRR Infrared Multispectral Data, Report of the International Satellite Cloud Climatology Project (ISCCP) Workshop of Cloud Algorithms in the Polar Regions Appendix C.2, World Climate Researche Programme, Report WCP-131, 1987a.

Yamanouchi, T., Suzuki, K., and Kawagouchi, S., Detection of Clouds in Antarctica from Infrared Multispectral Data of AVHRR, J. Meteorol. Soc. Jpn., 65, 949-961, 1987b.

Yamanouchi, T., Suzuki, K., and Kawagouchi, S., Discrimination of Clouds in Antarctica from Multispectral Satellite Images, Symposium on Remote Sensing and the Polar Regions, Honolulu, 1985.